DESY 11-153
CP3-11-28
LPN 11-51
SFB/CPP-11-50
September 2011

Vector boson fusion at NNLO in QCD: SM Higgs and beyond

Paolo Bolzoni[a], Fabio Maltoni[b], Sven-Olaf Moch[c] and Marco Zaro[b]

[a] *II. Institut für Theoretische Physik, Universität Hamburg*
Luruper Chaussee 149, D–22761 Hamburg, Germany

[b] *Center for Cosmology, Particle Physics and Phenomenology (CP3),*
Université Catholique de Louvain,
Chemin du Cyclotron 2, B–1348 Louvain-la-Neuve, Belgium

[c] *Deutsches Elektronensynchrotron DESY*
Platanenallee 6, D–15738 Zeuthen, Germany

Abstract

Weak vector boson fusion provides a unique channel to directly probe the mechanism of electroweak symmetry breaking at hadron colliders. We present a method that allows to calculate total cross sections to next-to-next-to-leading order (NNLO) in QCD for an arbitrary $V^*V^* \to X$ process, the so-called structure function approach. By discussing the case of Higgs production in detail, we estimate several classes of previously neglected contributions and we argue that such method is accurate at a precision level well above the typical residual scale and PDF uncertainties at NNLO. Predictions for cross sections at the Tevatron and the LHC are presented for a variety of cases: the Standard Model Higgs (including anomalous couplings), neutral and charged scalars in extended Higgs sectors and (fermiophobic) vector resonance production. Further results can be easily obtained through the public use of the VBF@NNLO code.

1 Introduction

The central theme of the physics program at the Large Hadron Collider (LHC) is the search for the Standard Model (SM) Higgs boson and more in general the elucidation of the mechanism of electroweak symmetry breaking. The three dominant production mechanisms for the SM Higgs boson are, (in order of importance) gluon-gluon fusion via a top-quark loop, vector-boson fusion (VBF) and Higgs-Strahlung, *i.e.* associated production with W and Z-bosons (see e.g. [1, 2]). In extensions of the SM with a richer Higgs sector, such as in supersymmetry, or in strongly interacting light Higgs scenarios [3], the relative importance of the various channels might depend on the details or parameters of the model. In any case, VBF remains of primary importance, being the channel where longitudinal vector boson scattering gives rise to violation of unitarity at around 1 TeV, if no other particle or interaction is present than what it is currently known from experiments.

Precise knowledge of the expected rates for the Higgs boson production processes is an essential prerequisite for any experimental search and, after discovery, will be a crucial input to proceed to accurate measurements. At a hadron collider such as the LHC, precision predictions need to include higher-order radiative corrections which usually implies the next-to-next-to-leading order (NNLO) in Quantum Chromodynamics (QCD) and the next-to-leading order (NLO) as far as electroweak corrections are concerned. If accounted for, these higher-order quantum corrections generally stabilize the theoretical predictions through an apparent convergence of the perturbative expansion and a substantially reduced dependence on the choice of the factorization and renormalization scales. For inclusive Higgs boson production in gluon-gluon fusion and the WH and ZH mode, the exact NNLO corrections in QCD are available [4–7] and have been shown to be very important (see e.g. [8]).

Higgs boson production via VBF is the mechanism with the second largest rate in the SM and offers a clean experimental signature with the presence of at least two jets in the forward/backward rapidity region [9–11] and a variety of Higgs boson decay modes to be searched for [12–15] . In extensions of the SM which feature scalar or vector state(s) with reduced couplings to fermions, VBF can become the leading production mechanism. VBF is a pure electroweak process at leading order (LO) and it acquires corrections at NLO in QCD [16, 17] as well as in the electroweak sector [18, 19] leading to a typical accuracy for the total cross-section in the $5-10\%$ range. Recently, the NNLO QCD corrections for the VBF process have been computed [20] in the so-called structure function approach [16], which builds upon the approximate, although very accurate, factorization of the QCD corrections between the two parton lines associated with the colliding hadrons. At NNLO the results are very stable with respect to variations of the renormalization and factorization scales, μ_r and μ_f, and can take full advantage of modern sets of precise parton distribution functions (PDFs) at the same accuracy. The small theoretical uncertainty for the inclusive rate due to missing higher order QCD corrections as well as the PDF uncertainties are estimated to be at the 2% level each for a wide range of Higgs boson masses.

The purpose of the present article is two-fold. First, it provides an extensive documentation of the NNLO computation of Refs. [20, 21] and a broad phenomenological study for the LHC at various center-of-mass energies and for the Tevatron. Second, it exploits the universality of the structure function approach to describe the production of any color-neutral final state from the fusion of vector bosons and applies it to a number of new physics models, e.g. with an extended Higgs sector, or to vector resonance production (see e.g., [22, 23]).

The outline is as follows: In Sec. 2 we define the VBF process as a signal, discuss carefully its contributions and give arguments for the ultimate theoretical precision one could possibly aim

at in predictions of its rates. Sec. 3 is devoted to a discussion of the structure function approach at NNLO in QCD along with detailed computations of neglected contributions as a means of estimating the accuracy. In particular, we study the non-factorizable diagrams and the ones involving heavy quarks, all of which are not accounted for in the structure function approach. Phenomenological results for inclusive rates at the LHC and Tevatron are presented in Sec. 4. Extensions of the structure function approach to Higgs boson production via VBF in specific classes of models beyond the SM (see e.g., [24] for charged Higgs bosons) as well as modifications due to anomalous couplings (WWH, ZZH, etc.) and vector resonances are discussed in Sec. 5. Finally, we conclude in Sec. 6 and document some technical aspects and tables with VBF cross sections in the Appendices.

2 Setting the stage

Processes in collider physics are always defined on simple conventions typically based on leading-order Feynman diagrams. While this normally poses no problems, it might lead to ambiguities when decays of resonant states and/or higher order effects are included. Consider, as a simple example, the class of processes which involve only the electroweak coupling α_{EW} at the leading order, such as Drell-Yan (with the decay into two jets), single-top production and Higgs boson production via coupling with a vector boson. Most of such processes can be easily defined at leading order considering the corresponding resonant intermediate or final states, while some, such as VBF are (quantum-mechanically) ambiguous already at the leading order: $pp \to Hjj$ with vector bosons in the t-channel can interfere with $pp \to HV^{(*)} \to Hjj$, *i.e.*, with Higgs associated production with a vector boson then decaying into two jets. Such interference, however, is quite small everywhere in the phase space and it can formally be reduced to zero by just taking the narrow width limit. This suggests that considering the two processes distinct is a handy approximation, at least at the leading order. For all of the processes in this class, *i.e.*, single-top and Higgs electroweak production, aiming at a better precision by including higher-order QCD effects creates further ambiguities as it opens up more possibilities for interferences (one notable example is tW at NLO overlapping with $t\bar{t}$ production) and the reliability of the approximations made has to be carefully assessed.

In general two complementary approaches can be followed. The first is to consider all interferences exactly, and introduce a gauge-invariant scheme to properly handle the width effects. This can be consistently done at NLO order in QCD and electroweak corrections, following well-known and established techniques, such as the use of the complex-mass scheme [25]. This is the path followed for instance in Ref. [19] for the calculation of QCD and electroweak effects in the order α_{EW}^3 process $pp \to Hjj$. The advantage of this approach is that all interference effects are correctly taken into account in any region of phase space, including where tight cuts might create significant enhancements. This is the only way to proceed when interference effects are similar to or larger than the corrections from higher orders. However, when such effects are small, it offers several drawbacks. The first is the unnecessary complexity of the calculation itself. The second is that the operational separation between the two processes, which can be quite useful at the practical level, for example in experimental analyses, is lost. In this context, even the definition of signal and background might not be meaningful and the distinction possibly leads to confusion. In this case another approach can be followed. Use a simple process definition and systematically check the impact of higher-order corrections as well as those from interferences to set the ultimate practical precision that can be achieved. In this section we argue that for vector-boson fusion this

procedure is sound and can lead to a definition which is unambiguous to better than 1%, *i.e.* more than sufficient for all practical applications at hadron colliders.

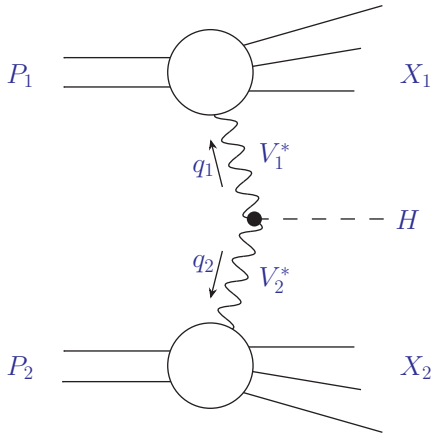

Figure 2.1: Higgs production via the VBF process.

In short, we define VBF as the Higgs production for vanishing quark masses, through direct coupling to vector bosons in the *t*-channel, and with no color exchange between the two colliding hadrons, *i.e.*, all the processes that can be represented by the diagram in Fig. 2.1, where no heavy-quark loop is to be included in the blobs while additional vector bosons in a color singlet state might appear at one or more loops (not shown).

The definition above, while academic in nature, fits extremely well with what is looked for and associated to in the current experimental searches. For example, it excludes the interfering effects with *s*-channel associated production, but includes the additional exchange of two gluons in a color singlet state in the *t*-channel. These two effects, as we will argue in the following, are tiny and can be neglected in the numerical evaluation of the total cross section. However, it is useful to keep in mind that our definition put them on a different ground. The main reason/motivation is that among the most important characteristics exploited in the experimental analyses is the presence of two high-invariant mass forward-backward jets and the absence of radiation in the central region. Both these effects are present in the case of the color-singlet component of double-gluon exchange in the *t*-channel, while they are not typical of the *s*-channel contribution.

The definition given above allows us to systematically classify processes for Higgs boson production as VBF and non-VBF. In the latter we include also possible interferences between amplitudes belonging to the VBF class and those in the non-VBF one.

"VBF" processes:

- Factorizable contributions in QCD, see Fig. 2.1. This class is evaluated exactly in this work for massless quarks. It provides the bulk of all QCD corrections up to order α_s^2 to a precision better than 1%.

- Non-factorizable contributions in QCD. This class starts at order α_s^2/N_c^2. It is estimated in Sec. 3.2 to contribute less than 1% to the total VBF cross section.

- Electroweak corrections to diagrams in Fig. 2.1. These are relevant corrections which have been calculated in Ref. [19]. A combination with the NNLO QCD ones calculated in this work has been reported in Ref. [8].

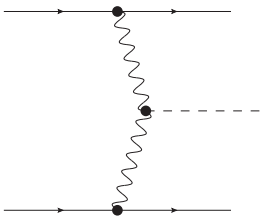

Figure 3.1: Higgs production via the VBF process at LO in QCD.

"Non-VBF" processes:

- Single-quark line contributions, as calculated in Ref. [26]. These effects are smaller than 1% in differential cross sections.
- Interferences in VBF itself known at NLO in QCD and electroweak, as calculated in Ref. [19]. These effects can be calculated at LO and are found to be very small.
- Interferences between VBF and associated WH and WZ production at NLO in QCD and electroweak, as calculated in Ref. [19]. These effects can be easily calculated at LO and are found to be very small.
- Interferences with the top-loop mediated Higgs production, Refs. [27, 28] and contributions calculated in Sec. 3.3. These effects are found to contribute less than 1% to the total cross section.
- t-channel vector boson production in presence of heavy-quark loops (triangles and boxes), see Sec. 3.3. These effects are estimated to contribute less than 1% to the total cross section.

We conclude this section by mentioning that the same kind of difficulties/ambiguities arise when the Higgs width becomes non-negligible, *i.e.* for large Higgs masses, let us say $m_H > 500$ GeV. Apart from the need of a Breit-Wigner smearing of cross sections calculated in the narrow-width limit that can be easily implemented, interference effects with "background" processes can become important and need to be accounted for. Such effects have been considered in full generality at LO in studies of vector boson scattering [29, 30] and, for leptonic final states of the vector bosons, in EW production of V_1V_2jj at NLO in QCD [31–34].

3 VBF at higher orders

Let us discuss the radiative corrections to the VBF process with emphasis on the QCD contributions. As mentioned above, at LO the Higgs production in VBF proceeds purely through electroweak interactions (see Fig. 3.1), with the cross section for $pp \to Hjj$ being of order α_{EW}^3.

In the QCD improved parton model, higher order corrections arise. All NLO QCD contributions to the VBF cross section (order $\alpha_{EW}^3\alpha_s$) can be treated exactly in the structure function approach, which we discuss in detail and extend to NNLO below in Sec. 3.1. At NNLO, *i.e.* at order $\alpha_{EW}^3\alpha_s^2$, certain other contributions arise, which we estimate. These are diagrams involving gluon exchange between the two quark lines (cf. Sec. 3.2), and diagrams involving closed heavy-quark loops (cf. Sec. 3.3). We also comment briefly on electroweak corrections at one-loop in Sec. 3.4.

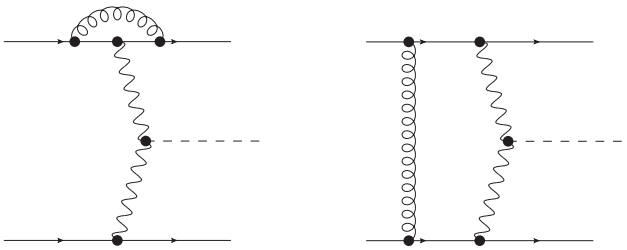

Figure 3.2: Higgs production via the VBF process at NLO in QCD.

3.1 Structure function approach

The structure function approach is based on the observation that to a very good approximation the VBF process can be described as a double deep-inelastic scattering process (DIS), see Fig. 2.1, where two (virtual) vector-bosons V_i (independently) emitted from the hadronic initial states fuse into a Higgs boson. This approximation builds on the absence (or smallness) of the QCD interference between the two inclusive final states X_1 and X_2. In this case the total cross section is given as a product of the matrix element $\mathcal{M}^{\mu\rho}$ for VBF, *i.e.*, $V_1^\mu V_2^\rho \to H$, which in the SM reads

$$\mathcal{M}^{\mu\nu} = 2\left(\sqrt{2}G_F\right)^{1/2} M_{V_i}^2 g^{\mu\nu}, \tag{3.1}$$

and of the DIS hadronic tensor $W_{\mu\nu}$:

$$\begin{aligned} d\sigma &= \frac{1}{2S} 2G_F^2 M_{V_1}^2 M_{V_2}^2 \frac{1}{\left(Q_1^2 + M_{V_1}^2\right)^2} \frac{1}{\left(Q_2^2 + M_{V_2}^2\right)^2} W_{\mu\nu}\left(x_1, Q_1^2\right) \mathcal{M}^{\mu\rho} \mathcal{M}^{*\nu\sigma} W_{\rho\sigma}\left(x_2, Q_2^2\right) \times \\ &\quad \times \frac{d^3P_{X_1}}{(2\pi)^3 2E_{X_1}} \frac{d^3P_{X_2}}{(2\pi)^3 2E_{X_2}} ds_1 ds_2 \frac{d^3P_H}{(2\pi)^3 2E_H} (2\pi)^4 \delta^4\left(P_1 + P_2 - P_{X_1} - P_{X_2} - P_H\right). \end{aligned} \tag{3.2}$$

Here G_F is Fermi's constant and $\sqrt{S}$ is the center-of-mass energy of the collider. $Q_i^2 = -q_i^2$, $x_i = Q_i^2/(2P_i \cdot q_i)$ are the usual DIS variables, $s_i = (P_i + q_i)^2$ are the invariant masses of the i-th proton remnant, and M_{V_i} denote the vector-boson masses, see Fig. 2.1. The three-particle phase space dPS of the VBF process is given in the second line of Eq. (3.2). It is discussed in detail in Sec. A.1.

Higgs production in VBF requires the hadronic tensor $W_{\mu\nu}$ for DIS neutral and charged current reactions, *i.e.*, the scattering off a Z as well as off a $W^\pm$-boson. It is commonly expressed in terms of the standard DIS structure functions $F_i(x, Q^2)$ with $i = 1,2,3$. *i.e.* F_i^V with $i = 1,2,3$ and $V \in \{Z, W^\pm\}$ and we employ the particle data group (PDG) conventions [35]. Thus,

$$W_{\mu\nu}\left(x_i, Q_i^2\right) = \left(-g_{\mu\nu} + \frac{q_{i,\mu} q_{i,\nu}}{q_i^2}\right) F_1(x_i, Q_i^2) + \frac{\hat{P}_{i,\mu}\hat{P}_{i,\nu}}{P_i \cdot q_i} F_2(x_i, Q_i^2) + \mathrm{i}\epsilon_{\mu\nu\alpha\beta} \frac{P_i^\alpha q_i^\beta}{2P_i \cdot q_i} F_3(x_i, Q_i^2), \tag{3.3}$$

where $\epsilon_{\mu\nu\alpha\beta}$ is the completely antisymmetric tensor and the momentum $\hat{P}_i$ reads

$$\hat{P}_{i,\mu} = P_{i,\mu} - \frac{P_i \cdot q_i}{q_i^2} q_{i,\mu}. \tag{3.4}$$

The factorization underlying Eq. (3.2) does not hold exactly already at LO, because interference can occur either between identical final state quarks (*i.e.*, $uu \to Huu$) or between processes where

either a W or a Z can be exchanged (*i.e.*, $ud \to Hud$). However, at LO, these contributions can be easily computed and they have been included in our results. On the other hand, simple arguments of kinematics (based on the behavior of the propagators in the matrix element [36]) show that such contributions are heavily suppressed already at LO and contribute to the total cross section well below the 1% level, a fact that has been confirmed by a complete calculation even through NLO [19]. Apart from these interference effects, the factorization of Eq. (3.2) is still exact at NLO. This is due to color conservation: QCD corrections to the upper quark line are independent from those of the lower line. Fig. 3.2 (left) shows a sample diagram accounted for by the structure function approach, while the diagram Fig. 3.2 (right) vanishes at NLO due to color conservation, *i.e.*, $\mathrm{Tr}(t^a) = 0$ for generators t^a of the color $\mathrm{SU}(N_c)$ gauge group.

The evaluation of Eq. (3.1) and Eq. (3.3) leads to the explicit result for the squared hadronic tensor in Eq. (3.2) in terms of the DIS structure functions [16] (see also the review [1]) :

$$
\begin{aligned}
&W_{\mu\nu}\left(x_1,Q_1^2\right)\mathcal{M}^{\mu\rho}\mathcal{M}^{*\nu\sigma}W_{\rho\sigma}\left(x_2,Q_2^2\right) = 4\sqrt{2}G_F M_{V_i}^4 \times \\
&\times \quad \left\{F_1\left(x_1,Q_1^2\right)F_1\left(x_2,Q_2^2\right)\left[2+\frac{(q_1\cdot q_2)^2}{q_1^2 q_2^2}\right]+\right. \\
&\quad +\frac{F_1\left(x_1,Q_1^2\right)F_2\left(x_2,Q_2^2\right)}{P_2\cdot q_2}\left[\frac{(P_2\cdot q_2)^2}{q_2^2}+\frac{1}{q_1^2}\left(P_2\cdot q_1-\frac{P_2\cdot q_2}{q_2^2}q_1\cdot q_2\right)^2\right] \\
&\quad +\frac{F_2\left(x_1,Q_1^2\right)F_1\left(x_2,Q_2^2\right)}{P_1\cdot q_1}\left[\frac{(P_1\cdot q_1)^2}{q_1^2}+\frac{1}{q_2^2}\left(P_1\cdot q_2-\frac{P_1\cdot q_1}{q_1^2}q_1\cdot q_2\right)^2\right] \\
&\quad +\frac{F_2\left(x_1,Q_1^2\right)F_2\left(x_2,Q_2^2\right)}{(P_1\cdot q_1)(P_2\cdot q_2)}\times \\
&\qquad \times\left(P_1\cdot P_2-\frac{(P_1\cdot q_1)(P_2\cdot q_1)}{q_1^2}-\frac{(P_1\cdot q_2)(P_2\cdot q_2)}{q_2^2}+\frac{(P_1\cdot q_1)(P_2\cdot q_2)(q_1\cdot q_2)}{q_1^2 q_2^2}\right)^2 \\
&\quad \left.+\frac{F_3\left(x_1,Q_1^2\right)F_3\left(x_2,Q_2^2\right)}{2(P_1\cdot q_1)(P_2\cdot q_2)}\Big((P_1\cdot P_2)(q_1\cdot q_2)-(P_1\cdot q_2)(P_2\cdot q_1)\Big)\right\}. \qquad (3.5)
\end{aligned}
$$

At this stage it remains to insert the DIS structure functions F_i^V with $i = 1,2,3$ and $V \in \{Z, W^\pm\}$. At NLO in QCD, explicit expression have been given in Ref. [16] using the results of Ref. [37]. For the necessary generalization beyond NLO, let us briefly review the basic formulae. QCD factorization allows to express the structure functions as convolutions of the PDFs in the proton and the short-distance Wilson coefficient functions C_i. The gluon PDF at the factorization scale μ_f is denoted by $g(x,\mu_f)$ and the quark (or anti-quark) PDF by $q_i(x,\mu_f)$ (or $\bar{q}_i(x,\mu_f)$) for a specific quark flavor i. The latter PDFs appear in the following combinations,

$$
q_{\mathrm{s}} = \sum_{i=1}^{n_f}\left(q_i+\bar{q}_i\right), \qquad q_{\mathrm{ns}}^{\mathrm{v}} = \sum_{i=1}^{n_f}\left(q_i-\bar{q}_i\right), \qquad (3.6)
$$

$$
q_{\mathrm{ns},i}^{+} = \left(q_i+\bar{q}_i\right)-q_{\mathrm{s}}, \qquad q_{\mathrm{ns},i}^{-} = \left(q_i-\bar{q}_i\right)-q_{\mathrm{ns}}^{\mathrm{v}}, \qquad (3.7)
$$

as the singlet distribution q_{s}, the (non-singlet) valence distribution $q_{\mathrm{ns}}^{\mathrm{v}}$ as well as flavor asymmetries of $q_{\mathrm{ns},i}^{\pm}$. All of them are subject to well-defined transformation properties under the flavor isospin, see e.g. [38, 39].

For the neutral current Z-boson exchange the DIS structure functions F_i^Z can be written as follows:

$$F_i^Z(x,Q^2) = f_i(x)\int_0^1 dz\int_0^1 dy\,\delta(x-yz)\sum_{j=1}^{n_f}\left(v_j^2+a_j^2\right)\times \tag{3.8}$$
$$\times\left\{q^+_{\mathrm{ns},j}(y,\mu_f)C^+_{i,\mathrm{ns}}(z,Q,\mu_r,\mu_f)+q_{\mathrm{s}}(y,\mu_f)C_{i,\mathrm{q}}(z,Q,\mu_r,\mu_f)+g(y,\mu_f)C_{i,\mathrm{g}}(z,Q,\mu_r,\mu_f)\right\},$$
$$F_3^Z(x,Q^2) = \int_0^1 dz\int_0^1 dy\,\delta(x-yz)\sum_{i=1}^{n_f}2\,v_i\,a_i\times \tag{3.9}$$
$$\times\left\{q^-_{\mathrm{ns},i}(y,\mu_f)C^-_{3,\mathrm{ns}}(z,Q,\mu_r,\mu_f)+q^{\mathrm{v}}_{\mathrm{ns}}(y,\mu_f)C^{\mathrm{v}}_{3,\mathrm{ns}}(z,Q,\mu_r,\mu_f)\right\},$$

where $i=1,2$ and the pre-factors in Eq. (3.8) are $f_1(x)=1/2$, $f_2(x)=x$. The vector- and axial-vector coupling constants v_i and a_i in Eq. (3.8) are given by

$$v_i^2+a_i^2 \;=\; \begin{cases} \frac{1}{4}+\left(\frac{1}{2}-\frac{4}{3}\sin^2\theta_w\right)^2 & u\text{-type quarks},\\ \frac{1}{4}+\left(\frac{1}{2}-\frac{2}{3}\sin^2\theta_w\right)^2 & d\text{-type quarks}, \end{cases} \tag{3.10}$$

and, likewise, in Eq. (3.9),

$$2v_ia_i \;=\; \begin{cases} \frac{1}{2}-\frac{4}{3}\sin^2\theta_w & u\text{-type quarks},\\ \frac{1}{2}-\frac{2}{3}\sin^2\theta_w & d\text{-type quarks}. \end{cases} \tag{3.11}$$

The coefficient functions C_i in Eqs. (3.8)–(3.9) parameterize the hard partonic scattering process. They depend only on the scaling variable x, and on dimensionless ratios of Q^2, μ_f and the renormalization scale μ_r. The perturbative expansion of C_i in the strong coupling α_s up to two loops reads in the non-singlet sector,

$$\begin{aligned} C^+_{i,\mathrm{ns}}(x) &= \delta(1-x)+a_s\left\{c^{(1)}_{i,\mathrm{q}}+L_M P^{(0)}_{\mathrm{qq}}\right\} \\ &\quad +a_s^2\left\{c^{(2),+}_{i,\mathrm{ns}}+L_M\left(P^{(1),+}_{\mathrm{ns}}+c^{(1)}_{i,\mathrm{q}}(P^{(0)}_{\mathrm{qq}}-\beta_0)\right)+L_M^2\left(\frac{1}{2}P^{(0)}_{\mathrm{qq}}(P^{(0)}_{\mathrm{qq}}-\beta_0)\right)\right. \\ &\quad \left.+L_R\,\beta_0 c^{(1)}_{i,\mathrm{q}}+L_RL_M\,\beta_0 P^{(0)}_{\mathrm{qq}}\right\}, \end{aligned} \tag{3.12}$$

$$\begin{aligned} C^-_{3,\mathrm{ns}}(x) &= \delta(1-x)+a_s\left\{c^{(1)}_{3,\mathrm{q}}+L_M P^{(0)}_{\mathrm{qq}}\right\} \\ &\quad +a_s^2\left\{c^{(2),-}_{3,\mathrm{ns}}+L_M\left(P^{(1),-}_{\mathrm{ns}}+c^{(1)}_{3,\mathrm{q}}(P^{(0)}_{\mathrm{qq}}-\beta_0)\right)+L_M^2\left(\frac{1}{2}P^{(0)}_{\mathrm{qq}}(P^{(0)}_{\mathrm{qq}}-\beta_0)\right)\right. \\ &\quad \left.+L_R\,\beta_0 c^{(1)}_{3,\mathrm{q}}+L_RL_M\,\beta_0 P^{(0)}_{\mathrm{qq}}\right\}, \end{aligned} \tag{3.13}$$

where $a_s=\alpha_s(\mu_r)/(4\pi)$ and $i=1,2$ in Eq. (3.12). The complete scale dependence, *i.e.* the towers of logarithms in $L_M=\ln(Q^2/\mu_f^2)$ and $L_R=\ln(\mu_r^2/\mu_f^2)$ (keeping $\mu_r\neq\mu_f$), has been derived by renormalization group methods (see, e.g. [40]) in terms of splitting functions $P^{(l)}_{ij}$ and the coefficients

of the QCD beta function, β_l. In our normalization of the expansion parameter, $a_s = \alpha_s/(4\pi)$, the conventions for the running coupling are

$$\frac{d}{d\ln\mu^2}\frac{\alpha_s}{4\pi} \equiv \frac{da_s}{d\ln\mu^2} = -\beta_0 a_s^2 - \dots, \qquad \underline{0} = \frac{11}{3}C_A - \frac{2}{3}n_f, \tag{3.14}$$

with β_0 the usual expansion coefficient of the QCD beta function, $C_A = 3$ and n_f the number of light flavors.

Note, that the valence coefficient function $C^{\rm v}_{3,\rm ns}$ in Eq. (3.9) is defined as $C^{\rm v}_{3,\rm ns} = C^-_{3,\rm ns} + C^{\rm s}_{3,\rm ns}$. However, we have $C^{\rm s}_{3,\rm ns} \neq 0$ starting at three-loop order only, so that Eq. (3.9) suffices with $C^{\rm v}_{3,\rm ns} = C^-_{3,\rm ns}$ up to NNLO. In the singlet sector we have

$$\begin{aligned} C_{i,\rm q}(x) &= \delta(1-x) + a_s\left\{c^{(1)}_{i,\rm q} + L_M P^{(0)}_{\rm qq}\right\} \qquad (3.15)\\ &+a_s^2\left\{c^{(2)}_{i,\rm q} + L_M\left(P^{(1)}_{\rm qq} + c^{(1)}_{i,\rm q}(P^{(0)}_{\rm qq} - \underline{0}) + c^{(1)}_{i,\rm g}P^{(0)}_{\rm gq}\right) + L_M^2\left(\frac{1}{2}P^{(0)}_{\rm qq}(P^{(0)}_{\rm qq} - \underline{0}) + \frac{1}{2}P^{(0)}_{\rm qg}P^{(0)}_{\rm gq}\right)\right.\\ &\left.+L_R\,\underline{0}c^{(1)}_{i,\rm q} + L_R L_M\,\underline{0}P^{(0)}_{\rm qq}\right\},\\ C_{i,\rm g}(x) &= a_s\left\{c^{(1)}_{i,\rm g} + L_M\,P^{(0)}_{\rm qg}\right\} \qquad (3.16)\\ &+a_s^2\left\{c^{(2)}_{i,\rm g} + L_M\left(P^{(1)}_{\rm qg} + c^{(1)}_{i,\rm q}P^{(0)}_{\rm qg} + c^{(1)}_{i,\rm g}(P^{(0)}_{\rm gg} - \underline{0})\right) + L_M^2\left(\frac{1}{2}P^{(0)}_{\rm qq}P^{(0)}_{\rm qg} + \frac{1}{2}P^{(0)}_{\rm qg}(P^{(0)}_{\rm gg} - \underline{0})\right)\right.\\ &\left.+L_R\,\underline{0}c^{(1)}_{i,\rm g} + L_R L_M\,\underline{0}P^{(0)}_{\rm qg}\right\}, \end{aligned}$$

where again $i = 1, 2$ in Eq. (3.15). The quark-singlet contribution contains the so-called pure-singlet part, $C_{i,\rm q} = C^+_{i,\rm ns} + C_{i,\rm ps}$, *i.e.* $P^{(1)}_{\rm qq} = P^{(1),+}_{\rm ns} + P^{(1)}_{\rm ps}$ and $c^{(2)}_{i,\rm q} = c^{(2),+}_{i,\rm ns} + c^{(2)}_{i,\rm ps}$ in Eq. (3.15). Note, that starting at two-loop order we have $C_{i,\rm ps} \neq 0$. The DIS coefficient functions $c^{(l)}_{i,\rm k}$ are known to NNLO from Refs. [41–44], likewise, NNLO evolution of the PDFs has been determined in Refs. [38, 45] and even the hard corrections at order α_s^3 are available [46, 47]. Accurate parametrizations of all coefficient functions in Eqs. (3.12)–(3.16) can be taken e.g. from Refs. [46, 47] and the splitting functions $P^{(l)}_{ij}$ are given e.g. in Refs. [38, 45] [1]. All products in Eqs. (3.12)–(3.16) are understood as Mellin convolutions. They can be easily evaluated in terms of harmonic polylogarithms $H_{\vec{m}}(x)/(1 \pm x)$ up to weight 4, see [48], and for their numerical evaluation we have used the FORTRAN package [49].

For the charged current case with $W^\pm$-boson exchange the DIS structure functions $F_i^{W^\pm}$ are given by,

$$\begin{aligned} F_i^{W^-}(x,Q^2) &= \frac{1}{2}f_i(x)\int_0^1 dz\int_0^1 dy\,\delta(x-yz)\frac{1}{n_f}\sum_{j=1}^{n_f}\left(v_j^2 + a_j^2\right)\times \qquad (3.17)\\ &\times\left\{\delta q^-_{\rm ns}(y,\mu_f)C^-_{i,\rm ns}(z,Q,\mu_r,\mu_f) + q_{\rm s}(y,\mu_f)C_{i,\rm q}(z,Q,\mu_r,\mu_f) + g(y,\mu_f)C_{i,\rm g}(z,Q,\mu_r,\mu_f)\right\},\\ F_3^{W^-}(x,Q^2) &= \frac{1}{2}\int_0^1 dz\int_0^1 dy\,\delta(x-yz)\frac{1}{n_f}\sum_{i=1}^{n_f} 2\,v_i\,a_i\times \qquad (3.18) \end{aligned}$$

[1] Note, that with the conventions of Refs. [38, 45–47] both the pure-singlet and the gluon coefficient functions as well as the the splitting functions $P^{(0)}_{\rm qg}$ and $P^{(1)}_{\rm qg}$ in Eqs. (3.12)–(3.16) need to be divided by a factor $2n_f$ to account for the contribution of **one** individual quark flavor (not the anti-quark).

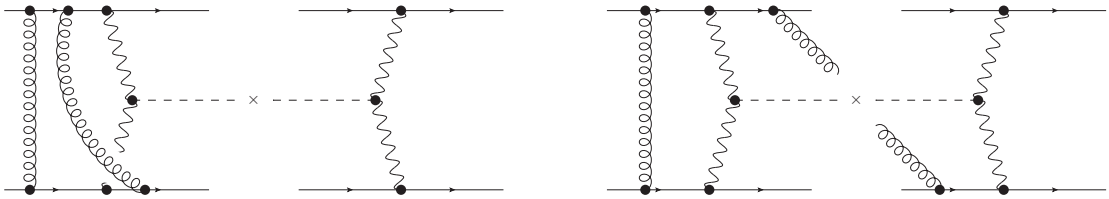

Figure 3.3: Examples of squared matrix elements contributing at NNLO to VBF involving a double gluon exchange between the two quark lines.

$$\times\left\{\delta q_{\rm ns}^{+}(y,\mu_f)\,C_{3,\rm ns}^{+}(z,Q,\mu_r,\mu_f)+q_{\rm ns}^{\rm v}(y,\mu_f)\,C_{3,\rm ns}^{\rm v}(z,Q,\mu_r,\mu_f)\right\},$$

where, as above, $C_{i,\rm q}=C_{i,\rm ns}^{+}+C_{i,\rm ps}$ and, also, $C_{3,\rm ns}^{\rm v}=C_{i,\rm ns}^{-}$ up to two-loop order. The asymmetry $\delta q_{\rm ns}^{\pm}$ parametrizes the iso-triplet component of the proton, *i.e.* $u\neq d$ and so on. It is defined as

$$\delta q_{\rm ns}^{\pm} \;=\; \sum_{i\in u-\rm type}\;\sum_{j\in d-\rm type}\left\{\left(q_i\pm\bar{q}_i\right)-\left(q_j\pm\bar{q}_j\right)\right\}. \tag{3.19}$$

Its numerical impact is expected to be small though. The respective results for $F_i^{W^+}$ are obtained from Eqs. (3.17)–(3.18) with the simple replacement $\delta q_{\rm ns}^{\pm}\to-\delta q_{\rm ns}^{\pm}$.

The vector- and axial-vector coupling constants v_i and a_i are given by

$$v_i=a_i=\frac{1}{\sqrt{2}}. \tag{3.20}$$

The coefficient functions in Eqs. (3.17)–(3.18) including their dependence on the factorization and the renormalization scales can be obtained from Eqs. (3.12)–(3.16) with the help of the following simple substitutions $c_{i,\rm ns}^{(2),+}\leftrightarrow c_{i,\rm ns}^{(2),-}$, $c_{3,\rm ns}^{(2),-}\leftrightarrow c_{3,\rm ns}^{(2),+}$ and $P_{\rm ns}^{(1),+}\leftrightarrow P_{\rm ns}^{(1),-}$ and so on. Again, all expressions for the coefficient and splitting functions are given in Refs. [46,47] and [38,45], respectively.

Eq. (3.2) with the explicit expressions for the DIS structure functions inserted provides the backbone of our NNLO QCD predictions for Higgs production in VBF. However, as emphasized above, the underlying factorization is not exact beyond NLO and therefore, the non-factorizable corrections need to be estimated. This will be done in the following.

3.2 Non-factorizable contributions

In order to assess the quality of the factorization approach, we now estimate the size of the non-factorizable contributions, *i.e.* those coming from diagrams involving the exchange of gluons between the two quark lines and not included in the structure function approach. Neglecting interferences between t- and u-channel diagrams, which are kinematically suppressed, this class of diagrams vanishes at NLO because of color conservation, but contributes at NNLO for the first time. Here, the notion "class of diagrams" refers to a gauge invariant subset of the diagrams that contributes to a certain process. Examples of non-factorizable diagrams are shown in Fig. 3.3. Before we present a detailed numerical estimate of the size of the non-factorizable contributions, we briefly recall two general arguments from Refs. [20, 21] justifying their omission.

The first argument is based on the study of the associated color factors. The possible color configurations for factorizable and non-factorizable corrections are shown in Figs. 3.4 and 3.5, respectively, together with the associated color factors. The leading color factor of the factorizable

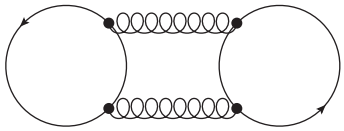

Figure 3.4: Color configurations associated to non-factorizable double-gluon exchange corrections to VBF at NNLO.

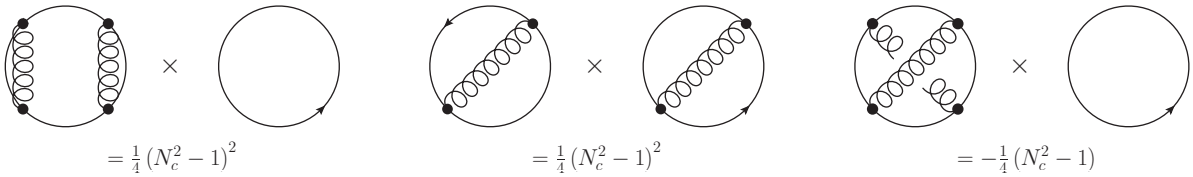

Figure 3.5: Color configurations associated to factorizable corrections to VBF at NNLO.

corrections is $(N_c^2-1)^2/4 = 16$, while we have $(N_c^2-1)/4 = 2$ (for $N_c = 3$) for the double gluon exchange consisting of a double color-traces. Hence the non-factorizable corrections are suppressed by a factor $O(1/N_c^2)$ with respect to the leading factorizable ones.

The second argument is based on the kinematical dependence of diagrams like those shown in Fig. 3.3. Such contributions, see e.g., Fig. 3.3 (right), come from the interference of diagrams with one or two gluons radiated by the upper quark line with diagrams where gluons are radiated by the lower line. Angular ordering in gluon emission, however, leads to radiation close to the quark from which it is emitted, and since these quarks tend to be very forward (or backward) due to the exchange of a spin-1 particle in the *t*-channel, there is generally very little overlap in phase space. Those arguments have already been used in [50] to justify neglecting real-virtual double gluon exchange diagrams in the computation of NLO QCD corrections for Higgs in VBF in association with three jets.

We now corroborate these considerations with a quantitative analysis. Let us express the total cross section at order α_s^2 as

$$\sigma_{NNLO} = \sigma_0 \left(1 + \alpha_s \Delta_1 + \alpha_s^2 \Delta_2\right), \tag{3.21}$$

with $\Delta_2 = \Delta_2^{fact} + \Delta_2^{non-fact}$. As already said, Δ_1 receives contributions mainly from factorizable corrections. The non-factorizable ones that are not kinematically suppressed are exactly zero due to color while interference effects between amplitudes with identical quark lines in the final state are highly suppressed (and not included beyond LO in our approach).

The exact calculation of $\Delta_2^{non-fact}$ being out of reach, we estimate the ratio of the non-factorizable contributions, $\Delta_2^{non-fact}$, vs. the factorizable ones, Δ_2^{fact}, as follows

$$R_2 \equiv \frac{\Delta_2^{non-fact}}{\Delta_2^{fact}} \simeq \frac{1}{N_c^2-1} R_1 \equiv \frac{1}{N_c^2-1} \frac{\Delta_1^{non-fact,U(1)}}{\Delta_1^{fact,U(1)}}, \tag{3.22}$$

where $\Delta_1^{fact,U(1)} = \Delta_1^{fact}/C_F$ and $\Delta_1^{non-fact,U(1)}$ denotes the "would-be" impact of the corrections coming from non-factorizable diagrams at NLO, *i.e.*, the class of diagrams involving the exchange

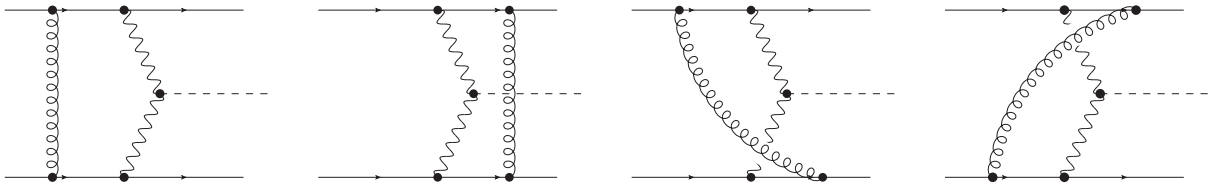

Figure 3.6: The four virtual topologies with one gluon exchange between the quark lines that would contribute at NLO, barring the vanishing color factor. Those diagrams represent the virtual part included in $\Delta_{NLO}^{non-fact}$.

of one gluon between the two quark lines, computed as if the color factor were non-vanishing. In other words, $\Delta_1^{non-fact,U(1)}$ can be thought of as the correction due to the gauge invariant class of diagrams where an extra $U(1)$ gauge boson is exchanged between the two quark lines including real and virtual diagrams. The $R_2 \simeq R_1$ approximation assumes, of course, that the ratios will not dramatically change in going from NLO to NNLO. As there is no substantial difference in the kinematics and no non-Abelian vertices enter at NNLO in diagrams where two gluons are exchanged in a color singlet in the t-channel, we can conclude that Eq. (3.22) should provide a reasonable estimate.

To compute $\Delta_1^{non-fact}$ we need to account for the four diagrams shown in Fig. 3.6 along with the analogous real emission terms. As our argument only needs to provide an estimate of the corrections and it is based on the kinematics we can slightly simplify the calculation of the tensor integrals by considering only vector couplings of the vector boson to the quarks, which eliminates all but the scalar five-point functions. The latter can be reduced in terms of scalar four-point functions [51–53] and then evaluated, together with the scalar four- and three-point functions coming from the Passarino-Veltmann reduction, with the help of the QcdLoop package [54]. For completeness, we stress that the results for the virtual diagrams have been checked against the amplitude automatically generated by MadLoop [55], where machine precision agreement has been found point by point in the phase space.

The combination of the virtual and the real emission part, with the subtraction of the soft divergences (no collinear divergences occur in this class of diagrams), has been done via MadFKS [56] that generates all the needed counterterms automatically and performs also the integration over phase space. In practice, the computation of the $O(\alpha_s)$ part of the cross section that enters in $\Delta_1^{non-fact}$, has been obtained as the difference of the complete NLO and the corresponding Born cross sections, and special attention has been paid to controlling the uncertainty of the numerical integration of the real emission contributions.

In Tabs. 3.1–3.3 we present the results for the non-factorizable corrections, $\Delta_1^{non-fact}$, at the Tevatron and at the LHC, compared with the quark-initiated factorizable ones, Δ_1^{fact}, and we have used the same color factor of the Born term. For the sake of simplicity, we have focused on the $ud \to udH$ channel, with Z-boson exchange and, as mentioned above, we have considered only the vector coupling of the Z-boson to the quarks. Interestingly, the numbers in Tabs. 3.1–3.3 display a sudden change of sign for $\Delta_1^{non-fact}$ at around $m_H = 180\,\text{GeV} = 2\,M_Z$, *i.e.*, the threshold of the $h \to ZZ$ process, which is due to the use of the zero-width approximation for the Z-bosons in the loop propagators, cf. also Refs. [58, 59]. A consistent inclusion of Z-boson width effects, which is beyond the scope of our analysis, would regularize this behavior.

The results of Tabs. 3.1–3.3 show an R_1 always well below unity. Once the $O(1/N_c^2)$ color

m_H [GeV]	σ_0 [pb]	$\Delta_1^{non-fact,U(1)}$	$\Delta_1^{fact,U(1)}$	R_1
100	$3.06 \cdot 10^{-5}$	$3.00(4) \cdot 10^{-2}$	$8.79 \cdot 10^{-2}$	0.34
120	$2.09 \cdot 10^{-5}$	$2.90(5) \cdot 10^{-2}$	$9.22 \cdot 10^{-2}$	0.31
150	$1.19 \cdot 10^{-5}$	$2.21(5) \cdot 10^{-2}$	$9.91 \cdot 10^{-2}$	0.22
200	$4.87 \cdot 10^{-6}$	$-3.2(5) \cdot 10^{-3}$	$1.12 \cdot 10^{-1}$	−0.03
250	$2.04 \cdot 10^{-6}$	$8(4) \cdot 10^{-4}$	$1.25 \cdot 10^{-1}$	0.01
300	$8.68 \cdot 10^{-7}$	$2.7(4) \cdot 10^{-3}$	$1.39 \cdot 10^{-1}$	0.02

Table 3.1: Non-diagonal NLO QCD corrections to VBF at the Tevatron, $\sqrt{S} = 1.96\,\text{TeV}$. Numbers have been computed ignoring the vanishing color factors of the diagrams in Fig. 3.6. The MRST2002 [57] NLO PDF set has been used. Renormalization and factorization scales have been set to M_W. Integration errors, if relevant, are shown in parenthesis.

m_H [GeV]	σ_0 [pb]	$\Delta_1^{non-fact,U(1)}$	$\Delta_1^{fact,U(1)}$	R_1
100	$2.04 \cdot 10^{-3}$	$6.6(3) \cdot 10^{-3}$	$1.57 \cdot 10^{-2}$	0.42
120	$1.74 \cdot 10^{-3}$	$5.4(4) \cdot 10^{-3}$	$1.54 \cdot 10^{-2}$	0.35
150	$1.39 \cdot 10^{-3}$	$3.4(2) \cdot 10^{-3}$	$1.53 \cdot 10^{-2}$	0.22
200	$9.84 \cdot 10^{-4}$	$-3.6(3) \cdot 10^{-3}$	$1.59 \cdot 10^{-2}$	−0.22
250	$7.12 \cdot 10^{-4}$	$-1.2(2) \cdot 10^{-3}$	$1.71 \cdot 10^{-2}$	−0.07
300	$5.26 \cdot 10^{-4}$	$-4(2) \cdot 10^{-4}$	$1.85 \cdot 10^{-2}$	−0.02
400	$3.00 \cdot 10^{-4}$	$2(2) \cdot 10^{-4}$	$2.24 \cdot 10^{-2}$	0.01
500	$1.78 \cdot 10^{-4}$	$1(2) \cdot 10^{-4}$	$2.69 \cdot 10^{-2}$	0.00
650	$8.66 \cdot 10^{-5}$	$5(2) \cdot 10^{-4}$	$3.45 \cdot 10^{-2}$	0.01
800	$4.41 \cdot 10^{-5}$	$2(2) \cdot 10^{-4}$	$4.28 \cdot 10^{-2}$	0.00
1000	$1.88 \cdot 10^{-5}$	$5(2) \cdot 10^{-4}$	$5.46 \cdot 10^{-2}$	0.01

Table 3.2: Non-diagonal NLO QCD corrections to VBF at the LHC, $\sqrt{S} = 7\,\text{TeV}$. Numbers have been computed ignoring the vanishing color factors of the diagrams in Fig. 3.6. The MRST2002 [57] NLO PDF set has been used. Renormalization and factorization scales have been set to M_W. Integration errors, if relevant, are shown in parenthesis.

suppression in Eq. (3.22) is taken into account, one finds an upper bound on $R_2 < 10\%$. As the impact of Δ_2^{fact} on the total cross-section is at the 1% level, we estimate the contribution of the omitted non-factorizable corrections at most at the per-mil level, hence negligible in our scheme. Finally, note that $\Delta_1^{non-fact}$ decreases with increasing Higgs boson masses m_H, so that, as expected from the fact that the Higgs boson acts as a "kinematical de-correlator" between the two jets, the size of the non-factorizable corrections becomes totally negligible for $m_H > 300$ GeV.

3.3 Contributions from heavy-quark loops

Diagrams with heavy-quark loops can also provide contributions at NNLO in QCD that are not included in the structure function approach. Following our definition of VBF given in Sec. 2 these contributions are classified in the strict sense as "non-VBF" processes. However, given that such effects are genuinely new at NNLO and, moreover, that they have not been subject to extensive consideration in the context of VBF in the literature before, cf. the previous discussions

m_H [GeV]	σ_0 [pb]	$\Delta_1^{non-fact,U(1)}$	$\Delta_1^{fact,U(1)}$	R_1
100	$5.63\cdot10^{-3}$	$4.0(4)\cdot10^{-3}$	$6.34\cdot10^{-3}$	0.63
120	$4.97\cdot10^{-3}$	$3.1(3)\cdot10^{-3}$	$5.76\cdot10^{-3}$	0.54
140	$4.42\cdot10^{-3}$	$2.8(3)\cdot10^{-3}$	$4.94\cdot10^{-3}$	0.56
150	$4.17\cdot10^{-3}$	$2.4(3)\cdot10^{-3}$	$4.62\cdot10^{-3}$	0.51
155	$4.06\cdot10^{-3}$	$1.7(3)\cdot10^{-3}$	$4.51\cdot10^{-3}$	0.37
160	$3.95\cdot10^{-3}$	$1.5(3)\cdot10^{-3}$	$4.39\cdot10^{-3}$	0.33
165	$3.84\cdot10^{-3}$	$8(2)\cdot10^{-4}$	$4.28\cdot10^{-3}$	0.18
170	$3.74\cdot10^{-3}$	$10(3)\cdot10^{-5}$	$4.20\cdot10^{-3}$	0.02
175	$3.64\cdot10^{-3}$	$-8(3)\cdot10^{-4}$	$4.08\cdot10^{-3}$	−0.21
180	$3.54\cdot10^{-3}$	$-1.3(2)\cdot10^{-3}$	$3.87\cdot10^{-3}$	−0.35
185	$3.45\cdot10^{-3}$	$-3.4(4)\cdot10^{-3}$	$3.86\cdot10^{-3}$	−0.89
190	$3.36\cdot10^{-3}$	$-2.8(3)\cdot10^{-3}$	$3.82\cdot10^{-3}$	−0.73
195	$3.27\cdot10^{-3}$	$-2.5(3)\cdot10^{-3}$	$3.74\cdot10^{-3}$	−0.67
200	$3.19\cdot10^{-3}$	$-2.6(2)\cdot10^{-3}$	$3.74\cdot10^{-3}$	−0.71
210	$3.03\cdot10^{-3}$	$-1.6(3)\cdot10^{-3}$	$3.62\cdot10^{-3}$	−0.43
230	$2.75\cdot10^{-3}$	$-7(5)\cdot10^{-4}$	$3.40\cdot10^{-3}$	−0.21
250	$2.50\cdot10^{-3}$	$-9(2)\cdot10^{-4}$	$3.32\cdot10^{-3}$	−0.26
300	$1.99\cdot10^{-3}$	$-5(2)\cdot10^{-4}$	$3.21\cdot10^{-3}$	−0.14
400	$1.32\cdot10^{-3}$	$2(2)\cdot10^{-4}$	$3.98\cdot10^{-3}$	0.05
500	$9.17\cdot10^{-4}$	$3(2)\cdot10^{-4}$	$5.32\cdot10^{-3}$	0.06
650	$5.59\cdot10^{-4}$	$6(2)\cdot10^{-4}$	$7.98\cdot10^{-3}$	0.07
800	$3.57\cdot10^{-4}$	$2(2)\cdot10^{-4}$	$1.11\cdot10^{-2}$	0.01
1000	$2.06\cdot10^{-4}$	$3(1)\cdot10^{-4}$	$1.63\cdot10^{-2}$	0.02

Table 3.3: Non-diagonal NLO QCD corrections to VBF at the LHC, $\sqrt{S} = 14\,\text{TeV}$. Numbers have been computed ignoring the vanishing color factors of the diagrams in Fig. 3.6. The MRST2002 [57] NLO PDF set has been used. Renormalization and factorization scales have been set to M_W. Integration errors, if relevant, are shown in parenthesis.

in Refs. [21, 60], they deserve detailed study here.

We distinguish three different classes of contributions: the modulo squared of one-loop diagrams with no extra radiation requiring a quark-gluon initial state, Fig. 3.7; the interference of one-loop diagrams with an extra parton in the final state, Fig. 3.8, with the VBF real tree-level diagrams; and the interference of two-loop diagrams, Fig. 3.9, with VBF diagrams at the Born level. Each of the three classes of loop diagrams has no soft/collinear divergencies and is gauge invariant, thus can be treated independently.

Such contributions appear only for neutral weak currents. Moreover, in both boxes and triangles only the axial coupling of the Z-boson to the quarks survives, so that a mass-degenerate quark doublet gives zero contribution. Therefore only the top and bottom quarks need to be considered.

3.3.1 Quark-gluon initiated contributions via the square of one-loop diagrams

Let us start with the diagrams shown in Fig. 3.7. A simple estimate [20] obtained in the limit $m_b \to 0$, $m_t \to \infty$, where only the contribution from the triangle is parametrically relevant, associates to

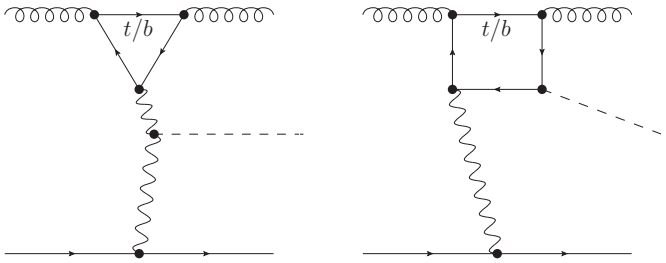

Figure 3.7: Next-to-next-to-leading order QCD corrections due to heavy-quarks (t/b) loops: pure one-loop diagrams contributing through their modulo squared.

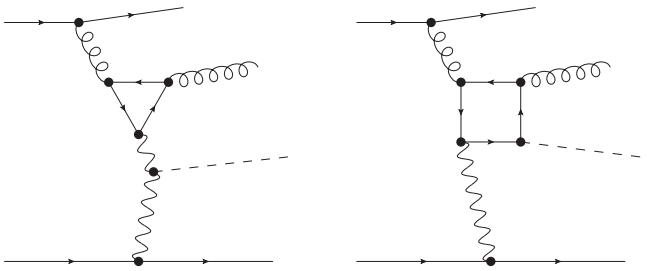

Figure 3.8: Next-to-next-to-leading order QCD corrections due to heavy-quarks (t/b) loops: one-loop plus extra parton diagrams interfering with VBF NLO real corrections.

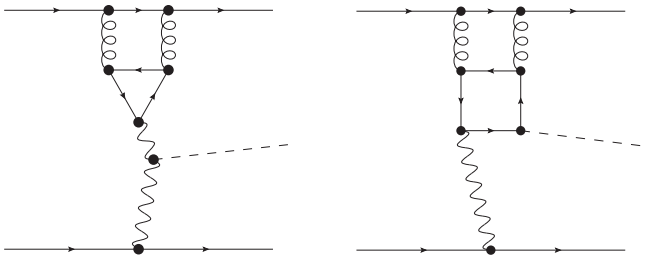

Figure 3.9: Next-to-next-to-leading order QCD corrections due to heavy-quarks (t/b) loops two-loop diagrams interfering with VBF LO diagrams.

this class an effect of less than one per-mil of the total cross section [21, 60]. By itself this result is non-trivial given that the contributions of the diagrams in Fig. 3.7 are proportional to the quark-gluon parton luminosity, which is potentially large, especially at LHC. Thus, based on considering the triangle alone, it can be argued that contributions from the heavy-quark loops in Fig. 3.7 can be safely neglected.

We now investigate to which extent the conclusion above is confirmed by a complete calculation of these contributions. Note that the corresponding one-loop diagrams are long known [61, 62] (see also [7]), although in a different kinematic regime (*i.e.*, time-like) for the Z-boson. Our results confirm previous findings and extend them for the first time to the t-channel regime. The contribution of these diagrams to Higgs boson production in VBF are shown in Fig. 3.10, where the sum of the triangle and the box, the triangle and the box alone and the limit $m_t \to \infty$ at $\sqrt{S} = 7\,\text{TeV}$ and $14\,\text{TeV}$ for the LHC and $\sqrt{S} = 1.96\,\text{TeV}$ for the Tevatron have been plotted. The pole mass values $m_b = 4.62\,\text{GeV}$, $m_t = 174.3\,\text{GeV}$ have been used. The numbers for the LHC corresponding to the various scenarios in Fig. 3.10 are reported in Tabs. 3.4–3.5. From these numbers we can see that the limit $m_t \to \infty$, $m_b \to 0$ is a good estimate of the upper bound of the integrated cross section.

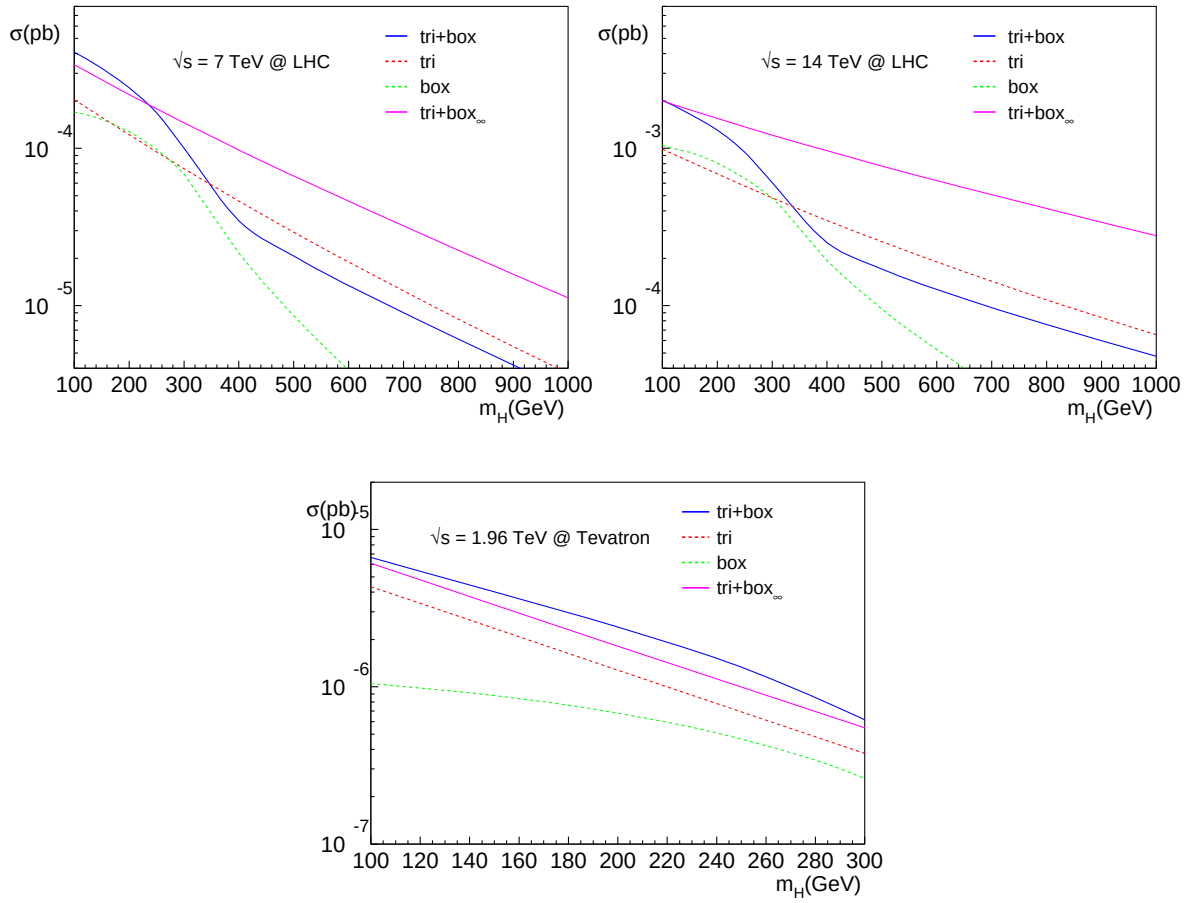

Figure 3.10: Contribution of the heavy-quarks (t/b) loops to the total NNLO VBF cross section, at the LHC with $\sqrt{S} = 7\,\text{TeV}$ (top-left), $\sqrt{S} = 14\,\text{TeV}$ (top-right) and at the Tevatron, $\sqrt{S} = 1.96\,\text{TeV}$. Numbers are computed with the MSTW 2008 [63] NNLO PDF set. The renormalization and factorization scales have been set to M_W.

In this case we verified that, as reported also in [61], the contribution of the box goes to zero. Moreover, specially for large m_H, the triangle alone is also an upper bound, while for small m_H it approximates the total cross-section within a factor of 2. Therefore, given our aim to asses the importance of these contributions relative to the VBF cross section, it gives a reasonable estimate of the exact value.

Our results have been obtained by two independent computations of the squared amplitude, and also agree point-by-point in phase space with the results of a code automatically generated by MadLoop [55]. The upshot is that the exact computation corroborates the findings of [20]. The impact of the diagrams in Fig. 3.7 on the VBF Higgs production cross section is always below the per-mil level of the Born contribution, and therefore can be safely neglected.

The exact result for the VBF cross section in the quark-gluon channel at NNLO allows for a comparison with the Higgs-Strahlung case. In this case a sizable destructive interference between the triangle and the box diagrams takes place [7, 62], while this does not happen for VBF (see also the plots in Fig. 3.10). It is instructive to find the origin of such a different behavior of the triangle and the box diagrams contributions in an s-channel process [62] compared to a t-channel one (cf. Fig. 3.10). To this aim it is useful to define the relative phase angle ϕ between the triangle and the

m_H [GeV]	$\sigma_{\rm LO}$	$\sigma_{\rm tri+box}$	$\sigma_{\rm tri}$	$\sigma_{\rm box}$	$\sigma^{\infty}_{\rm tri+box}$
100	1.49	$4.09\cdot10^{-4}$	$2.04\cdot10^{-4}$	$1.70\cdot10^{-4}$	$3.40\cdot10^{-4}$
120	1.22	$3.75\cdot10^{-4}$	$1.84\cdot10^{-4}$	$1.65\cdot10^{-4}$	$3.12\cdot10^{-4}$
150	$9.19\cdot10^{-1}$	$3.23\cdot10^{-4}$	$1.58\cdot10^{-4}$	$1.53\cdot10^{-4}$	$2.73\cdot10^{-4}$
200	$6.01\cdot10^{-1}$	$2.43\cdot10^{-4}$	$1.22\cdot10^{-4}$	$1.27\cdot10^{-4}$	$2.20\cdot10^{-4}$
250	$4.09\cdot10^{-1}$	$1.69\cdot10^{-4}$	$9.49\cdot10^{-5}$	$9.87\cdot10^{-5}$	$1.78\cdot10^{-4}$
300	$2.87\cdot10^{-1}$	$1.00\cdot10^{-4}$	$7.42\cdot10^{-5}$	$6.85\cdot10^{-5}$	$1.45\cdot10^{-4}$
400	$1.52\cdot10^{-1}$	$3.47\cdot10^{-5}$	$4.62\cdot10^{-5}$	$2.16\cdot10^{-5}$	$9.76\cdot10^{-5}$
500	$8.58\cdot10^{-2}$	$2.07\cdot10^{-5}$	$2.93\cdot10^{-5}$	$8.64\cdot10^{-6}$	$6.67\cdot10^{-5}$
650	$3.95\cdot10^{-2}$	$1.10\cdot10^{-5}$	$1.53\cdot10^{-5}$	$2.75\cdot10^{-6}$	$3.85\cdot10^{-5}$
800	$1.93\cdot10^{-2}$	$6.12\cdot10^{-6}$	$8.20\cdot10^{-6}$	$1.00\cdot10^{-6}$	$2.25\cdot10^{-5}$
1000	$8.00\cdot10^{-3}$	$2.89\cdot10^{-6}$	$3.71\cdot10^{-6}$	$2.97\cdot10^{-7}$	$1.12\cdot10^{-5}$

Table 3.4: Values of the contributions to the total NNLO VBF cross-section due to the heavy-quark loop diagrams shown in Fig. 3.7 at the LHC, $\sqrt{S} = 7\,\text{TeV}$. The MSTW2008 [63] NNLO PDF set has been used. The LO cross-section, computed with LO PDFs, is also shown for comparison. Renormalization and factorization scales have been set to M_W. Integration errors are below the 1% level. Cross-sections are in pb.

m_H [GeV]	$\sigma_{\rm LO}$	$\sigma_{\rm tri+box}$	$\sigma_{\rm tri}$	$\sigma_{\rm box}$	$\sigma^{\infty}_{\rm tri+box}$
100	5.08	$2.02\cdot10^{-3}$	$9.86\cdot10^{-4}$	$1.05\cdot10^{-3}$	$2.01\cdot10^{-3}$
120	4.29	$1.88\cdot10^{-3}$	$9.18\cdot10^{-4}$	$9.99\cdot10^{-4}$	$1.90\cdot10^{-3}$
150	3.40	$1.65\cdot10^{-3}$	$8.24\cdot10^{-4}$	$9.44\cdot10^{-4}$	$1.76\cdot10^{-3}$
200	2.40	$1.31\cdot10^{-3}$	$6.88\cdot10^{-4}$	$8.06\cdot10^{-4}$	$1.55\cdot10^{-3}$
250	1.76	$9.44\cdot10^{-4}$	$5.76\cdot10^{-4}$	$6.46\cdot10^{-4}$	$1.37\cdot10^{-3}$
300	1.33	$6.05\cdot10^{-4}$	$4.85\cdot10^{-4}$	$4.82\cdot10^{-4}$	$1.21\cdot10^{-3}$
400	$8.09\cdot10^{-1}$	$2.52\cdot10^{-4}$	$3.48\cdot10^{-4}$	$1.94\cdot10^{-4}$	$9.66\cdot10^{-4}$
500	$5.25\cdot10^{-1}$	$1.71\cdot10^{-4}$	$2.55\cdot10^{-4}$	$9.52\cdot10^{-5}$	$7.72\cdot10^{-4}$
650	$2.97\cdot10^{-1}$	$1.11\cdot10^{-4}$	$1.64\cdot10^{-4}$	$4.02\cdot10^{-5}$	$5.62\cdot10^{-4}$
800	$1.80\cdot10^{-1}$	$7.59\cdot10^{-5}$	$1.09\cdot10^{-4}$	$1.93\cdot10^{-5}$	$4.14\cdot10^{-4}$
1000	$9.82\cdot10^{-2}$	$4.76\cdot10^{-5}$	$6.53\cdot10^{-5}$	$8.05\cdot10^{-6}$	$2.79\cdot10^{-4}$

Table 3.5: Values of the contributions to the total NNLO VBF cross-section due to the heavy-quark loop diagrams shown in Fig. 3.7 at the LHC, $\sqrt{S} = 14\,\text{TeV}$. The MSTW2008 [63] NNLO PDF set has been used. The LO cross-section, computed with LO PDFs, is also shown for comparison. Renormalization and factorization scales have been set to M_W. Integration errors are below the 1% level. Cross-sections are in pb.

box amplitudes $\mathcal{M}_{\rm tri}$ and $\mathcal{M}_{\rm box}$ by

$$|\mathcal{M}_{\rm tri} + \mathcal{M}_{\rm box}|^2 = |\mathcal{M}_{\rm tri}|^2 + |\mathcal{M}_{\rm box}|^2 + 2|\mathcal{M}_{\rm tri}||\mathcal{M}_{\rm box}|\cos\phi\,. \tag{3.23}$$

Recall that in the s-channel case in the large-m_t limit $\mathcal{M}_{\rm tri}$ and $\mathcal{M}_{\rm box}$ are real and opposite in sign thus implying $\phi \sim \pi$ [62]. This remains true for the crossed amplitudes in the t-channel case of Fig. 3.10 because, due to unitarity, the asymptotic behavior in the large-m_t limit remains the same. However, for finite top-quark masses and away from large-m_t limit, both $\mathcal{M}_{\rm tri}$ and $\mathcal{M}_{\rm box}$ acquire an imaginary part above the threshold $\sqrt{S} \simeq 2m_t$ in the s-channel process. This is due

to the gluon-gluon scattering process opening to real top-quark pair-production. Thus, $\mathcal{M}_{\rm tri}$ and $\mathcal{M}_{\rm box}$ become complex numbers pointing in opposite directions in the complex plane within a tolerance of less than 50° resulting in a strong destructive interference between them, see [62]. The different findings in the VBF case can now be easily understood: in the t-channel process of Fig. 3.7 only $\mathcal{M}_{\rm box}$ can develop an imaginary part due to an intermediate real top-quark pair while $\mathcal{M}_{\rm tri}$ remains real. As a net result $\mathcal{M}_{\rm tri}$ and $\mathcal{M}_{\rm box}$ are likely to be almost orthogonal in the complex plane thus suppressing the interference term in Eq. (3.23).

Finally, compared to the Higgs-Strahlung process, *i.e.*, the associated production of Higgs and a Z-boson in the gluon-fusion channel, the NNLO corrections in VBF from the heavy quarks are by far less important [7]. This difference has also a simple physical explanation, because in the Higgs-Strahlung this contribution proceeds through a gg initiated s-channel, whereas VBF has the vector boson in the t-channel. The s-channel propagator enhances the small x-region where the gluon luminosity steeply rises. In the crossed case, *i.e.*, in VBF, the dominant contribution to the cross section comes from effective parton momentum fractions $\langle x\rangle \sim 10^{-2}$, where the gluon luminosity is not large yet.

3.3.2 One-loop plus extra real parton diagrams

Let us now discuss the contributions coming from diagrams in Fig. 3.8 in the qq-channel and the crossed qg one. These diagrams feature one initial (final) state on-shell gluon attached to the heavy-quark loop, together with the Z-boson and a time-like (space-like) off-shell gluon. We estimate the overall contribution of this class of diagrams by computing only the triangles, yet keeping the m_t and m_b finite. This choice is justified by the fact that triangles are parametrically leading, especially for large values of m_H and, as shown in Sec. 3.3.1, provide an approximate estimate for the total contribution, although sufficiently accurate for our purposes. We also verified that the limit $m_t \to \infty$, which we expect to be close to the upper bound for the cross-section, is indeed quite close ($\simeq 20\%$) to the values we have computed. Note that triangle diagrams as in Fig. 3.8 have already been computed before in the context of Z-boson decay into hadrons [64] or hadro-production [65] in a different kinematic regime. As an additional simplification, we will consider only the parton channel with an extra gluon in the final state, *i.e.*, the reaction $qq' \to qq'Hg$, the other parton channels having similar or smaller impact. This latter assumption is supported by the previous studies of Z-boson hadro-production [65], where it was shown that the entire class of diagrams in Fig. 3.8 is heavily suppressed with respect to the two-loop ones of Fig. 3.9 considered below in Sec. 3.3.3.

We have computed the necessary expressions for the interference of the one-loop diagrams with the tree-level ones analytically using MATHEMATICA and FEYNCALC [66] and have performed the phase-space integration using MADGRAPH [67,68]. The respective numbers for the contribution to the VBF total cross-section of the process $qq' \to Hqq'g$ due to the heavy-quark triangle in Fig. 3.8 at the LHC, at $\sqrt{S} = 7\,\text{TeV}$ and $14\,\text{TeV}$ are given in Tab. 3.6. Again, we found these contributions to be totally negligible compared to the LO VBF cross-section, and also about one order of magnitude smaller than the ones studied in Sec. 3.3.1.

3.3.3 Two-loop diagrams

Finally, we consider the two-loop contributions of Fig. 3.9 where the heavy-quark loop is attached via two gluons to the light-quark line originating from one of the protons. These diagrams interfere with the Born VBF amplitudes. The effective coupling to the light-quark line singles out the iso-

m_H [GeV]	σ_{LO}	$\sigma_{\rm tri}^{\rm 1loop+glu}$
100	1.49	$5.10 \cdot 10^{-5}$
120	1.22	$4.02 \cdot 10^{-5}$
150	$9.19 \cdot 10^{-1}$	$2.89 \cdot 10^{-5}$
200	$6.01 \cdot 10^{-1}$	$1.74 \cdot 10^{-5}$
250	$4.09 \cdot 10^{-1}$	$1.11 \cdot 10^{-5}$
300	$2.87 \cdot 10^{-1}$	$7.41 \cdot 10^{-6}$
400	$1.52 \cdot 10^{-1}$	$3.53 \cdot 10^{-6}$
500	$8.58 \cdot 10^{-2}$	$1.84 \cdot 10^{-6}$
650	$3.95 \cdot 10^{-2}$	$7.72 \cdot 10^{-7}$
800	$1.93 \cdot 10^{-2}$	$3.52 \cdot 10^{-7}$
1000	$8.00 \cdot 10^{-3}$	$1.34 \cdot 10^{-7}$

m_H [GeV]	σ_{LO}	$\sigma_{\rm tri}^{\rm 1loop+glu}$
100	5.08	$2.66 \cdot 10^{-4}$
120	4.29	$2.20 \cdot 10^{-4}$
150	3.40	$1.67 \cdot 10^{-4}$
200	2.40	$1.11 \cdot 10^{-4}$
250	1.76	$7.62 \cdot 10^{-5}$
300	1.33	$5.48 \cdot 10^{-5}$
400	$8.09 \cdot 10^{-1}$	$3.02 \cdot 10^{-5}$
500	$5.25 \cdot 10^{-1}$	$1.82 \cdot 10^{-5}$
650	$2.97 \cdot 10^{-1}$	$9.21 \cdot 10^{-6}$
800	$1.80 \cdot 10^{-1}$	$5.12 \cdot 10^{-6}$
1000	$9.82 \cdot 10^{-2}$	$2.54 \cdot 10^{-6}$

Table 3.6: Values of the contributions to the total NNLO VBF cross-section due to the heavy-quark triangle plus gluon emission diagrams shown in Fig. 3.8 at the LHC, at $\sqrt{S} = 7\,\text{TeV}$ (left) and $\sqrt{S} = 14\,\text{TeV}$ (right). The MSTW2008 [63] NNLO PDF set has been used. The LO cross-section, computed with LO PDFs, is also shown for comparison. Renormalization and factorization scales have been set to M_W. Integration errors are below the 1% level. Cross-sections are in pb.

triplet component of the proton in the squared matrix elements, since only the axial part of the Z-boson coupling contributes for non-degenerate heavy-quarks in the loop. That is to say, this class of diagrams is proportional to the (non-singlet) distribution $\delta q_{\rm ns}^-$ of Eq. (3.19), which is generally small.

In analogy to the previous Sec. 3.3.2, we aim at an estimate of the size of the contributions of Fig. 3.9 rather than the exact result. To that end, we will restrict ourselves to the two-loop triangle diagrams. This choice is, of course, also driven by the fact that the two-loop double box in Fig. 3.9 is currently unknown for the required VBF kinematical configuration and its computation would be a tremendous task in itself.

The two-loop triangles for the $q\bar{q}Z$ vertex have been computed in [64] for the case $m_b = 0$ and $m_t \neq 0$, see also [65]. Rather compact results in terms of harmonic polylogarithms [48] (see [49] for numerical routines) for all kinematic configurations have been obtained in [69] and we use the latter expressions to compute the numbers shown in Tab. 3.7 for the LHC at $\sqrt{S} = 7\,\text{TeV}$ and $14\,\text{TeV}$. Again, a comparison of the cross section numbers in Tab. 3.7 for the reaction $qq' \to Hqq'$ at NNLO in QCD mediated by the two-loop triangle with the LO cross-section shows that such contributions are below the per-mil level.

In ending this discussion of heavy-quark loop contributions we briefly remark that, of course, the diagrams shown in Figs. 3.7–3.9, also contribute in heavy-quark DIS, if the full neutral-current reactions are considered, *i.e.*, both γ and Z-boson exchange at high Q^2. Currently available DIS data on heavy-quark production, however, is usually taken at Q^2 values where these contributions are not relevant. Their existence is an issue, though, to be recalled in the definition of variable-flavor number schemes, see e.g., [70].

3.4 One-loop electroweak corrections

We briefly discuss the electroweak corrections at one-loop. The combined strong and electroweak NLO corrections to Higgs production in VBF have been computed in [18, 19] and can be obtained

m_H [GeV]	σ_{LO}	$\sigma_{\rm tri}^{\rm 2loop}$
100	1.49	$8.38 \cdot 10^{-4}$
120	1.22	$7.08 \cdot 10^{-4}$
150	$9.19 \cdot 10^{-1}$	$5.60 \cdot 10^{-4}$
200	$6.01 \cdot 10^{-1}$	$3.90 \cdot 10^{-4}$
250	$4.09 \cdot 10^{-1}$	$2.81 \cdot 10^{-4}$
300	$2.87 \cdot 10^{-1}$	$2.06 \cdot 10^{-4}$
400	$1.52 \cdot 10^{-1}$	$1.18 \cdot 10^{-4}$
500	$8.58 \cdot 10^{-2}$	$7.08 \cdot 10^{-5}$
650	$3.95 \cdot 10^{-2}$	$3.52 \cdot 10^{-5}$
800	$1.93 \cdot 10^{-2}$	$1.84 \cdot 10^{-5}$
1000	$8.00 \cdot 10^{-3}$	$8.18 \cdot 10^{-6}$

m_H [GeV]	σ_{LO}	$\sigma_{\rm tri}^{\rm 2loop}$
100	5.08	$2.30 \cdot 10^{-3}$
120	4.29	$2.01 \cdot 10^{-3}$
150	3.40	$1.67 \cdot 10^{-3}$
200	2.40	$1.25 \cdot 10^{-3}$
250	1.76	$9.63 \cdot 10^{-4}$
300	1.33	$7.60 \cdot 10^{-4}$
400	$8.09 \cdot 10^{-1}$	$4.99 \cdot 10^{-4}$
500	$5.25 \cdot 10^{-1}$	$3.44 \cdot 10^{-4}$
650	$2.97 \cdot 10^{-1}$	$2.10 \cdot 10^{-4}$
800	$1.80 \cdot 10^{-1}$	$1.35 \cdot 10^{-4}$
1000	$9.82 \cdot 10^{-2}$	$7.91 \cdot 10^{-5}$

Table 3.7: Values of the contributions to the total NNLO VBF cross-section due to the two-loop trinagle diagram shown in Fig. 3.9 at the LHC, at $\sqrt{S} = 7\,\text{TeV}$ (left) and $\sqrt{S} = 14\,\text{TeV}$ (right). The MSTW2008 [63] NNLO PDF set has been used.The LO cross-section, computed with LO PDFs, is also shown for comparison. Renormalization and factorization scales have been set to M_W. Integration errors are below the 1% level. Cross-sections are in pb.

via the program HAWK [71].

In absence of a full calculation up to corrections of order $\alpha_s^2\alpha_{EW}$ with respect to the Born amplitude, which is currently beyond capabilities, a combination of EW and NNLO QCD corrections is possible, yet formally subject to ambiguities. A pragmatic way to proceed is to follow two different approaches, multiplicative or additive, and the corresponding differences used to assess the impact of neglected terms. Using a compact notation, we define

$$\sigma_{NNLO}^{QCD} = \sigma_0 + \alpha_s\sigma_1^{QCD} + \alpha_s^2\sigma_2^{QCD} \tag{3.24}$$

the total cross section at NNLO in QCD,

$$\sigma^{EW} = \sigma_0 + \alpha_{EW}\sigma_1^{EW} \tag{3.25}$$

the total cross sections including NLO EW corrections, and σ_{NLO+EW} the result of the full calculation at NLO in QCD and EW of Refs. [18, 19].

The additive scheme amounts to simply define

$$\sigma_{NNLO+EW} \equiv \sigma_{NLO+EW} + \alpha_s^2\sigma_2^{QCD}, \tag{3.26}$$

i.e., to add the missing α_s^2 terms to the full NLO+EW calculation. In this scheme no assumption on the factorization of QCD and EW corrections is made and only terms that are known are included. It demands, however, the two terms to be evaluated with exactly the same EW ($G_F, M_Z, M_W, \ldots$) and QCD (scales, α_s, and PDFs) parameters, something possibly error-prone when different codes are used.

The multiplicative scheme amounts to assuming that the QCD and EW corrections factorize to a very good approximation at NLO as well as at NNLO. In this case one can define

$$\sigma_{NNLO+EW} \equiv \sigma_{NNLO}^{QCD}\left(1 + \frac{\sigma_1^{EW}}{\sigma_0}\right). \tag{3.27}$$

This is a very handy approximation: it implies that the EW corrections can be evaluated independently as effects such as scale and PDF choices are mostly canceled in the ratio σ_1^{EW}/σ_0. Note, however, that it implies the inclusion of unknown higher order terms in the results. This is the approach followed in Ref. [8] and the results relevant for Higgs production at the LHC can be found there. We have explicitly checked for a few values of the Higgs mass, that the differences between the two schemes are very small and totally negligible at the LHC.

4 VBF production in the Standard Model

We are now in a position to present an extensive phenomenological analysis for the VBF production mechanism at the LHC at the center of mass energies of $\sqrt{S} = 7\,\text{TeV}$ and $\sqrt{S} = 14\,\text{TeV}$ and the Tevatron, $\sqrt{S} = 1.96\,\text{TeV}$, employing the structure function approach up to the NNLO in QCD. This is a significant extension of our previous studies in Refs. [20, 21]. For the numerical results we use the following values for the electroweak parameters (see also [8]): The masses of the vector bosons are $M_W = 80.398\,\text{GeV}$ and $M_Z = 91.1876\,\text{GeV}$, Fermi's constant and the weak mixing angle are taken to be $G_F = 1.16637 \cdot 10^{-5}$ and $\sin^2\theta_w = 0.23119$. The widths of the vector bosons, Γ_W and Γ_Z, have been set to zero for simplicity, their effect being of order 10^{-3} or less on the total rate. Moreover, we provide numbers for all PDFs currently available at NNLO accuracy in QCD, ABKM [70, 72], HERAPDF1.5 [73, 74], JR09 [75, 76], MSTW2008 [63] and NNPDF2.1 [77] always using the default value of the strong coupling α_s required by the respective set. A cut of $1\,\text{GeV}$ has been used to regulate the phase space integration over Q which extends to vanishing Q^2 (see Sec. A.1). In the numerical evaluation we have checked explicitly that the results remain unchanged upon variations of this cut on Q, a fact readily understood by realizing that the effective $\langle Q \rangle$ in VBF is much larger, typically $\langle Q \rangle \simeq 20\,\text{GeV}$, see the discussion in [20].

All results presented here can also be obtained through our publicly usable VBF@NNLO code [78].

4.1 Cross section predictions for the Tevatron

Let us start off with the Tevatron, where the cross section is roughly 0.1 pb for a Higgs boson with mass $m_H = 100\,\text{GeV}$ and steeply falling as a function of m_H. An exhaustive list of cross-sections, for different values of the Higgs boson mass in the range $m_H \in [90, 300]\,\text{GeV}$ at LO, NLO and NNLO in QCD are given in Tabs. B.1–B.5.

The central values have been obtained by setting the factorization and the renormalization scales $\mu_r = \mu_f = Q$, where Q is the virtuality of the vector bosons which fuse into the Higgs, cf. Eq. (3.2). Our results in Tabs. B.1–B.5 show that the NLO corrections are always positive and not too large of the order of 1-2%, while the NNLO corrections are typically small of the order of ±1% depending on the chosen PDF set.

The theoretical uncertainty of the predictions has been determined by varying the scales independently in a large range $\mu_r, \mu_f \in [Q/4, 4Q]$. Here we find markedly a clear improvement due to the NNLO corrections computed. While we observe, e.g. for a Higgs mass of $m_H = 100\,\text{GeV}$, variations of order ±20-30% for σ_{LO}, this reduces to ±5-10% for σ_{NLO}, and to ±2% for σ_{NNLO}. The scale uncertainty increases slightly for larger Higgs masses, e.g. for $m_H = 250\,\text{GeV}$, we find order ±30-50%, ±10-12% and to ±3% at LO, NLO and NNLO, respectively, see also Fig. 4.1. Of course, other scale choices are possible relating μ_r, μ_f to the Higgs boson mass m_H or the W-boson mass M_W, see Fig. 4.2 for a comparison. As discussed in [20] the present choice, *i.e.*, relating

μ_r and μ_f to Q turns out to be the most natural one with the point of minimal sensitivity being $\mu_r, \mu_f \simeq Q$, as it exhibits the best pattern of apparent convergence of the perturbative expansion. Considering the size of the neglected contributions discussed at length above in Sec. 3 the residual theoretical uncertainty due to perturbative QCD corrections at higher orders at the Tevatron is of the order 2-3%.

The PDF dependence is clearly the dominating source of uncertainty at the Tevatron, the individual PDFs report an uncertainity in the PDFs at NNLO (sometimes combined with the one in the strong coupling α_s) of the order ±1-3%. Moreover the central values obtained from the various NNLO PDFs differ by roughly 5% at low Higgs masses, e.g. $m_H = 100\,\text{GeV}$, which is increasing towards larger Higgs masses, e.g., to 10% at $m_H = 250\,\text{GeV}$, see also Fig. 4.3. This is due to the larger values of effective $\langle x \rangle$ at which the parton luminosities are probed. In summary, thus, the uncertainty due to the non-perturbative parameters (PDFs, α_s) can be estimated to be of the order 5% for a light Higgs boson at the Tevatron.

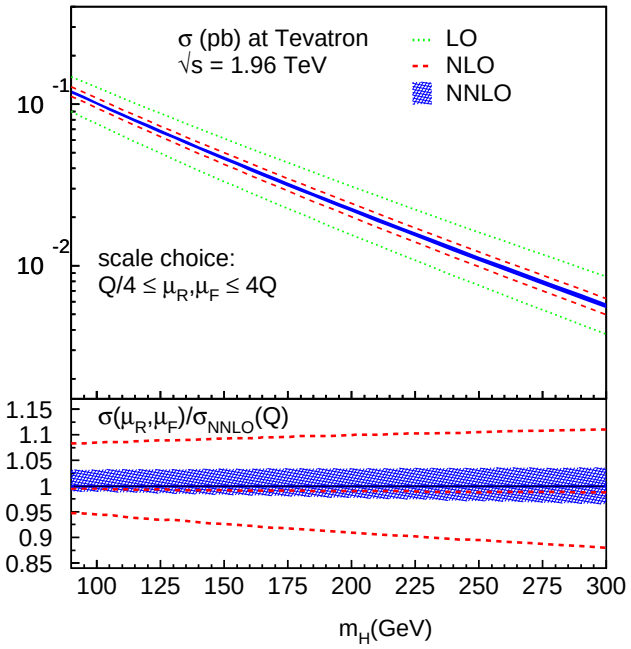

Figure 4.1: The total VBF cross sections at the Tevatron, $\sqrt{S} = 1.96\,\text{TeV}$, at LO, NLO and NNLO in QCD with the scale uncertainity from the variation $\mu_r, \mu_f \in [Q/4, 4Q]$. The MSTW2008 [63] PDF set (68% CL) has been used. Numbers are in pb.

4.2 Cross section predictions for the LHC

Let us now present the numbers for the current and foreseen center-of-mass energies of the LHC. For a Higgs boson with a mass $m_H = 100\,\text{GeV}$ the cross section is roughly 1.6(5.5) pb at $\sqrt{S} = 7(14)\,\text{TeV}$ and, again, steeply falling as a function of m_H, e.g. to 0.1(0.5) pb at $m_H = 500\,\text{GeV}$. This is illustrated in Figs. 4.4 and 4.7. The complete listings of cross-sections at LO, NLO and NNLO in QCD for Higgs boson masses in the range $m_H \in [90, 1000]\,\text{GeV}$ for $\mu_r = \mu_f = Q$ are given in Tabs. B.6–B.10 ($\sqrt{S} = 7\,\text{TeV}$) and in Tabs. B.11–B.15 ($\sqrt{S} = 14\,\text{TeV}$), respectively.

In analogy to the preceeding discussion in Sec. 4.1 our results in Tabs. B.6–B.10 demonstrate a very good apparent convergence of the perturbative expansion, *i.e.*, the NLO corrections of the order of 5%, while the NNLO corrections are of the order of ±1%, only. The NNLO results

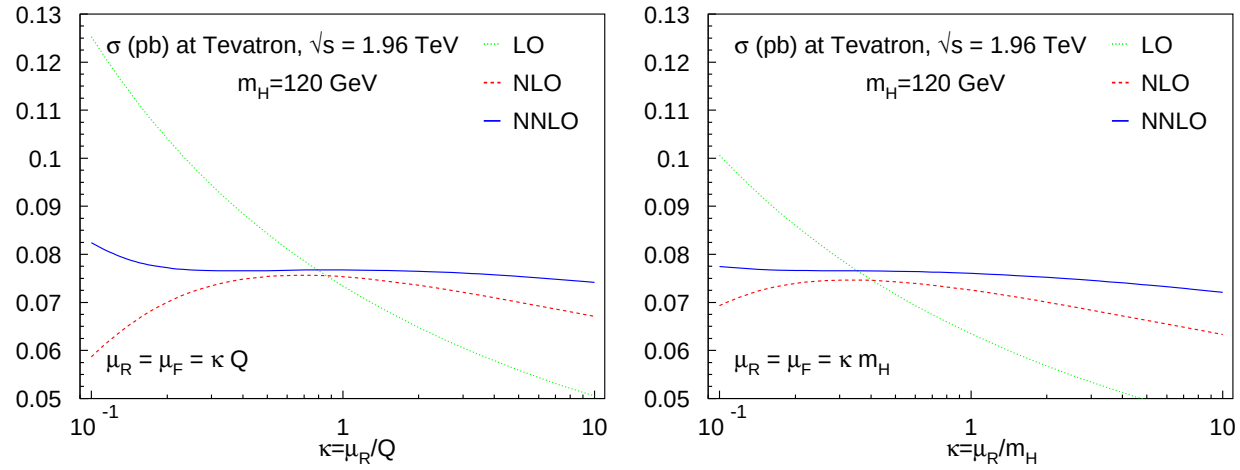

Figure 4.2: Scale dependence of the VBF cross sections at the Tevatron, $\sqrt{S} = 1.96\,\text{TeV}$ at LO, NLO and NNLO in QCD for $m_H = 120\,\text{GeV}$ and the choice $\mu_r = \mu_f = \kappa Q$ (left) and $\mu_r = \mu_f = \kappa m_H$ (right). The ABKM [70] PDF set has been used. Numbers are in pb.

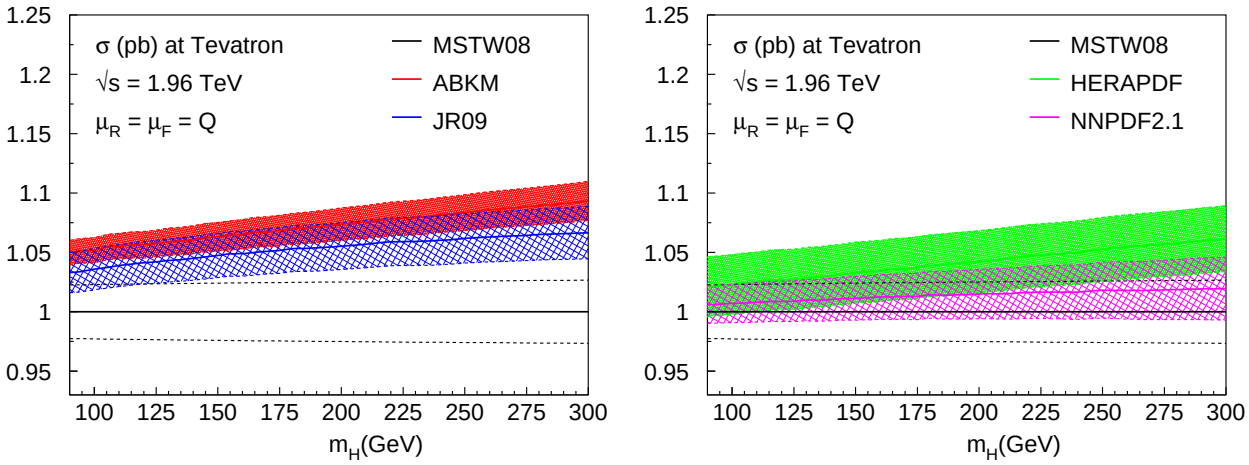

Figure 4.3: The PDF uncertainity of the VBF cross sections at the Tevatron, $\sqrt{S} = 1.96\,\text{TeV}$, at NNLO in QCD for PDF sets of ABKM [70], HERAPDF1.5 [73, 74], JR09 [75, 76], MSTW2008 [63] (68 % CL), and NNPDF [77]. All results have been normalized to the best fit of MSTW2008.

display also an impressive perturbative stability with respect to scale variations, see Figs. 4.5 and 4.8 also for a comparison of the scale choice relating μ_r and μ_f to Q and to m_H, respectively. The preference to low scales is obvious from those plots, again with the point of minimal sensitivity being of the order $\mu_r, \mu_f \simeq Q$. Given that all the perturbative QCD corrections not accounted for in the structure function approach are very small and negligible, as discussed in Sec. 3, we can estimate the residual theoretical uncertainty due to uncalculated higher orders in QCD at the LHC to be of order 2% for the entire Higgs mass range up to $m_H = 1\,\text{TeV}$.

Let us also comment on the uncertainties coming from the PDFs (and the associated value of α_s as provided by the respective PDF set). All PDF sets under consideration are displayed in Figs. 4.6 and 4.9. In comparison to the Tevatron, we see that over a large range of Higgs masses, $m_H \simeq 100 \ldots 300\,\text{GeV}$, there are rather small differences between these sets only, because quark PDFs are well constrained in the relevant x-region. Generally, the PDF uncertainties are larger for the lower running energy of the LHC. The plots in Figs. 4.6 and 4.9 show that an almost constant 2% PDF uncertainty can be associated to the cross section for the LHC for a light Higgs boson.

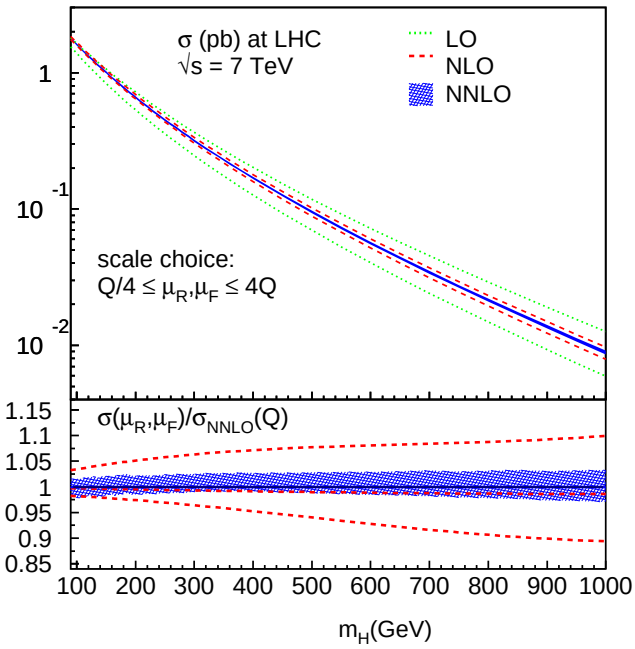

Figure 4.4: The total VBF cross sections at the LHC, $\sqrt{S} = 7\,\text{TeV}$, at LO, NLO and NNLO in QCD with the scale uncertainity from the variation $\mu_r, \mu_f \in [Q/4, 4Q]$. The MSTW2008 [63] PDF set (68% CL) has been used. Numbers are in pb.

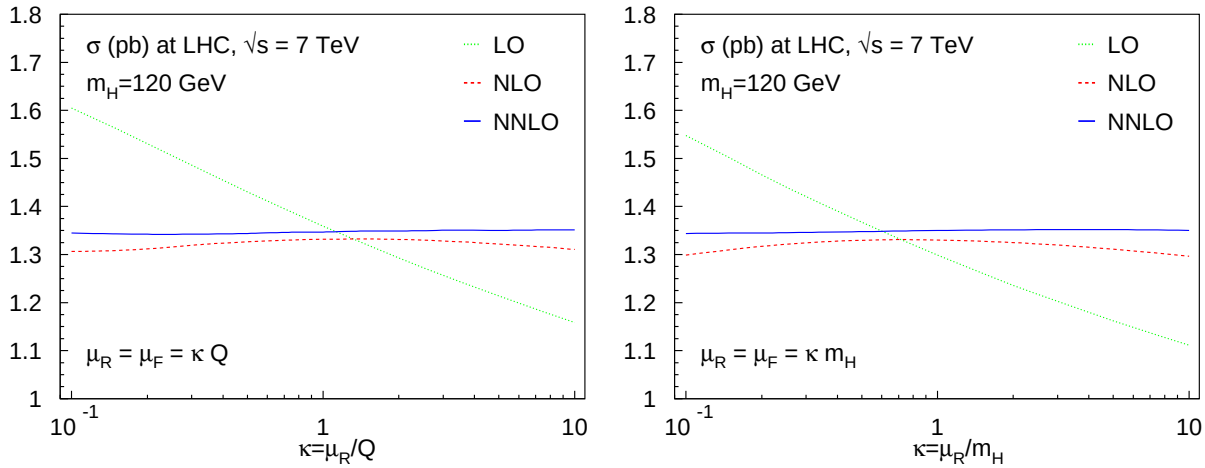

Figure 4.5: Scale dependence of the VBF cross sections at the LHC, $\sqrt{S} = 7\,\text{TeV}$, at LO, NLO and NNLO in QCD for $m_H = 120\,\text{GeV}$ and the choice $\mu_r = \mu_f = \kappa Q$ (left) and $\mu_r = \mu_f = \kappa m_H$ (right). The ABKM [70] PDF set has been used. Numbers are in pb.

This deteriorates towards larger Higgs masses, e.g., the uncertainty being of order ±10-12% for $m_H = 1\,\text{TeV}$.

In summary, our results demonstrate that at NNLO in QCD the theoretical uncertainty is reduced to about 2% reaching the same level of ambiguity at which the Higgs production signal via VBF can be defined phenomenologically, as discussed in Sec. 2. Moreover, the study of the available NNLO PDF sets shows that all non-perturbative parameters (PDFs and α_s) needed for VBF precision predictions are well under control. For larger Higgs masses, the PDF uncertainty is the dominating.

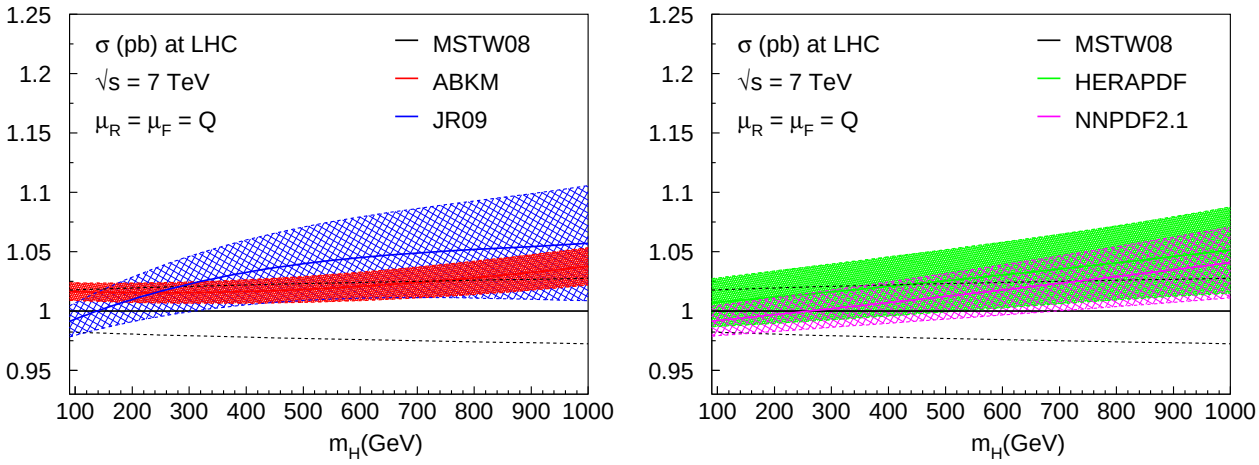

Figure 4.6: The PDF uncertainity of the VBF cross sections at the LHC, $\sqrt{S} = 7\,\text{TeV}$, at NNLO in QCD for PDF sets of ABKM [70], HERAPDF1.5 [73, 74], JR09 [75, 76], MSTW2008 [63] (68 % CL), and NNPDF [77]. All results have been normalized to the best fit of MSTW2008.

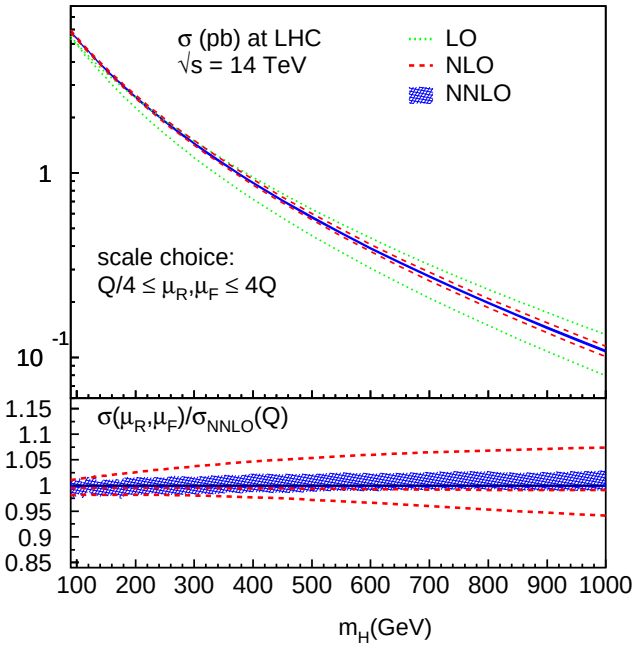

Figure 4.7: The total VBF cross sections at the LHC, $\sqrt{S} = 14\,\text{TeV}$, at LO, NLO and NNLO in QCD with the scale uncertainity from the variation $\mu_r, \mu_f \in [Q/4, 4Q]$. The MSTW2008 [63] PDF set (68% CL) has been used. Numbers are in pb.

5 VBF production beyond the Standard Model

One of the most important features of the structure function approach resides in its universality: as long as the final state X in $V^*V^* \to X$ fusion process does not interact (strongly) with the quark lines, the cross section can be factorized using Eq. (3.2) and QCD corrections decouple from the nature of the fusion process. This property allows the computation of production cross sections at NNLO in QCD for a variety of processes relevant for new physics searches in a straightforward way. In this section we present results for a few examples: Higgs production through anomalous couplings which are relevant when new physics states are heavy and the effects enter only at loop

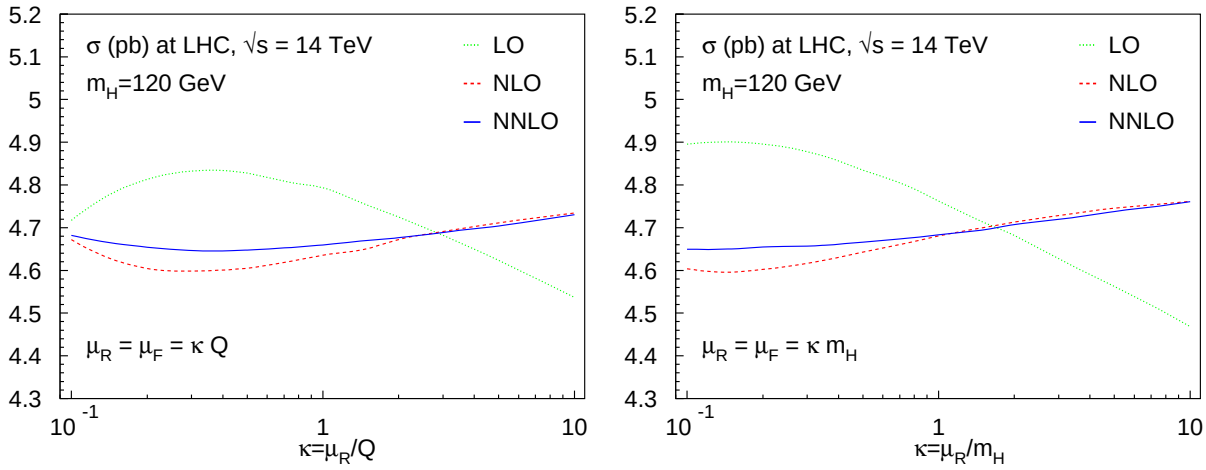

Figure 4.8: Scale dependence of the VBF cross sections at the LHC, $\sqrt{S} = 14\,\text{TeV}$, at LO, NLO and NNLO in QCD for $m_H = 120\,\text{GeV}$ and the choice $\mu_r = \mu_f = \kappa Q$ (left) and $\mu_r = \mu_f = \kappa m_H$ (right). The ABKM [70] PDF set has been used. Numbers are in pb.

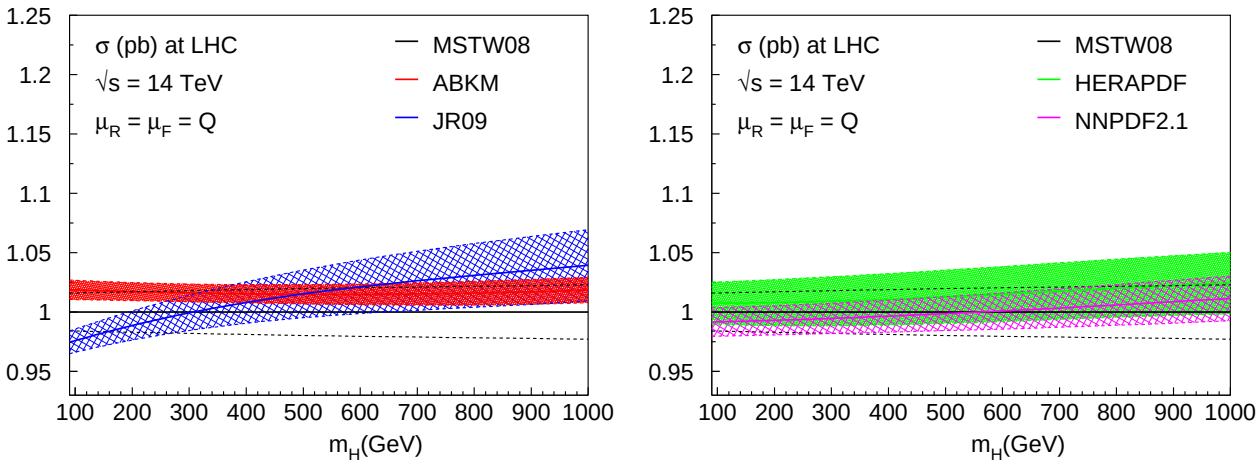

Figure 4.9: The PDF uncertainity of the VBF cross sections at the LHC, $\sqrt{S} = 14\,\text{TeV}$, at NNLO in QCD for PDF sets of ABKM [70], HERAPDF1.5 [73, 74], JR09 [75, 76], MSTW2008 [63] (68 % CL), and NNPDF [77]. All results have been normalized to the best fit of MSTW2008.

level; extra neutral and charged scalar production in extended Higgs sectors, such as in two Higgs doublet and triplet Higgs models; neutral and charged vector fermiophobic resonance production.

5.1 Anomalous VVH couplings

Due to its very peculiar signature with two forward tagging jets, whose angular correlations can also be studied and related to the Higgs CP properties independently of the Higgs decay channel, VBF can be a powerful means to discover new physics residing at a scale Λ and responsible for anomalous VVH vertices [79]. The most generic structure for the VVH vertex which generalizes Eq. (3.1), has the form [80]:

$$\Gamma^{\mu\nu}(q_1,q_2) = 2M_V^2\left(\left(\sqrt{2}G_F\right)^{1/2} + \frac{a_1}{\Lambda}\right)g_{\mu\nu} + \frac{a_2}{\Lambda}\left(q_1\cdot q_2 g^{\mu\nu} - q_2^{\mu}q_1^{\nu}\right) + \frac{a_3}{\Lambda}\varepsilon^{\mu\nu\rho\sigma}q_{1\rho}q_{2\sigma}, \qquad (5.1)$$

where the effective coefficients a_i are dimensionless and vanish in the SM. The VBF cross-section including anomalous vertices is known at NLO in QCD [81], and has been included in the program

VBFNLO [82].

As discussed in [79], at high energies one expects the effective coefficients a_i to become form factors, *i.e.* to display a dependence on the scattering energy such that unitarity would be preserved. However, since at the LHC the typical scales in a VBF process can be still considered small with respect to a new physics scale of the order of 1 TeV, we will present numbers for constant values of a_i and $\Lambda = 500$ GeV. With the vertex in Eq. (5.1), the expression corresponding to Eq. (3.5) becomes a bit more involved than its SM counterpart and it is given in the Appendix, Sec. A.2.

Since a_1 only changes the cross-section by an overall factor, we set it to 0. We therefore plot in Fig. 5.1 the total cross-sections at the LHC for different values of a_2 and a_3. Uncertainties at NNLO are again found to be of the order of a few percent.

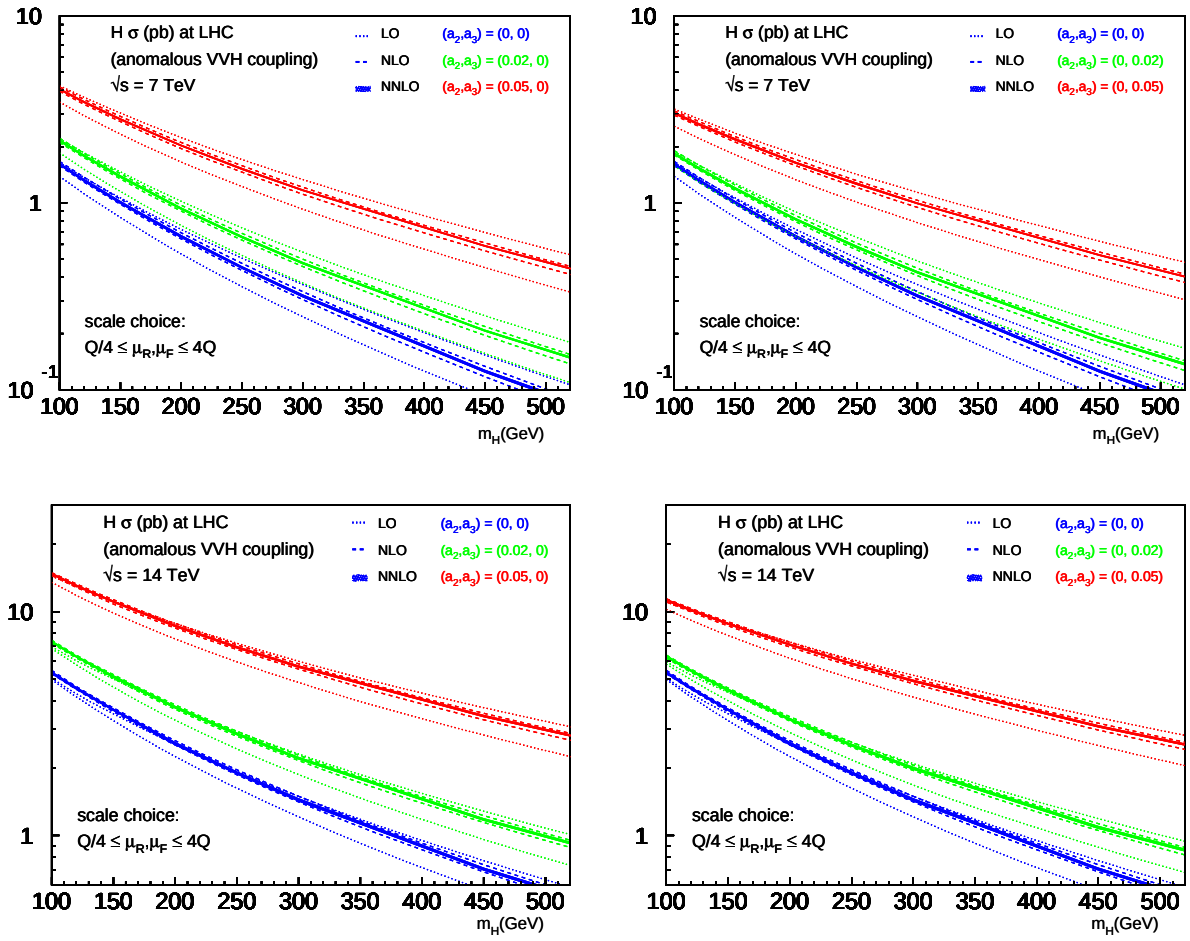

Figure 5.1: The total cross-section for Higgs production via VBF at the LHC, with $\sqrt{S} = 7\,\text{TeV}$ (top) and $\sqrt{S} = 14\,\text{TeV}$ (bottom). The values used for the parameters a_2, a_3 are written on the plots. We have assumed $\Lambda = 500\,\text{GeV}$. The MSTW 2008 [63] PDF set has been used. The uncertainty bands are obtained from the variation of the renormalization and factorization scale in the interval $Q/4 < \mu_f, \mu_r < 4Q$, where Q is the virtuality of the vector boson.

5.2 New neutral and charged Higgs bosons

Many extension of the SM feature an Higgs sector with an extra SU(2) doublet and/or triplet, that lead to a particle spectrum including several neutral Higgs bosons, as well as single- and, possibly,

double-charged scalars. Because of the particular signature with forward jets, VBF can be a really powerful search channel also for these states.

In a generic two Higgs doublet model (2HDM), such as that in the Minimal Supersymmetric Standard Model (MSSM) [83], the production rate of a CP-even light or heavy Higgs scalar via VBF is equal to the SM one times overall factors [84–86]. Therefore, to obtain the total cross-section including QCD NNLO corrections for the h^0 or H^0 production, one just needs to rescale the SM results given in Sec. 4.

Pseudo-scalar states do not couple to vector bosons at the tree level, therefore VBF is not really relevant in this case. On the other hand, it is of great phenomenological interest to study the production of charged Higgs bosons. As we will briefly see, there exist a class of models in which charged Higgs boson production via VBF can be observed.

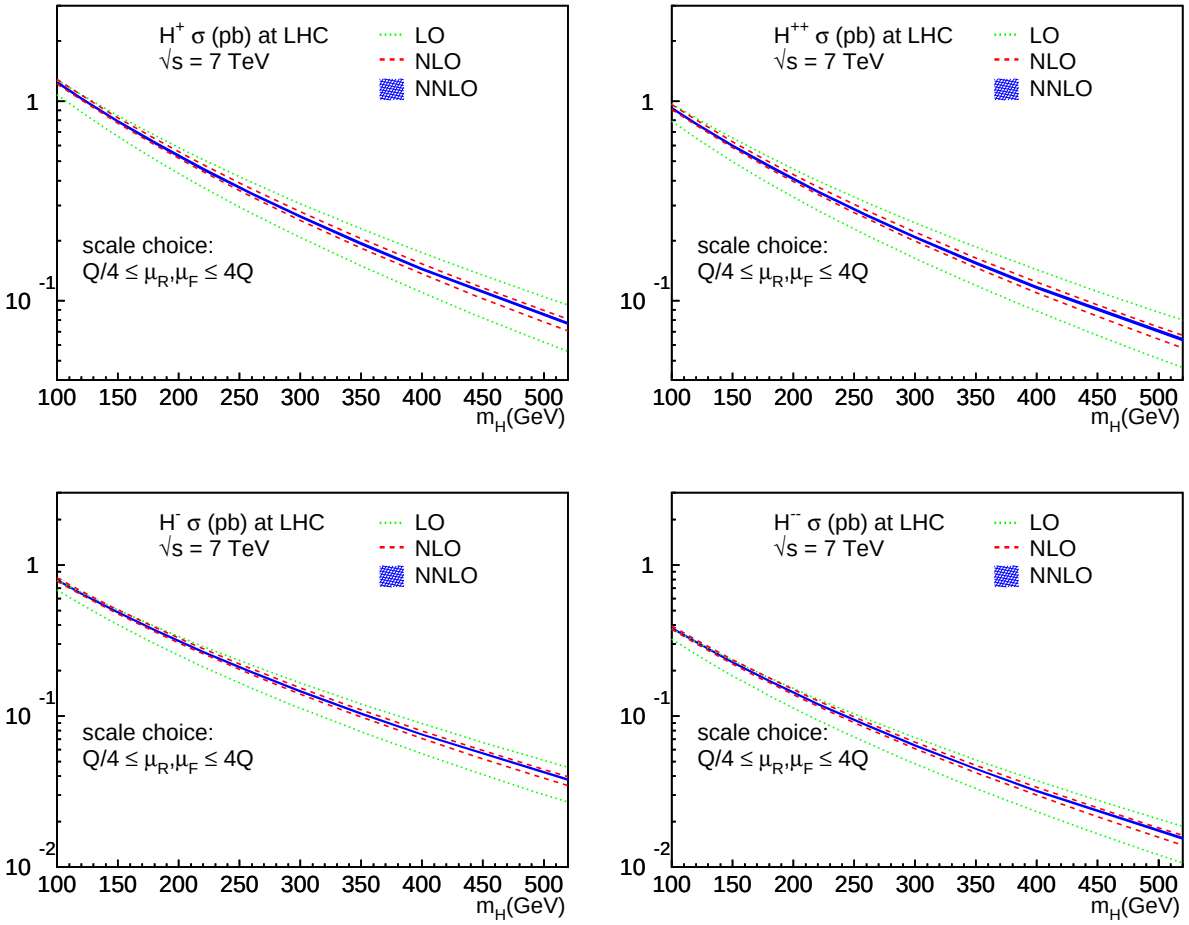

Figure 5.2: The total cross-section for charged Higgs production via VBF at the LHC, with $\sqrt{S} = 7\,\text{TeV}$. The MSTW 2008 [63] PDF set has been used. The uncertainty bands are obtained from the variation of the renormalization and factorization scale in the interval $Q/4 < \mu_f, \mu_r < 4Q$, where Q is the virtuality of the vector boson. Plots refer to: H^+ production (top-left), H^{++} production (top-right), H^- production (bottom-left), H^{--} production (bottom-right).

In models where the extra Higgs bosons are included in SU(2) doublets, like the MSSM or the 2HDM, isospin conservation forbids (at the tree level) the appearance of $W^\pm H^\mp Z$ and $W^\pm H^\mp \gamma$ vertices, while they can be loop-induced [87]. However, in this case the corresponding total cross-section for VBF is totally negligible [88], leaving the associated production of a charged Higgs

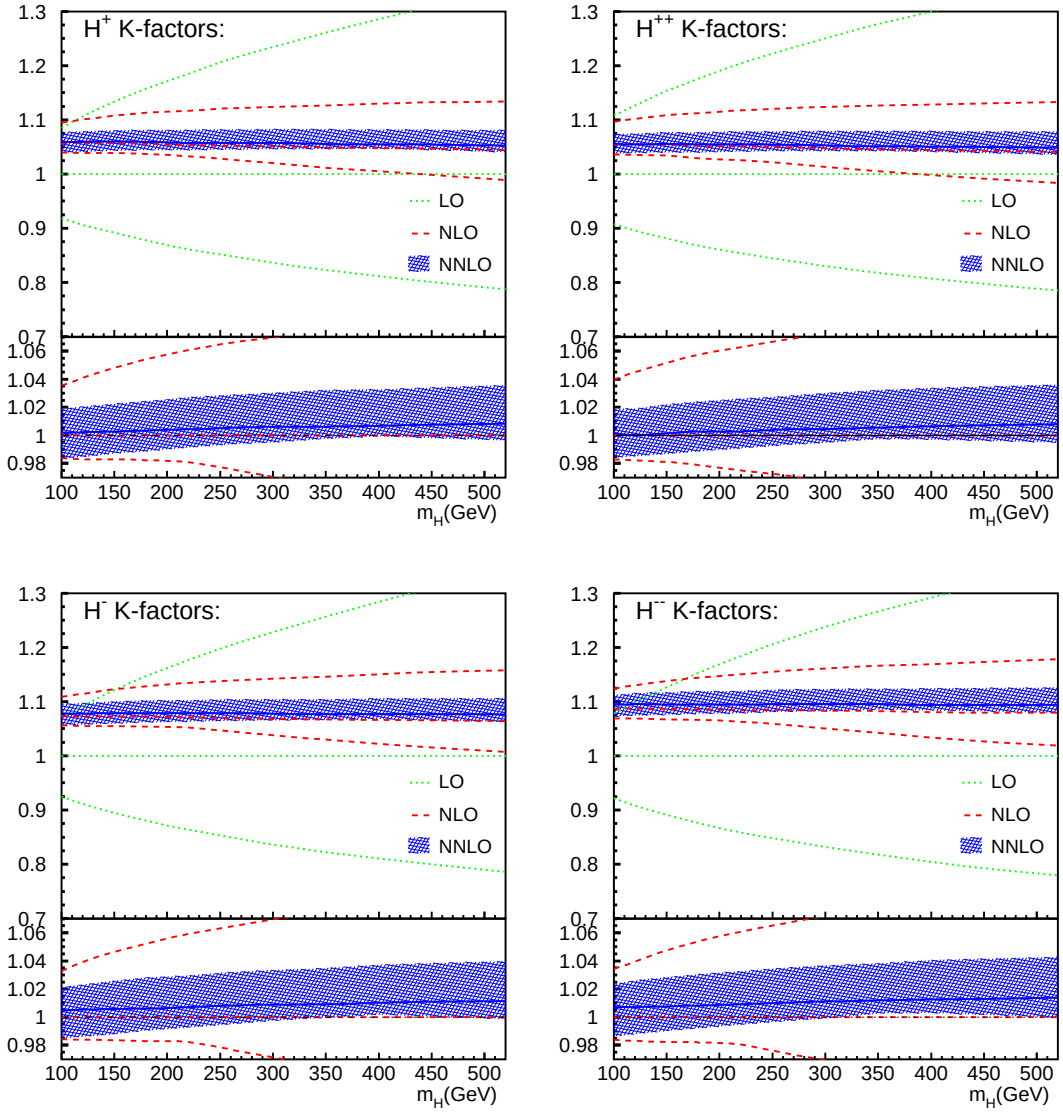

Figure 5.3: The (N)NLO/LO (upper inlay) and NNLO/NLO (lower inlay) K-factors for charged Higgs production via VBF at the LHC, with $\sqrt{S} = 7\,\text{TeV}$. The MSTW 2008 [63] PDF set has been used. The uncertainty bands are obtained from the variation of the renormalization and factorization scale in the interval $Q/4 < \mu_f, \mu_r < 4Q$, where Q is the virtuality of the vector boson. Plots refer to: H^+ production (top-left), H^{++} production (top-right), H^- production (bottom-left), H^{--} production (bottom-right).

boson and a top-quark from a bottom-gluon initial state [89, 90] as the only phenomenologically relevant production channel.

This situation changes when models with isospin triplets in the Higgs-sector are considered. Many versions of such models exist in literature, with a very interesting particle content including double-charged Higgs bosons. In many of such models the coupling of the charged Higgs bosons to gauge bosons is allowed with a strength proportional to the ratio v'/v, where v' is the triplet vacuum expectation value (vev) and v the SM one. Even though v' is constrained by electroweak data, in particular by the ρ parameter of the SM, to be at most a few GeV, this bound can be loosened by including more triplets [91]. In this case, the production of single- and double-charged Higgs bosons via VBF can be relevant at colliders [88, 92, 93]. The Lorentz structure of the VVH vertex

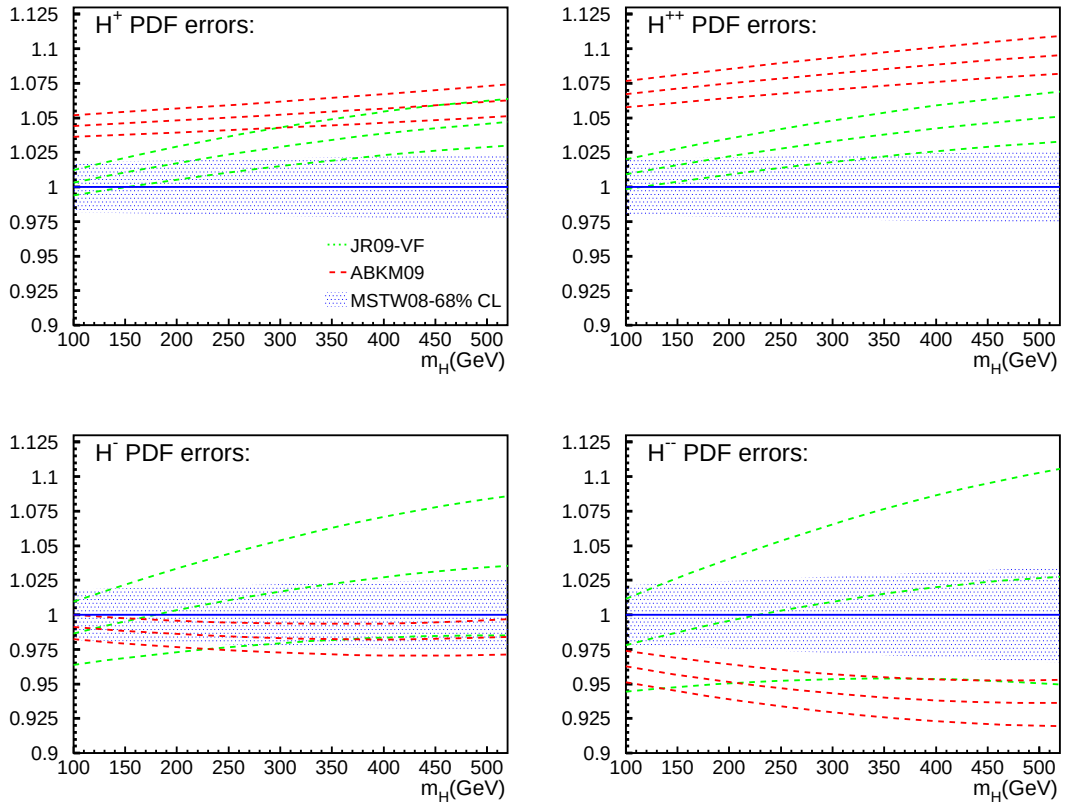

Figure 5.4: The PDF uncertainties to the NNLO total cross section for charged Higgs boson production in VBF at the LHC, with $\sqrt{S} = 7\,\text{TeV}$. Plots are normalized to the MSTW 2008 [63] central value. The errors for the MSTW set are at 68% CL. The plots show also the central value and error band for the JR09-VF NNLO set [75, 76] and for the ABKM09 NNLO set [70, 72]. Plots refer to: H^+ production (top-left), H^{++} production (top-right), H^- production (bottom-left), H^{--} production (bottom-right)

is, like the SM one in Eq. (3.1), proportional to the metric tensor (see, e.g., the Feynman rules given in Ref. [94]), and it can be cast in the generic form

$$\Gamma^{\mu\nu}_{V_iV_jH} = 2\left(\sqrt{2}G_F\right)^{1/2} m_i m_j \, F_{ij}(-ig^{\mu\nu}), \tag{5.2}$$

where the dimensionless constant F_{ij} depends on the particular model (in the SM the non-vanishing ones are $F_{ZZ} = F_{W^\pm W^\mp} = 1$). Because of the rich variety of available models, and in order to be as much general as possible, we will present numbers with $\left|F_{ij}\right| = 1$.

In Fig. 5.2 we show the total cross section for $H^\pm, H^{\pm\pm}$ production via VBF at the LHC with $\sqrt{S} = 7\,\text{TeV}$. The plots clearly display the excellent convergence of the perturbative series and the reduction of theoretical uncertainties obtained by the inclusion of higher order corrections, as it can be also be appreciated by inspecting Fig. 5.3, where the K-factors are shown. In particular we find that the NNLO K-factor for the nominal scale choice ($\mu_r = \mu_f = Q$) differs from one for less than 1% in almost the whole mass range shown. From Fig. 5.4 it is clear that the uncertainty coming from the PDFs is sizable, in particular for large values of the charged Higgs masses, where the PDFs are probed at larger values of x, *i.e.*, in a region, where the PDF uncertainties generally increase.

5.3 Production of fermiophobic vector boson resonances

In many extensions of the SM, additional vector bosons can appear in the particle spectrum, together with or as an alternative to the Higgs boson, see e.g. [22, 23, 95, 96]. The existence of heavy vector bosons, however, is severely constrained by electroweak precision data and direct searches and masses are pushed to the multi-TeV scale. This holds unless their couplings to (light) fermions are for some reason suppressed and only couplings to the SM weak vector bosons take place. In such models, where the new heavy vector resonances are dubbed "fermiophobic", VBF can become the dominant production channel.

While a detailed phenomenological analysis is beyond our scope, we just limit ourselves to presenting a few results motivated by warped scenarios [97, 98] for the production of a neutral and a single-charged vector resonance, which couples to SM vector bosons via a trilinear vertex of the form

$$\Gamma^{\mu_1\mu_2\mu_3}(p_1,p_2,p_3) = g_{123}\left[g^{\mu_1\mu_2}\left(p_1^{\mu_3}-p_2^{\mu_3}\right)-g^{\mu_2\mu_3}\left(p_2^{\mu_1}-p_3^{\mu_1}\right)-g^{\mu_3\mu_1}\left(p_3^{\mu_2}-p_1^{\mu_2}\right)\right]. \tag{5.3}$$

This particular choice assumes that the new vector bosons are explicit or "hidden" gauge vectors of a new sector. Different vertices are also possible (see e.g., [99, 100]) and can be easily implemented in our calculation.

The expression for the total cross-section in terms of structure functions and particle momenta is given in Sec. A.3. The results we present are for neutral and charged vector boson production, which we call $W'^{\pm}$ or Z' and which we assume not to be coupled to photons. (This is in fact not a real limitation as in practice forward jets are required entailing de facto a minimum Q^2 for the exchanged particle in the t-channel and such a cut could also be effectively included in the structure function approach). For the sake of simplicity, we also assume that no ZZZ' vertex exists in our model and that in the WZW' and WWZ' vertices the coupling constants are equal to those appearing in the respective WWZ SM vertex:

$$g_{WWZ'} = g_{WZW'} = g_{WWZ} = g_w \cos\theta_w. \tag{5.4}$$

The corresponding results are shown in Fig. 5.5.

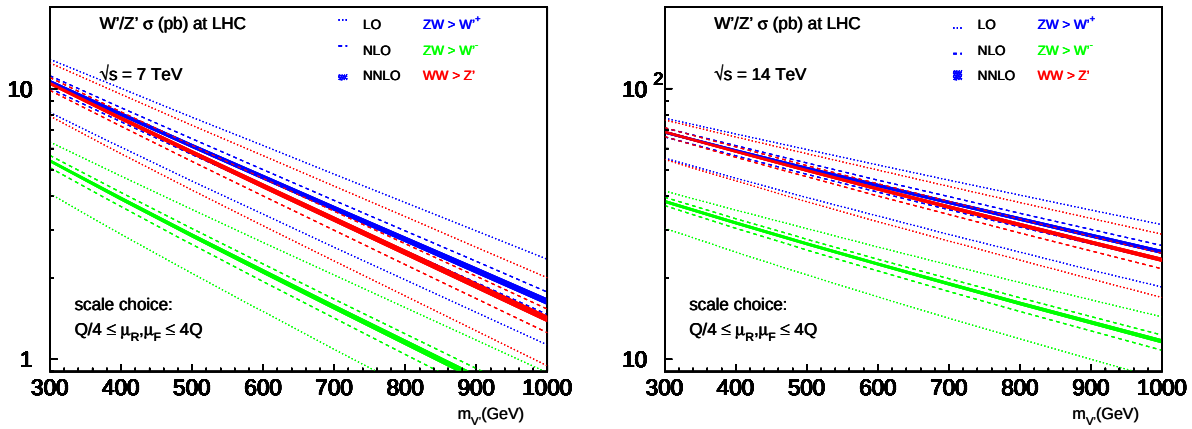

Figure 5.5: The total cross-section for a vector resonance (Z' or W') via VBF at the LHC, $\sqrt{S} = 7\,\text{TeV}$ (top) and $\sqrt{S} = 14\,\text{TeV}$ (bottom). The trilinear coupling between vector bosons is assumed to be equal to the one for ZWW in the SM. The MSTW 2008 [63] PDF set has been used. The uncertainty bands are obtained from the variation of the renormalization and factorization scale in the interval $Q/4 < \mu_f, \mu_r < 4Q$, where Q is the virtuality of the vector boson.

6 Conclusions

The computation of NNLO in QCD predictions for production cross sections at the LHC is in general a formidable, but nevertheless strongly motivated task. To date only a handful of very simple processes (with $2 \to 1$ kinematics at the Born level) are known at this order: Drell-Yan, Higgs production in gluon-gluon fusion, and $V^* \to VH$. In this work we have argued that VBF processes provide a notable exception, being the only class of processes beyond one-body final states at the Born level (actually starting from a genuine three-body one) whose total cross section can be calculated at NNLO through the use of currently available techniques and results. We have shown that the key reason for this unique possibility is that the structure function approach and the factorization approximation on which it is based, work extremely well up to order α_s^2, corrections being kinematically and parametrically (by α_s^2/N_c^2) suppressed and de facto negligible. Considering also contributions coming from processes involving virtual heavy quarks, neglected in the past, we find that the residual theoretical uncertainty from higher order QCD corrections is at the 2% level over a wide range of Higgs boson masses. With the PDF uncertainties being also of the same order, one concludes that cross sections for this class of processes are among the most precise rate predictions available in LHC phenomenology. In this respect, our results strongly encourage the efforts towards the calculation of the differential NNLO rates in DIS, which is now in sight [101]. A fully exclusive DIS computation at NNLO would put VBF on par with gluon-gluon fusion, and $V^* \to VH$ (see e.g., [102] for recent progress). It would allow to mimic experimental selection cuts on the forward jets and to estimate non-trivial effects such as central jet-veto efficiencies, for the first time at NNLO.

Another very pleasant feature of the structure function approach is its universality: any weak boson fusion process to an arbitrary n-body final state X_n (of particles not or very weakly interacting with the quark lines), *i.e.*, $V^*V^* \to X_n$, can be easily computed at the NNLO. As first simple applications we have considered fusion of V^*V^* to one-particle BSM final states: neutral scalar production with the full set of anomalous vector-vector-scalar couplings, single-charged and double-charged scalars, neutral and charged heavy vector resonances. Other models and scat-

tering processes, such as two-body (scalar-scalar, scalar-vector, vector-vector, and fermion-anti-fermion) final states can be easily implemented. In fact, thanks to its modularity, the structure function approach to VBF cross sections via VBF@NNLO could be automatized using tools like FeynRules [103] and MadGraph 5 [104] for matrix element evaluation in arbitrary new physics models. NNLO results could then be used to provide the best normalization to fully exclusive NLO-accurate event samples automatically generated via, for example, aMC@NLO [55, 56, 105]. Work in this direction is in progress. In the meantime, all results presented in this article can also be easily obtained through the public use of our VBF@NNLO code [78].

Acknowledgments

We thank R. Frederix, S. Frixione and V. Hirschi for their help in using MadFKS [56] and MadLoop [55], and A. Akeroyd, G. Bozzi, C. Grojean, B. Kniehl and A. Vicini for discussions. The Feynman diagrams in this article have been prepared using Jaxodraw [106] and Axodraw [107]. This work is partially supported by the Belgian Federal Office for Scientific, Technical and Cultural Affairs through Interuniversity Attraction Pole No. P6/11, by the Deutsche Forschungsgemeinschaft in Sonderforschungsbereich/Transregio 9 and by the European Commission through contract PITN-GA-2010-264564 (*LHCPhenoNet*).

A Useful formulae

A.1 The VBF phase space

In this appendix we briefly document the parameterization for the phase space of the VBF process. We will first take the most general case, which is the production of an n-particles final state via VBF with momenta $K_1, \ldots, K_n$, then we will specialize to the case of one particle.
In the structure function approach we can consider the proton remnants as massive particles, and integrate over their masses, which we label s_1, s_2.
We will call P_1, P_2 the momenta of the incoming protons, and P_{X_1}, P_{X_2} the momenta of the proton remnants. The choice of kinematical variables is guided by the requirement to resemble the DIS kinematics as much as possible. We work in the hadronic center-of-mass reference frame, with

$$P_1 = \frac{1}{2}\left(\sqrt{S}, 0, 0, \sqrt{S}\right), \qquad P_2 = \frac{1}{2}\left(\sqrt{S}, 0, 0, -\sqrt{S}\right). \tag{A.1}$$

Then, the Lorentz invariant phase space for this process is (cf. Eq. (3.2)),

$$dPS = \prod_{i=1,2} ds_i \, \frac{d^4 P_{X_i}}{(2\pi)^4} \, 2\pi\delta\left(P_{X_i}^2 - s_i\right) \, dPS_n(K_1, \ldots, K_n) \, (2\pi)^4 \delta^4\left(P_1 + P_2 - P_{X_1} - P_{X_2} - \sum_{j=1,n} K_j\right). \tag{A.2}$$

In Eq. (A.2) we have separated the phase space of the proton remnants and the one of the particles produced via VBF. In order to solve the kinematics, let q_i be the momentum exchanged by each of the two protons, with the convention, as for DIS, that the direction of q_i is incoming with respect to the proton vertex (see Fig. 2.1),

$$q_i = P_{X_i} - P_i \,. \tag{A.3}$$

We parameterize q_i in terms of the two light-like momenta P_i and the transverse components $\mathbf{q_i^\perp}$:

$$q_1 = \frac{2P_1\cdot q_1}{2P_1\cdot P_2}P_2 + \frac{2P_2\cdot q_1}{2P_1\cdot P_2}P_1 + \mathbf{q_1^\perp}\,, \tag{A.4}$$

$$q_2 = \frac{2P_2\cdot q_2}{2P_1\cdot P_2}P_1 + \frac{2P_1\cdot q_2}{2P_1\cdot P_2}P_2 + \mathbf{q_2^\perp}\,. \tag{A.5}$$

The Bjorken scaling variables x_i for the DIS process are given by the scalar products $P_i\cdot q_i$

$$2P_i\cdot q_i = \frac{-q_i^2}{x_i} = \frac{Q_i^2}{x_i}, \tag{A.6}$$

where $Q_i^2 = -q_i^2$. In analogy one can also define variables y_i via the relation

$$2P_2\cdot q_1 = \frac{Q_1^2}{y_1}, \qquad 2P_1\cdot q_2 = \frac{Q_2^2}{y_2}, \tag{A.7}$$

so that

$$y_i = -\frac{Q_i^4}{x_i S\,(Q_i^2 - q_i^{\perp\,2})}, \tag{A.8}$$

with $q_i^\perp = \sqrt{\left|\mathbf{q_i^{\perp\,2}}\right|}$.
Then, the integration measure can be expressed as

$$d^4q_i = dQ_i^2\; d^2\mathbf{q_i^\perp}\;\frac{dx_i}{2x_i}, \tag{A.9}$$

and

$$P_{X_i}^2 = Q_i^2\left(\frac{1}{x_i} - 1\right). \tag{A.10}$$

The phase space Eq. (A.2) reduces now to the following form,

$$dPS \;=\; \frac{1}{(2\pi)^2}\prod_{i=1,2} dQ_i^2\; d^2\mathbf{q_i^\perp}\;\frac{dx_i}{2x_i}\; dPS_n(K_1,\ldots,K_n)\;(2\pi)^4\delta^4\left(q_1+q_2+\sum_{j=1,n}K_j\right), \tag{A.11}$$

and the integrations on the transverse components can be cast in polar coordinates,

$$d^2\mathbf{q_1^\perp}\; d^2\mathbf{q_2^\perp} \;=\; q_1^\perp\; dq_1^\perp d\varphi_1\; q_2^\perp\; dq_2^\perp d\varphi_2 = 2\pi\; q_1^\perp\; dq_1^\perp\; q_2^\perp\; dq_2^\perp d\varphi_{12}\,. \tag{A.12}$$

The momentum-conservation condition imposed by the Dirac delta-function in Eq. (A.11) allows to write a relation between the proton remnants variables and the total energy of the VBF products:

$$\begin{aligned} S_{VBF} &= (K_1+\ldots+K_n)^2 = (q_1+q_2)^2 = \\ &= \frac{1}{Q_1^2Q_2^2}S\,x_1x_2\left(Q_1^2 - q_1^{\perp\,2}\right)\left(Q_2^2 - q_2^{\perp\,2}\right) + \frac{Q_1^2Q_2^2}{S\,x_1x_2} - Q_1^2 - Q_2^2 - 2q_1^\perp q_2^\perp\cos\varphi_{12}\,. \end{aligned} \tag{A.13}$$

Using this equation one can generate the phase space of the VBF-produced particles once the proton remnants variables are fixed, simply in the same way as for the decay of a particle.

We will finally go through the details of the case in which only one particle with mass m and momentum K is produced via VBF. In this case we simply have

$$dPS_1(K) = \frac{d^4K}{(2\pi)^4}\, 2\pi\delta\left(K^2 - m^2\right), \tag{A.14}$$

and the d^4K integration can be eliminated using the momentum-conservation Dirac delta-function, so that we just need to solve the mass-shell condition imposed by the delta-function in Eq. (A.14) (which is nothing but Eq. (A.13) with $S_{VBF} = m^2$):

$$m^2 = \frac{1}{Q_1^2 Q_2^2} S\, x_1 x_2 \left(Q_1^2 - q_1^{\perp 2}\right)\left(Q_2^2 - q_2^{\perp 2}\right) + \frac{Q_1^2 Q_2^2}{S\, x_1 x_2} - Q_1^2 - Q_2^2 - 2q_1^\perp q_2^\perp \cos\varphi_{12}\,. \tag{A.15}$$

This equation can, of course, be easily solved for $\cos\varphi_{12}$, but in this case it would lead to an (integrable) singularity in the Jacobian, and therefore to numerical problems. Therefore, our choice has been to write Eq. (A.15) as a second degree equation for $q_2^\perp$:

$$A q_2^{\perp 2} + B q_2^\perp + C = 0\,, \tag{A.16}$$

with

$$A = \frac{S\, x_1 x_2 \left(q_1^{\perp 2} - Q_1^2\right)}{Q_1^2 Q_2^2}, \tag{A.17}$$

$$B = -2q_1^\perp \cos\varphi_{12}\,, \tag{A.18}$$

$$C = \frac{Q_1^2 Q_2^2}{S\, x_1 x_2} - \frac{S\, x_1 x_2 q_1^\perp}{Q_1^2} + S\, x_1 x_2 - m^2 - Q_1^2 - Q_2^2\,. \tag{A.19}$$

Since two solutions of $q_2^\perp$ exist for each set of parameters x_1, x_2, Q_1^2, Q_2^2, $q_1^\perp$, φ, two phase space points are evaluated. We require "physical" phase space points to have positive $q_2^\perp$ and the number of rejected points can be greatly reduced if one asks

$$0 < Q_2^2 < S\, x_1 x_2 \frac{\left(Q_1^2 - q_1^{\perp 2}\right)\left[Q_1^4 - Q_1^2\left(S\, x_1 x_2 - m^2\right) + q_1^{\perp 2} S\, x_1 x_2\right]}{Q_1^2\left[Q_1^4 - Q_1^2\left(q_1^{\perp 2}\sin^2\varphi_{12} + S\, x_1 x_2\right) + q_1^{\perp 2} S\, x_1 x_2\right]}, \tag{A.20}$$

which corresponds to the positivity of the discriminant of Eq. (A.16). The other parameters are generated in the following ranges:

$$\begin{aligned} &x_1 \cdot x_2 \in \left[\frac{m^2}{S}, 1\right], \qquad \log x_1 \in \left[\log\frac{m^2}{S}, 0\right], \qquad Q_1^2 \in \left[Q_0^2, \left(\sqrt{S} - m\right)^2\right], \\ &q_1^\perp \in [0, Q_1]\,, \qquad \varphi \in [0, 2\pi]\,, \end{aligned} \tag{A.21}$$

where Q_0 is a technical cut set to 1 GeV which prevents sampling PDFs and α_s at too low scales. It also sets the lower bound for Q_2 and we have checked the independence of the cross section results on value of Q_0. The differential cross-section from Eq. (3.2), multiplied by the Jacobian corresponding to Eqs. (A.20)–(A.21), is integrated using VEGAS [108].

A.2 The VBF cross-section with anomalous VVH couplings

We report here the formula corresponding to Eq. (3.5) for the vertex in Eq. (5.1). We rewrite it as:

$$\Gamma^{\mu\nu}(q_1,q_2) = A_1 g_{\mu\nu} + A_2\left(q_1\cdot q_2 g^{\mu\nu} - q_2^{\mu} q_1^{\nu}\right) + A_3 \varepsilon^{\mu\nu\rho\sigma} q_{1\rho} q_{2\sigma}, \tag{A.22}$$

where we have set

$$\begin{aligned} A_1 &= 2M_V^2\left(\left(\sqrt{2}G_F\right)^{1/2} + \frac{a_1}{\Lambda}\right), \\ A_2 &= \frac{a_2}{\Lambda}, \\ A_3 &= \frac{a_3}{\Lambda}. \end{aligned} \tag{A.23}$$

Eq. (3.5), with the replacement $\mathcal{M}^{\mu\nu} = \Gamma^{\mu\nu}(q_1,q_2)$ has now the form:

$$W_{\mu\nu}\left(x_1,Q_1^2\right)\mathcal{M}^{\mu\rho}\mathcal{M}^{*\nu\sigma}W_{\rho\sigma}\left(x_2,Q_2^2\right) = \sum_{i,j=1}^{3} C_{ij}F_i\left(x_1,Q_1^2\right)F_j\left(x_2,Q_2^2\right). \tag{A.24}$$

Defining

$$q_1\cdot q_2 = q_{12}, \qquad P_a\cdot q_b = P_{ab}, \tag{A.25}$$

the non-vanishing C_{ij} read

$$\begin{aligned} C_{11} &= \left(2+\frac{{q_{12}}^2}{{q_1}^2\,{q_2}^2}\right)|A_1|^2 + 6\,q_{12}\,\mathrm{Re}\left(A_1A_2^*\right) + \left({q_1}^2\,{q_2}^2 + 2\,{q_{12}}^2\right)|A_2|^2 \\ &\quad +2\left({q_{12}}^2 - {q_1}^2\,{q_2}^2\right)|A_3|^2, \end{aligned} \tag{A.26}$$

$$\begin{aligned} C_{12} &= \frac{1}{P_{22}}\left[\frac{{P_{22}}^2}{{q_2}^2} + \frac{1}{{q_1}^2}\left(P_{21} - \frac{P_{22}}{{q_2}^2}\,q_{12}\right)^2\right]|A_1|^2 + 2\frac{P_{22}\,q_{12}}{{q_2}^2}\,\mathrm{Re}\left(A_1A_2^*\right) \\ &\quad + P_{21}\left(2\,q_{12} - \frac{P_{21}\,{q_2}^2}{P_{22}}\right)|A_2|^2 + \left(2\,P_{21}\,q_{12} - \frac{{P_{21}}^2\,{q_2}^2}{P_{22}} - P_{22}\;{q_1}^2\right)|A_3|^2, \end{aligned} \tag{A.27}$$

$$\begin{aligned} C_{21} &= \frac{1}{P_{11}}\left[\frac{{P_{11}}^2}{{q_1}^2} + \frac{1}{{q_2}^2}\left(P_{12} - \frac{P_{11}}{{q_1}^2}\,q_{12}\right)^2\right]|A_1|^2 + 2\frac{P_{11}\,q_{12}}{{q_1}^2}\,\mathrm{Re}\left(A_1A_2^*\right) \\ &\quad + \left(2\,P_{12}\,q_{12} - \frac{{P_{12}}^2\;{q_1}^2}{P_{11}}\right)|A_2|^2 + \left(2\,P_{12}\,q_{12} - \frac{{P_{12}}^2\;{q_1}^2}{P_{11}} - P_{11}\,{q_2}^2\right)|A_3|^2, \end{aligned} \tag{A.28}$$

$$\begin{aligned} C_{22} &= \frac{1}{P_{11}\,P_{22}}\left(\frac{s}{2} - \frac{P_{11}\,P_{21}}{{q_1}^2} - \frac{P_{12}\,P_{22}}{{q_2}^2} + \frac{P_{11}\,P_{22}\,q_{12}}{{q_1}^2\,{q_2}^2}\right)^2|A_1|^2 \\ &\quad -2\left(P_{12}\,P_{21} - q_{12}\,\frac{s}{2}\right)\left(\frac{q_{12}}{{q_1}^2\,{q_2}^2} + \frac{s}{2\,P_{11}\,P_{22}} - \frac{P_{21}}{P_{22}\;{q_1}^2} - \frac{P_{12}}{P_{11}\,{q_2}^2}\right)\mathrm{Re}\left(A_1A_2^*\right) \\ &\quad +2\left(\frac{q_{12}}{{q_1}^2\,{q_2}^2} + \frac{s}{2\,P_{11}\,P_{22}} - \frac{P_{21}}{P_{22}\;{q_1}^2} - \frac{P_{12}}{P_{11}\,{q_2}^2}\right)\varepsilon_{\mu\nu\rho\sigma}P_1^{\mu}P_2^{\nu}\;{q_1}^{\rho}\,{q_2}^{\sigma}\;\mathrm{Re}\left(A_1A_3^*\right) \\ &\quad +\frac{(\,q_{12}\,s - 2\,P_{12}\,P_{21})^2}{4\,P_{11}\,P_{22}}|A_2|^2 - \frac{P_{12}\,P_{21} - q_{12}\,s}{P_{11}\,P_{22}}\,\varepsilon_{\mu\nu\rho\sigma}P_1^{\mu}P_2^{\nu}\;{q_1}^{\rho}\,{q_2}^{\sigma}\;\mathrm{Re}\left(A_2A_3^*\right) \\ &\quad +\left\{s\left(q_{12} - \frac{P_{21}\,{q_2}^2}{P_{22}} - \frac{P_{12}\;{q_1}^2}{P_{11}} + \frac{P_{12}\,P_{21}\,q_{12}}{P_{11}\,P_{22}}\right)\right. \end{aligned}$$

$$+\frac{1}{P_{11}\,P_{22}}\left[\frac{s^2}{4}\left(q_1{}^2\,q_2{}^2-q_{12}{}^2\right)-P_{12}{}^2\,P_{21}{}^2\right]-P_{11}\,P_{22}+2\,P_{12}\,P_{21}\Big\}|A_3|^2, \qquad \text{(A.29)}$$

$$\begin{aligned}
C_{33} \;=\;& \frac{q_{12}\,s-2\,P_{12}\,P_{21}}{2\,P_{11}\,P_{22}}|A_1|^2+\frac{1}{2}\left[\frac{s}{2\,P_{11}\,P_{22}}\left(q_1{}^2\,q_2{}^2+q_{12}{}^2\right)+q_{12}-\frac{P_{12}\;q_1{}^2}{P_{11}}-\frac{P_{21}\,q_2{}^2}{P_{22}}\right.\\
&\left.-\frac{P_{12}\,P_{21}\,q_{12}}{P_{11}\,P_{22}}\right]\mathrm{Re}\left(A_1A_2^*\right)+\frac{q_{12}}{2\,P_{11}\,P_{22}}\,\varepsilon_{\mu\nu\rho\sigma}P_1^\mu P_2^\nu\;q_1{}^\rho\,q_2{}^\sigma\;\mathrm{Re}\left(A_1A_3^*\right)\\
&+\frac{q_{12}}{2}\left(q_{12}-\frac{P_{12}\;q_1{}^2}{P_{11}}-\frac{P_{21}\,q_2{}^2}{P_{22}}+\frac{s\,q_1{}^2\,q_2{}^2}{2\,P_{11}\,P_{22}}\right)|A_2|^2\\
&+\frac{q_1{}^2\,q_2{}^2}{2\,P_{11}\,P_{22}}\,\varepsilon_{\mu\nu\rho\sigma}P_1^\mu P_2^\nu\;q_1{}^\rho\,q_2{}^\sigma\;\mathrm{Re}\left(A_2A_3^*\right)\\
&+\frac{q_{12}}{2}\left(q_{12}-\frac{P_{12}\;q_1{}^2}{P_{11}}-\frac{P_{21}\,q_2{}^2}{P_{22}}+\frac{P_{12}\,P_{21}\,q_1{}^2\,q_2{}^2}{P_{11}\,P_{22}\,q_{12}}\right)|A_3|^2. \qquad \text{(A.30)}
\end{aligned}$$

A.3 The VBF cross-section for a vector resonance

Finally, we give the formula for the total cross-section for the production of a vector resonance in the structure function approach.
We assume the usual gauge and Lorentz invariant tri-linear vertex:

$$\Gamma^{\mu_1\mu_2\mu_3}(p_1,p_2,p_3)=g_{123}\left[g^{\mu_1\mu_2}\left(p_1^{\mu_3}-p_2^{\mu_3}\right)+g^{\mu_2\mu_3}\left(p_2^{\mu_1}-p_3^{\mu_1}\right)+g^{\mu_3\mu_1}\left(p_3^{\mu_2}-p_1^{\mu_2}\right)\right], \qquad \text{(A.31)}$$

where all the momenta are taken to flow outside the vertex. Since in the processes that we have considered the coupling g_{123} can always be factorized from the total cross-section, we will set it to unity.
As in Sec. A.2, with the extra care to sum over the polarizations of the produced vector, we have

$$W_{\mu\nu}\left(x_1,Q_1^2\right)\sum_\lambda\left(\mathcal{M}_\lambda^{\mu\rho}\mathcal{M}^{*\nu\sigma}_{\;\lambda}\right)W_{\rho\sigma}\left(x_2,Q_2^2\right)=\sum_{i,j=1}^{3}C_{ij}F_i\left(x_1,Q_1^2\right)F_j\left(x_2,Q_2^2\right), \qquad \text{(A.32)}$$

where we have set

$$\mathcal{M}_\lambda^{\mu\nu}=\Gamma_\rho^{\mu\nu}(q_1,q_2,-q_1-q_2)\,\epsilon_\lambda^\rho(-q_1-q_2), \qquad \text{(A.33)}$$

and the non-vanishing coefficients C_{ij} are

$$\begin{aligned}
C_{11} \;=\;& \frac{1}{q_1{}^2\,q_2{}^2}\left[4\,q_1{}^2\,q_2{}^2\,q_{12}-14\,q_1{}^4\,q_2{}^2-14\;q_1{}^2\,q_2{}^4+11\;q_1{}^2\,q_{12}{}^2+11q_2^2\,q_{12}{}^2+2\,q_{12}{}^3\right.\\
&\left.+\frac{1}{m_{V'}^2}\left(q_1{}^2-q_2{}^2\right)^2\left(2\,q_1{}^2\,q_2{}^2+q_{12}{}^2\right)\right], \qquad \text{(A.34)}\\
C_{12} \;=\;& \frac{-1}{P_{22}\;q_1{}^2\,q_2{}^4}\left[-11\,P_{21}{}^2\;q_1{}^2\,q_2{}^4-2\,P_{21}{}^2\,q_{12}\,q_2{}^4+P_{21}{}^2\,q_2{}^6+22\,P_{21}\,P_{22}\;q_1{}^2\,q_{12}\,q_2{}^2\right.\\
&+4\,P_{21}\,P_{22}\,q_{12}{}^2\,q_2{}^2-2\,P_{21}\,P_{22}\,q_{12}\,q_2{}^4+P_{22}{}^2\;q_1{}^4\,q_2{}^2-11P_{22}{}^2\;q_1{}^2\,q_{12}{}^2\\
&-2\,P_{22}{}^2\;q_1{}^2\,q_{12}\,q_2{}^2+5P_{22}{}^2\;q_1{}^2\,q_2{}^4-2P_{22}{}^2\,q_{12}{}^3-3\,P_{22}{}^2\,q_{12}{}^2\,q_2{}^2\\
&\left.-\frac{1}{m_{V'}^2}\left(q_1{}^2-q_2{}^2\right)^2\left(P_2q_1{}^2\,q_2{}^{2\,2}-2\,P_{21}\,P_{22}\,q_{12}\,q_2{}^2+P_{22}{}^2\,q_1{}^2\,q_2{}^2+P_{22}{}^2\,q_{12}{}^2\right)\right],
\end{aligned}$$

(A.35)

$$C_{21} = C_{12}\ (1 \leftrightarrow 2), \tag{A.36}$$

$$\begin{aligned} C_{22} = {} & \frac{1}{P_{11}\,P_{22}\ {q_1}^4\,{q_2}^4} \Big\{ 3{P_{11}}^2\,{P_{21}}^2\ {q_1}^2\,{q_2}^4 + 2\,{P_{11}}^2\,{P_{21}}^2\,q_{12}\,{q_2}^4 - {P_{11}}^2\,{P_{21}}^2\,{q_2}^6 \\ & -6\,{P_{11}}^2\,P_{21}\,P_{22}\ {q_1}^2\,q_{12}\,{q_2}^2 - 4\,{P_{11}}^2\,P_{21}\,P_{22}\,{q_{12}}^2\,{q_2}^2 + 2\,{P_{11}}^2\,P_{21}\,P_{22}\,q_{12}\,{q_2}^4 \\ & +3\,{P_{11}}^2\,{P_{22}}^2\ {q_1}^2\,{q_{12}}^2 + 2\,{P_{11}}^2\,{P_{22}}^2\,{q_{12}}^3 + 3\,{P_{11}}^2\,{P_{22}}^2\,{q_{12}}^2\,{q_2}^2 \\ & -2\,P_{11}\,P_{12}\,P_{21}\,P_{22}\ {q_1}^4\,{q_2}^2 + 4\,P_{11}\,P_{12}\,P_{21}\,P_{22}\ {q_1}^2\,q_{12}\,{q_2}^2 - 2\,P_{11}\,P_{12}\,P_{21}\,P_{22}\ {q_1}^2\,{q_2}^4 \\ & +2\,P_{11}\,P_{12}\,{P_{22}}^2\ {q_1}^4\,q_{12} - 4\,P_{11}\,P_{12}\,{P_{22}}^2\ {q_1}^2\,{q_{12}}^2 - 6\,P_{11}\,P_{12}\,{P_{22}}^2\ {q_1}^2\,q_{12}\,{q_2}^2 \\ & -{P_{12}}^2\,{P_{22}}^2\ {q_1}^6 + 2\,{P_{12}}^2\,{P_{22}}^2\ {q_1}^4\,q_{12} + 3\,{P_{12}}^2\,{P_{22}}^2\ {q_1}^4\,{q_2}^2 \\ & +s\ {q_1}^2\,{q_2}^2\,(q_1 - q_2)^2 \left(P_{11}\,P_{21}\,{q_2}^2 - P_{11}\,P_{22}\,q_{12} + P_{12}\,P_{22}\ {q_1}^2 \right) - \frac{s^2}{4}\ {q_1}^4\,{q_2}^4\,(q_1 - q_2)^2 \\ & +\frac{1}{4\,m_{V'}^2} \left({q_1}^2 - {q_2}^2 \right)^2 \left(2\,P_{11}\,P_{21}\,{q_2}^2 - 2\,P_{11}\,P_{22}\,q_{12} + 2\,P_{12}\,P_{22}\,{q_1}^2 - s\,{q_1}^2\,{q_2}^2 \right)^2 \Big\}, \end{aligned} \tag{A.37}$$

$$\begin{aligned} C_{33} = {} & \frac{1}{2\,P_{11}\,P_{22}} \Bigg[-8\,P_{11}\,P_{21}\,{q_2}^2 + 8\,P_{11}\,P_{22}\,q_{12} + P_{12}\,P_{21}\ {q_1}^2 + 6\,P_{12}\,P_{21}\,q_{12} + \\ & P_{12}\,P_{21}\,{q_2}^2 - 8\,P_{12}\,P_{22}\ {q_1}^2 - \frac{s}{2} \left({q_1}^2\,q_{12} - 8\,{q_1}^2\,{q_2}^2 + 6\,{q_{12}}^2 + q_{12}\,{q_2}^2 \right) \\ & +\frac{1}{m_{V'}^2} \left({q_1}^2 - {q_2}^2 \right)^2 \left(-P_{12}\,P_{21} + \frac{s}{2}\,q_{12} \right) \Bigg]. \end{aligned} \tag{A.38}$$

B VBF cross sections

We present the VBF cross sections for the Tevatron in Tabs. B.1–B.5, and for the LHC in Tabs. B.6–B.10 and in Tabs. B.11–B.15, respectively. The PDF sets used and all other parameters are given in the table captions.

m_H [GeV]	σ_{LO}	σ_{NLO}	σ_{NNLO}
90	$1.206^{+0.363+0.012}_{-0.233-0.012}\cdot 10^{-1}$	$1.220^{+0.103+0.012}_{-0.056-0.012}\cdot 10^{-1}$	$1.241^{+0.034+0.012}_{-0.011-0.012}\cdot 10^{-1}$
95	$1.108^{+0.342+0.011}_{-0.218-0.011}\cdot 10^{-1}$	$1.123^{+0.096+0.011}_{-0.053-0.011}\cdot 10^{-1}$	$1.144^{+0.030+0.011}_{-0.012-0.011}\cdot 10^{-1}$
100	$1.019^{+0.322+0.010}_{-0.204-0.010}\cdot 10^{-1}$	$1.035^{+0.091+0.011}_{-0.052-0.011}\cdot 10^{-1}$	$1.054^{+0.029+0.011}_{-0.010-0.011}\cdot 10^{-1}$
105	$9.387^{+3.025+0.098}_{-1.906-0.098}\cdot 10^{-2}$	$9.551^{+0.841+0.100}_{-0.497-0.100}\cdot 10^{-2}$	$9.737^{+0.258+0.099}_{-0.113-0.099}\cdot 10^{-2}$
110	$8.652^{+2.847+0.092}_{-1.786-0.092}\cdot 10^{-2}$	$8.814^{+0.788+0.093}_{-0.474-0.093}\cdot 10^{-2}$	$8.990^{+0.247+0.093}_{-0.106-0.093}\cdot 10^{-2}$
115	$7.975^{+2.681+0.086}_{-1.666-0.086}\cdot 10^{-2}$	$8.146^{+0.724+0.088}_{-0.456-0.088}\cdot 10^{-2}$	$8.308^{+0.224+0.087}_{-0.107-0.087}\cdot 10^{-2}$
120	$7.360^{+2.519+0.081}_{-1.560-0.081}\cdot 10^{-2}$	$7.533^{+0.681+0.082}_{-0.427-0.082}\cdot 10^{-2}$	$7.679^{+0.214+0.082}_{-0.099-0.082}\cdot 10^{-2}$
125	$6.795^{+2.372+0.076}_{-1.457-0.076}\cdot 10^{-2}$	$6.965^{+0.635+0.077}_{-0.402-0.077}\cdot 10^{-2}$	$7.107^{+0.193+0.076}_{-0.094-0.076}\cdot 10^{-2}$
130	$6.280^{+2.234+0.071}_{-1.365-0.071}\cdot 10^{-2}$	$6.454^{+0.585+0.072}_{-0.388-0.072}\cdot 10^{-2}$	$6.581^{+0.183+0.072}_{-0.089-0.072}\cdot 10^{-2}$
135	$5.805^{+2.100+0.067}_{-1.275-0.067}\cdot 10^{-2}$	$5.972^{+0.561+0.068}_{-0.370-0.068}\cdot 10^{-2}$	$6.098^{+0.169+0.067}_{-0.088-0.067}\cdot 10^{-2}$
140	$5.370^{+1.981+0.063}_{-1.194-0.063}\cdot 10^{-2}$	$5.541^{+0.516+0.064}_{-0.358-0.064}\cdot 10^{-2}$	$5.652^{+0.158+0.063}_{-0.081-0.063}\cdot 10^{-2}$
145	$4.972^{+1.862+0.059}_{-1.116-0.059}\cdot 10^{-2}$	$5.133^{+0.488+0.060}_{-0.330-0.060}\cdot 10^{-2}$	$5.246^{+0.146+0.059}_{-0.084-0.059}\cdot 10^{-2}$
150	$4.608^{+1.748+0.055}_{-1.048-0.055}\cdot 10^{-2}$	$4.763^{+0.460+0.056}_{-0.314-0.056}\cdot 10^{-2}$	$4.867^{+0.136+0.056}_{-0.077-0.056}\cdot 10^{-2}$
155	$4.271^{+1.643+0.052}_{-0.981-0.052}\cdot 10^{-2}$	$4.423^{+0.426+0.053}_{-0.303-0.053}\cdot 10^{-2}$	$4.520^{+0.126+0.052}_{-0.076-0.052}\cdot 10^{-2}$
160	$3.958^{+1.551+0.049}_{-0.916-0.049}\cdot 10^{-2}$	$4.108^{+0.401+0.050}_{-0.287-0.050}\cdot 10^{-2}$	$4.199^{+0.119+0.049}_{-0.071-0.049}\cdot 10^{-2}$
165	$3.673^{+1.452+0.046}_{-0.860-0.046}\cdot 10^{-2}$	$3.818^{+0.375+0.047}_{-0.271-0.047}\cdot 10^{-2}$	$3.905^{+0.108+0.046}_{-0.071-0.046}\cdot 10^{-2}$
170	$3.410^{+1.367+0.043}_{-0.807-0.043}\cdot 10^{-2}$	$3.549^{+0.351+0.044}_{-0.257-0.044}\cdot 10^{-2}$	$3.630^{+0.102+0.043}_{-0.067-0.043}\cdot 10^{-2}$
175	$3.166^{+1.289+0.040}_{-0.757-0.040}\cdot 10^{-2}$	$3.302^{+0.328+0.041}_{-0.245-0.041}\cdot 10^{-2}$	$3.377^{+0.096+0.041}_{-0.064-0.041}\cdot 10^{-2}$
180	$2.941^{+1.211+0.038}_{-0.709-0.038}\cdot 10^{-2}$	$3.073^{+0.309+0.039}_{-0.231-0.039}\cdot 10^{-2}$	$3.143^{+0.089+0.038}_{-0.061-0.038}\cdot 10^{-2}$
185	$2.733^{+1.142+0.036}_{-0.664-0.036}\cdot 10^{-2}$	$2.861^{+0.290+0.036}_{-0.220-0.036}\cdot 10^{-2}$	$2.927^{+0.084+0.036}_{-0.059-0.036}\cdot 10^{-2}$
190	$2.541^{+1.076+0.034}_{-0.623-0.034}\cdot 10^{-2}$	$2.664^{+0.272+0.034}_{-0.208-0.034}\cdot 10^{-2}$	$2.727^{+0.077+0.034}_{-0.057-0.034}\cdot 10^{-2}$
195	$2.364^{+1.012+0.032}_{-0.585-0.032}\cdot 10^{-2}$	$2.482^{+0.255+0.032}_{-0.198-0.032}\cdot 10^{-2}$	$2.541^{+0.072+0.032}_{-0.054-0.032}\cdot 10^{-2}$
200	$2.199^{+0.953+0.030}_{-0.549-0.030}\cdot 10^{-2}$	$2.314^{+0.239+0.030}_{-0.188-0.030}\cdot 10^{-2}$	$2.369^{+0.069+0.030}_{-0.051-0.030}\cdot 10^{-2}$
210	$1.906^{+0.845+0.026}_{-0.483-0.026}\cdot 10^{-2}$	$2.012^{+0.211+0.027}_{-0.168-0.027}\cdot 10^{-2}$	$2.061^{+0.060+0.027}_{-0.046-0.027}\cdot 10^{-2}$
220	$1.654^{+0.750+0.023}_{-0.425-0.023}\cdot 10^{-2}$	$1.752^{+0.184+0.024}_{-0.151-0.024}\cdot 10^{-2}$	$1.795^{+0.051+0.024}_{-0.043-0.024}\cdot 10^{-2}$
230	$1.437^{+0.666+0.021}_{-0.375-0.021}\cdot 10^{-2}$	$1.527^{+0.164+0.021}_{-0.135-0.021}\cdot 10^{-2}$	$1.565^{+0.045+0.021}_{-0.039-0.021}\cdot 10^{-2}$
240	$1.249^{+0.592+0.018}_{-0.331-0.018}\cdot 10^{-2}$	$1.333^{+0.145+0.019}_{-0.122-0.019}\cdot 10^{-2}$	$1.367^{+0.039+0.019}_{-0.035-0.019}\cdot 10^{-2}$
250	$1.088^{+0.526+0.016}_{-0.292-0.016}\cdot 10^{-2}$	$1.164^{+0.128+0.017}_{-0.110-0.017}\cdot 10^{-2}$	$1.194^{+0.035+0.017}_{-0.032-0.017}\cdot 10^{-2}$
260	$9.480^{+4.669+0.145}_{-2.576-0.145}\cdot 10^{-3}$	$1.018^{+0.114+0.015}_{-0.099-0.015}\cdot 10^{-2}$	$1.045^{+0.030+0.015}_{-0.030-0.015}\cdot 10^{-2}$
270	$8.269^{+4.155+0.129}_{-2.276-0.129}\cdot 10^{-3}$	$8.912^{+1.007+0.132}_{-0.883-0.132}\cdot 10^{-3}$	$9.148^{+0.268+0.132}_{-0.268-0.132}\cdot 10^{-3}$
280	$7.220^{+3.690+0.114}_{-2.013-0.114}\cdot 10^{-3}$	$7.806^{+0.889+0.118}_{-0.795-0.118}\cdot 10^{-3}$	$8.016^{+0.239+0.117}_{-0.244-0.117}\cdot 10^{-3}$
290	$6.307^{+3.284+0.102}_{-1.778-0.102}\cdot 10^{-3}$	$6.843^{+0.789+0.105}_{-0.714-0.105}\cdot 10^{-3}$	$7.030^{+0.204+0.104}_{-0.221-0.104}\cdot 10^{-3}$
300	$5.517^{+2.918+0.091}_{-1.576-0.091}\cdot 10^{-3}$	$6.002^{+0.700+0.093}_{-0.642-0.093}\cdot 10^{-3}$	$6.171^{+0.180+0.093}_{-0.204-0.093}\cdot 10^{-3}$

Table B.1: Total VBF cross sections at the Tevatron, $\sqrt{S} = 1.96\,\text{TeV}$ at LO, NLO and NNLO in QCD. Errors shown are respectively scale and PDF uncertainities. Scale uncertainities are evaluated by varying μ_r and μ_f in the interval $\mu_r, \mu_f \in [Q/4, 4Q]$. The ABKM [70] PDF set has been used. Numbers are in pb.

m_H [GeV]	σ_{LO}	σ_{NLO}	σ_{NNLO}
90	$1.199^{+0.349+0.029}_{-0.226-0.029}\cdot 10^{-1}$	$1.210^{+0.103+0.030}_{-0.053-0.030}\cdot 10^{-1}$	$1.207^{+0.037+0.030}_{-0.010-0.030}\cdot 10^{-1}$
95	$1.103^{+0.329+0.026}_{-0.212-0.026}\cdot 10^{-1}$	$1.113^{+0.098+0.027}_{-0.050-0.027}\cdot 10^{-1}$	$1.112^{+0.033+0.027}_{-0.010-0.027}\cdot 10^{-1}$
100	$1.014^{+0.310+0.024}_{-0.198-0.024}\cdot 10^{-1}$	$1.028^{+0.088+0.025}_{-0.050-0.025}\cdot 10^{-1}$	$1.025^{+0.031+0.025}_{-0.009-0.025}\cdot 10^{-1}$
105	$9.332^{+2.923+0.225}_{-1.849-0.225}\cdot 10^{-2}$	$9.467^{+0.838+0.234}_{-0.465-0.234}\cdot 10^{-2}$	$9.458^{+0.293+0.234}_{-0.094-0.234}\cdot 10^{-2}$
110	$8.600^{+2.749+0.207}_{-1.733-0.207}\cdot 10^{-2}$	$8.744^{+0.784+0.216}_{-0.442-0.216}\cdot 10^{-2}$	$8.732^{+0.270+0.216}_{-0.088-0.216}\cdot 10^{-2}$
115	$7.930^{+2.593+0.191}_{-1.623-0.191}\cdot 10^{-2}$	$8.076^{+0.741+0.200}_{-0.425-0.200}\cdot 10^{-2}$	$8.074^{+0.247+0.200}_{-0.092-0.200}\cdot 10^{-2}$
120	$7.317^{+2.439+0.177}_{-1.519-0.177}\cdot 10^{-2}$	$7.467^{+0.692+0.185}_{-0.406-0.185}\cdot 10^{-2}$	$7.464^{+0.232+0.185}_{-0.087-0.185}\cdot 10^{-2}$
125	$6.755^{+2.298+0.163}_{-1.419-0.163}\cdot 10^{-2}$	$6.906^{+0.646+0.171}_{-0.385-0.171}\cdot 10^{-2}$	$6.904^{+0.217+0.171}_{-0.081-0.171}\cdot 10^{-2}$
130	$6.243^{+2.170+0.151}_{-1.330-0.151}\cdot 10^{-2}$	$6.389^{+0.603+0.159}_{-0.357-0.159}\cdot 10^{-2}$	$6.393^{+0.203+0.159}_{-0.079-0.159}\cdot 10^{-2}$
135	$5.771^{+2.036+0.140}_{-1.245-0.140}\cdot 10^{-2}$	$5.922^{+0.563+0.147}_{-0.353-0.147}\cdot 10^{-2}$	$5.923^{+0.188+0.147}_{-0.078-0.147}\cdot 10^{-2}$
140	$5.340^{+1.916+0.130}_{-1.166-0.130}\cdot 10^{-2}$	$5.488^{+0.527+0.137}_{-0.330-0.137}\cdot 10^{-2}$	$5.491^{+0.175+0.137}_{-0.076-0.137}\cdot 10^{-2}$
145	$4.944^{+1.803+0.120}_{-1.091-0.120}\cdot 10^{-2}$	$5.089^{+0.490+0.127}_{-0.313-0.127}\cdot 10^{-2}$	$5.093^{+0.163+0.127}_{-0.071-0.127}\cdot 10^{-2}$
150	$4.580^{+1.700+0.111}_{-1.023-0.111}\cdot 10^{-2}$	$4.722^{+0.462+0.118}_{-0.300-0.118}\cdot 10^{-2}$	$4.729^{+0.148+0.118}_{-0.072-0.118}\cdot 10^{-2}$
155	$4.242^{+1.605+0.103}_{-0.956-0.103}\cdot 10^{-2}$	$4.385^{+0.431+0.109}_{-0.285-0.109}\cdot 10^{-2}$	$4.390^{+0.140+0.110}_{-0.068-0.110}\cdot 10^{-2}$
160	$3.935^{+1.509+0.096}_{-0.897-0.096}\cdot 10^{-2}$	$4.072^{+0.404+0.102}_{-0.270-0.102}\cdot 10^{-2}$	$4.077^{+0.130+0.102}_{-0.065-0.102}\cdot 10^{-2}$
165	$3.652^{+1.419+0.089}_{-0.844-0.089}\cdot 10^{-2}$	$3.784^{+0.380+0.095}_{-0.257-0.095}\cdot 10^{-2}$	$3.791^{+0.120+0.095}_{-0.064-0.095}\cdot 10^{-2}$
170	$3.390^{+1.335+0.083}_{-0.791-0.083}\cdot 10^{-2}$	$3.518^{+0.353+0.088}_{-0.242-0.088}\cdot 10^{-2}$	$3.524^{+0.114+0.088}_{-0.061-0.088}\cdot 10^{-2}$
175	$3.146^{+1.258+0.077}_{-0.740-0.077}\cdot 10^{-2}$	$3.273^{+0.331+0.082}_{-0.232-0.082}\cdot 10^{-2}$	$3.279^{+0.107+0.082}_{-0.058-0.082}\cdot 10^{-2}$
180	$2.923^{+1.185+0.072}_{-0.695-0.072}\cdot 10^{-2}$	$3.045^{+0.312+0.076}_{-0.219-0.076}\cdot 10^{-2}$	$3.052^{+0.098+0.077}_{-0.057-0.077}\cdot 10^{-2}$
185	$2.716^{+1.117+0.067}_{-0.652-0.067}\cdot 10^{-2}$	$2.836^{+0.293+0.071}_{-0.209-0.071}\cdot 10^{-2}$	$2.842^{+0.092+0.071}_{-0.054-0.071}\cdot 10^{-2}$
190	$2.524^{+1.051+0.062}_{-0.610-0.062}\cdot 10^{-2}$	$2.640^{+0.275+0.066}_{-0.198-0.066}\cdot 10^{-2}$	$2.648^{+0.085+0.067}_{-0.052-0.067}\cdot 10^{-2}$
195	$2.348^{+0.990+0.058}_{-0.574-0.058}\cdot 10^{-2}$	$2.459^{+0.259+0.062}_{-0.188-0.062}\cdot 10^{-2}$	$2.467^{+0.080+0.062}_{-0.050-0.062}\cdot 10^{-2}$
200	$2.184^{+0.933+0.054}_{-0.538-0.054}\cdot 10^{-2}$	$2.294^{+0.240+0.058}_{-0.180-0.058}\cdot 10^{-2}$	$2.299^{+0.075+0.058}_{-0.048-0.058}\cdot 10^{-2}$
210	$1.893^{+0.827+0.047}_{-0.474-0.047}\cdot 10^{-2}$	$1.993^{+0.212+0.050}_{-0.160-0.050}\cdot 10^{-2}$	$2.001^{+0.065+0.051}_{-0.044-0.051}\cdot 10^{-2}$
220	$1.643^{+0.736+0.041}_{-0.418-0.041}\cdot 10^{-2}$	$1.736^{+0.187+0.044}_{-0.144-0.044}\cdot 10^{-2}$	$1.743^{+0.057+0.044}_{-0.040-0.044}\cdot 10^{-2}$
230	$1.427^{+0.653+0.036}_{-0.369-0.036}\cdot 10^{-2}$	$1.513^{+0.165+0.038}_{-0.130-0.038}\cdot 10^{-2}$	$1.520^{+0.050+0.039}_{-0.037-0.039}\cdot 10^{-2}$
240	$1.241^{+0.581+0.031}_{-0.326-0.031}\cdot 10^{-2}$	$1.320^{+0.147+0.034}_{-0.117-0.034}\cdot 10^{-2}$	$1.327^{+0.043+0.034}_{-0.034-0.034}\cdot 10^{-2}$
250	$1.080^{+0.517+0.027}_{-0.287-0.027}\cdot 10^{-2}$	$1.153^{+0.129+0.029}_{-0.105-0.029}\cdot 10^{-2}$	$1.160^{+0.038+0.030}_{-0.030-0.030}\cdot 10^{-2}$
260	$9.409^{+4.595+0.238}_{-2.537-0.238}\cdot 10^{-3}$	$1.008^{+0.115+0.026}_{-0.095-0.026}\cdot 10^{-2}$	$1.015^{+0.034+0.026}_{-0.028-0.026}\cdot 10^{-2}$
270	$8.206^{+4.089+0.209}_{-2.242-0.209}\cdot 10^{-3}$	$8.827^{+1.011+0.228}_{-0.851-0.228}\cdot 10^{-3}$	$8.885^{+0.296+0.229}_{-0.258-0.229}\cdot 10^{-3}$
280	$7.163^{+3.636+0.183}_{-1.984-0.183}\cdot 10^{-3}$	$7.727^{+0.897+0.200}_{-0.764-0.200}\cdot 10^{-3}$	$7.784^{+0.260+0.202}_{-0.233-0.202}\cdot 10^{-3}$
290	$6.255^{+3.238+0.161}_{-1.753-0.161}\cdot 10^{-3}$	$6.770^{+0.800+0.176}_{-0.685-0.176}\cdot 10^{-3}$	$6.828^{+0.230+0.178}_{-0.215-0.178}\cdot 10^{-3}$
300	$5.468^{+2.881+0.142}_{-1.552-0.142}\cdot 10^{-3}$	$5.940^{+0.707+0.156}_{-0.620-0.156}\cdot 10^{-3}$	$5.991^{+0.203+0.157}_{-0.193-0.157}\cdot 10^{-3}$

Table B.2: Total VBF cross sections at the Tevatron, $\sqrt{S} = 1.96\,\text{TeV}$ at LO, NLO and NNLO in QCD. Errors shown are respectively scale and PDF uncertainities. Scale uncertainities are evaluated by varying μ_r and μ_f in the interval $\mu_r, \mu_f \in [Q/4, 4Q]$. The HERAPDF1.5 [73, 74] PDF set has been used. Numbers are in pb.

m_H [GeV]	σ_{LO}	σ_{NLO}	σ_{NNLO}
90	$1.227^{+0.324+0.015}_{-0.219-0.015}\cdot 10^{-1}$	$1.235^{+0.092+0.015}_{-0.045-0.015}\cdot 10^{-1}$	$1.221^{+0.031+0.020}_{-0.008-0.020}\cdot 10^{-1}$
95	$1.129^{+0.306+0.014}_{-0.205-0.014}\cdot 10^{-1}$	$1.140^{+0.085+0.014}_{-0.047-0.014}\cdot 10^{-1}$	$1.125^{+0.029+0.019}_{-0.007-0.019}\cdot 10^{-1}$
100	$1.040^{+0.289+0.013}_{-0.192-0.013}\cdot 10^{-1}$	$1.049^{+0.082+0.013}_{-0.043-0.013}\cdot 10^{-1}$	$1.038^{+0.027+0.017}_{-0.008-0.017}\cdot 10^{-1}$
105	$9.581^{+2.730+0.124}_{-1.801-0.124}\cdot 10^{-2}$	$9.699^{+0.751+0.123}_{-0.411-0.123}\cdot 10^{-2}$	$9.580^{+0.248+0.162}_{-0.072-0.162}\cdot 10^{-2}$
110	$8.835^{+2.576+0.116}_{-1.691-0.116}\cdot 10^{-2}$	$8.961^{+0.698+0.115}_{-0.401-0.115}\cdot 10^{-2}$	$8.851^{+0.228+0.151}_{-0.078-0.151}\cdot 10^{-2}$
115	$8.152^{+2.433+0.109}_{-1.583-0.109}\cdot 10^{-2}$	$8.290^{+0.650+0.108}_{-0.401-0.108}\cdot 10^{-2}$	$8.182^{+0.213+0.140}_{-0.076-0.140}\cdot 10^{-2}$
120	$7.526^{+2.294+0.102}_{-1.485-0.102}\cdot 10^{-2}$	$7.665^{+0.614+0.101}_{-0.367-0.101}\cdot 10^{-2}$	$7.568^{+0.194+0.131}_{-0.073-0.131}\cdot 10^{-2}$
125	$6.954^{+2.165+0.096}_{-1.391-0.096}\cdot 10^{-2}$	$7.089^{+0.580+0.095}_{-0.349-0.095}\cdot 10^{-2}$	$7.003^{+0.183+0.122}_{-0.072-0.122}\cdot 10^{-2}$
130	$6.428^{+2.049+0.090}_{-1.304-0.090}\cdot 10^{-2}$	$6.567^{+0.538+0.090}_{-0.337-0.090}\cdot 10^{-2}$	$6.483^{+0.172+0.113}_{-0.071-0.113}\cdot 10^{-2}$
135	$5.948^{+1.927+0.085}_{-1.223-0.085}\cdot 10^{-2}$	$6.084^{+0.509+0.084}_{-0.320-0.084}\cdot 10^{-2}$	$6.008^{+0.157+0.106}_{-0.068-0.106}\cdot 10^{-2}$
140	$5.505^{+1.819+0.080}_{-1.147-0.080}\cdot 10^{-2}$	$5.644^{+0.474+0.079}_{-0.308-0.079}\cdot 10^{-2}$	$5.569^{+0.151+0.098}_{-0.064-0.098}\cdot 10^{-2}$
145	$5.099^{+1.708+0.075}_{-1.075-0.075}\cdot 10^{-2}$	$5.233^{+0.448+0.075}_{-0.289-0.075}\cdot 10^{-2}$	$5.166^{+0.138+0.092}_{-0.063-0.092}\cdot 10^{-2}$
150	$4.729^{+1.612+0.071}_{-1.012-0.071}\cdot 10^{-2}$	$4.860^{+0.419+0.070}_{-0.276-0.070}\cdot 10^{-2}$	$4.795^{+0.128+0.086}_{-0.062-0.086}\cdot 10^{-2}$
155	$4.384^{+1.519+0.067}_{-0.947-0.067}\cdot 10^{-2}$	$4.511^{+0.394+0.066}_{-0.263-0.066}\cdot 10^{-2}$	$4.454^{+0.119+0.080}_{-0.062-0.080}\cdot 10^{-2}$
160	$4.065^{+1.433+0.063}_{-0.889-0.063}\cdot 10^{-2}$	$4.193^{+0.369+0.062}_{-0.252-0.062}\cdot 10^{-2}$	$4.135^{+0.115+0.075}_{-0.055-0.075}\cdot 10^{-2}$
165	$3.773^{+1.351+0.059}_{-0.834-0.059}\cdot 10^{-2}$	$3.897^{+0.345+0.059}_{-0.238-0.059}\cdot 10^{-2}$	$3.843^{+0.103+0.070}_{-0.056-0.070}\cdot 10^{-2}$
170	$3.502^{+1.273+0.056}_{-0.782-0.056}\cdot 10^{-2}$	$3.624^{+0.325+0.055}_{-0.226-0.055}\cdot 10^{-2}$	$3.574^{+0.096+0.065}_{-0.054-0.065}\cdot 10^{-2}$
175	$3.253^{+1.199+0.052}_{-0.735-0.052}\cdot 10^{-2}$	$3.371^{+0.304+0.052}_{-0.215-0.052}\cdot 10^{-2}$	$3.324^{+0.090+0.061}_{-0.051-0.061}\cdot 10^{-2}$
180	$3.022^{+1.131+0.049}_{-0.689-0.049}\cdot 10^{-2}$	$3.138^{+0.285+0.049}_{-0.205-0.049}\cdot 10^{-2}$	$3.094^{+0.085+0.057}_{-0.050-0.057}\cdot 10^{-2}$
185	$2.809^{+1.066+0.046}_{-0.646-0.046}\cdot 10^{-2}$	$2.922^{+0.270+0.046}_{-0.195-0.046}\cdot 10^{-2}$	$2.880^{+0.079+0.053}_{-0.049-0.053}\cdot 10^{-2}$
190	$2.612^{+1.005+0.044}_{-0.606-0.044}\cdot 10^{-2}$	$2.722^{+0.251+0.044}_{-0.186-0.044}\cdot 10^{-2}$	$2.682^{+0.074+0.050}_{-0.047-0.050}\cdot 10^{-2}$
195	$2.430^{+0.945+0.041}_{-0.570-0.041}\cdot 10^{-2}$	$2.536^{+0.237+0.041}_{-0.176-0.041}\cdot 10^{-2}$	$2.498^{+0.068+0.046}_{-0.044-0.046}\cdot 10^{-2}$
200	$2.261^{+0.893+0.039}_{-0.535-0.039}\cdot 10^{-2}$	$2.363^{+0.224+0.039}_{-0.166-0.039}\cdot 10^{-2}$	$2.328^{+0.064+0.044}_{-0.042-0.044}\cdot 10^{-2}$
210	$1.959^{+0.795+0.035}_{-0.472-0.035}\cdot 10^{-2}$	$2.056^{+0.196+0.035}_{-0.151-0.035}\cdot 10^{-2}$	$2.025^{+0.055+0.038}_{-0.039-0.038}\cdot 10^{-2}$
220	$1.700^{+0.706+0.031}_{-0.416-0.031}\cdot 10^{-2}$	$1.790^{+0.173+0.031}_{-0.136-0.031}\cdot 10^{-2}$	$1.763^{+0.049+0.034}_{-0.036-0.034}\cdot 10^{-2}$
230	$1.477^{+0.628+0.027}_{-0.368-0.027}\cdot 10^{-2}$	$1.561^{+0.153+0.028}_{-0.123-0.028}\cdot 10^{-2}$	$1.536^{+0.042+0.029}_{-0.033-0.029}\cdot 10^{-2}$
240	$1.284^{+0.558+0.024}_{-0.324-0.024}\cdot 10^{-2}$	$1.362^{+0.135+0.025}_{-0.111-0.025}\cdot 10^{-2}$	$1.340^{+0.037+0.026}_{-0.030-0.026}\cdot 10^{-2}$
250	$1.118^{+0.497+0.022}_{-0.287-0.022}\cdot 10^{-2}$	$1.189^{+0.120+0.022}_{-0.099-0.022}\cdot 10^{-2}$	$1.170^{+0.033+0.023}_{-0.028-0.023}\cdot 10^{-2}$
260	$9.741^{+4.425+0.193}_{-2.532-0.193}\cdot 10^{-3}$	$1.040^{+0.106+0.020}_{-0.090-0.020}\cdot 10^{-2}$	$1.023^{+0.029+0.020}_{-0.026-0.020}\cdot 10^{-2}$
270	$8.497^{+3.937+0.172}_{-2.241-0.172}\cdot 10^{-3}$	$9.099^{+0.943+0.174}_{-0.812-0.174}\cdot 10^{-3}$	$8.949^{+0.252+0.179}_{-0.231-0.179}\cdot 10^{-3}$
280	$7.415^{+3.511+0.153}_{-1.981-0.153}\cdot 10^{-3}$	$7.969^{+0.831+0.155}_{-0.732-0.155}\cdot 10^{-3}$	$7.838^{+0.222+0.158}_{-0.215-0.158}\cdot 10^{-3}$
290	$6.477^{+3.122+0.136}_{-1.754-0.136}\cdot 10^{-3}$	$6.983^{+0.739+0.138}_{-0.657-0.138}\cdot 10^{-3}$	$6.867^{+0.195+0.140}_{-0.194-0.140}\cdot 10^{-3}$
300	$5.659^{+2.788+0.121}_{-1.550-0.121}\cdot 10^{-3}$	$6.123^{+0.656+0.124}_{-0.593-0.124}\cdot 10^{-3}$	$6.020^{+0.171+0.124}_{-0.177-0.124}\cdot 10^{-3}$

Table B.3: Total VBF cross sections at the Tevatron, $\sqrt{S} = 1.96\,\text{TeV}$ at LO, NLO and NNLO in QCD. Errors shown are respectively scale and PDF uncertainities. Scale uncertainities are evaluated by varying μ_r and μ_f in the interval $\mu_r, \mu_f \in [Q/4, 4Q]$. The JR09 [75, 76] PDF set has been used. Numbers are in pb.

m_H [GeV]	σ_{LO}	σ_{NLO}	σ_{NNLO}
90	$1.125^{+0.354+0.019}_{-0.227-0.019}\cdot 10^{-1}$	$1.176^{+0.104+0.028}_{-0.055-0.028}\cdot 10^{-1}$	$1.182^{+0.038+0.027}_{-0.011-0.027}\cdot 10^{-1}$
95	$1.035^{+0.335+0.018}_{-0.212-0.018}\cdot 10^{-1}$	$1.083^{+0.096+0.026}_{-0.053-0.026}\cdot 10^{-1}$	$1.088^{+0.035+0.025}_{-0.012-0.025}\cdot 10^{-1}$
100	$9.541^{+3.156+0.166}_{-1.991-0.166}\cdot 10^{-2}$	$9.974^{+0.892+0.240}_{-0.511-0.240}\cdot 10^{-2}$	$1.002^{+0.032+0.023}_{-0.011-0.023}\cdot 10^{-1}$
105	$8.794^{+2.984+0.154}_{-1.865-0.154}\cdot 10^{-2}$	$9.181^{+0.848+0.222}_{-0.469-0.222}\cdot 10^{-2}$	$9.235^{+0.298+0.213}_{-0.102-0.213}\cdot 10^{-2}$
110	$8.117^{+2.810+0.143}_{-1.752-0.143}\cdot 10^{-2}$	$8.465^{+0.786+0.206}_{-0.453-0.206}\cdot 10^{-2}$	$8.520^{+0.277+0.197}_{-0.104-0.197}\cdot 10^{-2}$
115	$7.494^{+2.652+0.133}_{-1.641-0.133}\cdot 10^{-2}$	$7.813^{+0.739+0.191}_{-0.431-0.191}\cdot 10^{-2}$	$7.866^{+0.257+0.183}_{-0.098-0.183}\cdot 10^{-2}$
120	$6.923^{+2.502+0.123}_{-1.536-0.123}\cdot 10^{-2}$	$7.217^{+0.691+0.177}_{-0.414-0.177}\cdot 10^{-2}$	$7.268^{+0.239+0.170}_{-0.095-0.170}\cdot 10^{-2}$
125	$6.401^{+2.363+0.115}_{-1.440-0.115}\cdot 10^{-2}$	$6.678^{+0.641+0.165}_{-0.399-0.165}\cdot 10^{-2}$	$6.721^{+0.219+0.158}_{-0.095-0.158}\cdot 10^{-2}$
130	$5.923^{+2.235+0.107}_{-1.351-0.107}\cdot 10^{-2}$	$6.169^{+0.602+0.153}_{-0.365-0.153}\cdot 10^{-2}$	$6.215^{+0.204+0.147}_{-0.089-0.147}\cdot 10^{-2}$
135	$5.483^{+2.108+0.099}_{-1.268-0.099}\cdot 10^{-2}$	$5.709^{+0.563+0.142}_{-0.346-0.142}\cdot 10^{-2}$	$5.755^{+0.188+0.137}_{-0.089-0.137}\cdot 10^{-2}$
140	$5.081^{+1.978+0.093}_{-1.189-0.093}\cdot 10^{-2}$	$5.286^{+0.525+0.132}_{-0.333-0.132}\cdot 10^{-2}$	$5.329^{+0.178+0.127}_{-0.082-0.127}\cdot 10^{-2}$
145	$4.709^{+1.873+0.086}_{-1.114-0.086}\cdot 10^{-2}$	$4.898^{+0.492+0.123}_{-0.320-0.123}\cdot 10^{-2}$	$4.938^{+0.165+0.118}_{-0.081-0.118}\cdot 10^{-2}$
150	$4.365^{+1.763+0.080}_{-1.046-0.080}\cdot 10^{-2}$	$4.540^{+0.462+0.115}_{-0.302-0.115}\cdot 10^{-2}$	$4.578^{+0.156+0.110}_{-0.075-0.110}\cdot 10^{-2}$
155	$4.052^{+1.659+0.075}_{-0.979-0.075}\cdot 10^{-2}$	$4.211^{+0.432+0.107}_{-0.287-0.107}\cdot 10^{-2}$	$4.247^{+0.142+0.103}_{-0.074-0.103}\cdot 10^{-2}$
160	$3.760^{+1.573+0.070}_{-0.918-0.070}\cdot 10^{-2}$	$3.908^{+0.403+0.099}_{-0.271-0.099}\cdot 10^{-2}$	$3.942^{+0.133+0.096}_{-0.070-0.096}\cdot 10^{-2}$
165	$3.495^{+1.481+0.065}_{-0.864-0.065}\cdot 10^{-2}$	$3.628^{+0.378+0.093}_{-0.259-0.093}\cdot 10^{-2}$	$3.660^{+0.125+0.089}_{-0.066-0.089}\cdot 10^{-2}$
170	$3.246^{+1.396+0.061}_{-0.811-0.061}\cdot 10^{-2}$	$3.370^{+0.355+0.086}_{-0.245-0.086}\cdot 10^{-2}$	$3.401^{+0.116+0.083}_{-0.065-0.083}\cdot 10^{-2}$
175	$3.019^{+1.317+0.057}_{-0.761-0.057}\cdot 10^{-2}$	$3.132^{+0.332+0.081}_{-0.233-0.081}\cdot 10^{-2}$	$3.161^{+0.107+0.078}_{-0.063-0.078}\cdot 10^{-2}$
180	$2.806^{+1.241+0.053}_{-0.714-0.053}\cdot 10^{-2}$	$2.912^{+0.312+0.075}_{-0.221-0.075}\cdot 10^{-2}$	$2.938^{+0.102+0.073}_{-0.060-0.073}\cdot 10^{-2}$
185	$2.611^{+1.173+0.049}_{-0.670-0.049}\cdot 10^{-2}$	$2.708^{+0.293+0.070}_{-0.209-0.070}\cdot 10^{-2}$	$2.734^{+0.093+0.068}_{-0.058-0.068}\cdot 10^{-2}$
190	$2.430^{+1.106+0.046}_{-0.629-0.046}\cdot 10^{-2}$	$2.521^{+0.273+0.066}_{-0.199-0.066}\cdot 10^{-2}$	$2.545^{+0.088+0.063}_{-0.056-0.063}\cdot 10^{-2}$
195	$2.263^{+1.044+0.043}_{-0.591-0.043}\cdot 10^{-2}$	$2.347^{+0.256+0.061}_{-0.189-0.061}\cdot 10^{-2}$	$2.369^{+0.082+0.059}_{-0.053-0.059}\cdot 10^{-2}$
200	$2.108^{+0.985+0.040}_{-0.556-0.040}\cdot 10^{-2}$	$2.185^{+0.241+0.057}_{-0.178-0.057}\cdot 10^{-2}$	$2.206^{+0.075+0.055}_{-0.051-0.055}\cdot 10^{-2}$
210	$1.831^{+0.878+0.035}_{-0.490-0.035}\cdot 10^{-2}$	$1.897^{+0.211+0.050}_{-0.162-0.050}\cdot 10^{-2}$	$1.916^{+0.065+0.048}_{-0.046-0.048}\cdot 10^{-2}$
220	$1.592^{+0.782+0.031}_{-0.434-0.031}\cdot 10^{-2}$	$1.649^{+0.186+0.044}_{-0.144-0.044}\cdot 10^{-2}$	$1.665^{+0.058+0.042}_{-0.042-0.042}\cdot 10^{-2}$
230	$1.387^{+0.698+0.027}_{-0.384-0.027}\cdot 10^{-2}$	$1.434^{+0.164+0.038}_{-0.129-0.038}\cdot 10^{-2}$	$1.450^{+0.051+0.037}_{-0.038-0.037}\cdot 10^{-2}$
240	$1.209^{+0.623+0.024}_{-0.339-0.024}\cdot 10^{-2}$	$1.250^{+0.145+0.034}_{-0.117-0.034}\cdot 10^{-2}$	$1.264^{+0.044+0.033}_{-0.035-0.033}\cdot 10^{-2}$
250	$1.055^{+0.555+0.021}_{-0.300-0.021}\cdot 10^{-2}$	$1.089^{+0.129+0.029}_{-0.103-0.029}\cdot 10^{-2}$	$1.102^{+0.039+0.029}_{-0.032-0.029}\cdot 10^{-2}$
260	$9.216^{+4.955+0.182}_{-2.660-0.182}\cdot 10^{-3}$	$9.518^{+1.128+0.258}_{-0.937-0.258}\cdot 10^{-3}$	$9.624^{+0.344+0.251}_{-0.287-0.251}\cdot 10^{-3}$
270	$8.058^{+4.421+0.160}_{-2.356-0.160}\cdot 10^{-3}$	$8.313^{+1.003+0.227}_{-0.837-0.227}\cdot 10^{-3}$	$8.412^{+0.300+0.220}_{-0.264-0.220}\cdot 10^{-3}$
280	$7.052^{+3.947+0.141}_{-2.089-0.141}\cdot 10^{-3}$	$7.275^{+0.883+0.199}_{-0.755-0.199}\cdot 10^{-3}$	$7.359^{+0.260+0.194}_{-0.240-0.194}\cdot 10^{-3}$
290	$6.174^{+3.529+0.124}_{-1.851-0.124}\cdot 10^{-3}$	$6.365^{+0.783+0.175}_{-0.678-0.175}\cdot 10^{-3}$	$6.443^{+0.231+0.170}_{-0.218-0.170}\cdot 10^{-3}$
300	$5.410^{+3.155+0.109}_{-1.641-0.109}\cdot 10^{-3}$	$5.575^{+0.692+0.154}_{-0.608-0.154}\cdot 10^{-3}$	$5.644^{+0.204+0.150}_{-0.198-0.150}\cdot 10^{-3}$

Table B.4: Total VBF cross sections at the Tevatron, $\sqrt{S} = 1.96\,\text{TeV}$ at LO, NLO and NNLO in QCD. Errors shown are respectively scale and PDF uncertainities. Scale uncertainities are evaluated by varying μ_r and μ_f in the interval $\mu_r, \mu_f \in [Q/4, 4Q]$. The MSTW2008 [63] PDF set (68% CL) has been used. Numbers are in pb.

m_H [GeV]	σ_{LO}	σ_{NLO}	σ_{NNLO}
90	$1.180^{+0.342+0.023}_{-0.224-0.023}\cdot 10^{-1}$	$1.191^{+0.100+0.024}_{-0.053-0.024}\cdot 10^{-1}$	$1.189^{+0.036+0.019}_{-0.012-0.019}\cdot 10^{-1}$
95	$1.085^{+0.323+0.022}_{-0.209-0.022}\cdot 10^{-1}$	$1.096^{+0.094+0.022}_{-0.049-0.022}\cdot 10^{-1}$	$1.095^{+0.034+0.017}_{-0.010-0.017}\cdot 10^{-1}$
100	$9.983^{+3.045+0.202}_{-1.962-0.202}\cdot 10^{-2}$	$1.011^{+0.087+0.021}_{-0.048-0.021}\cdot 10^{-1}$	$1.009^{+0.031+0.016}_{-0.009-0.016}\cdot 10^{-1}$
105	$9.190^{+2.875+0.188}_{-1.838-0.188}\cdot 10^{-2}$	$9.324^{+0.828+0.194}_{-0.459-0.194}\cdot 10^{-2}$	$9.303^{+0.293+0.151}_{-0.093-0.151}\cdot 10^{-2}$
110	$8.469^{+2.708+0.176}_{-1.721-0.176}\cdot 10^{-2}$	$8.608^{+0.763+0.181}_{-0.440-0.181}\cdot 10^{-2}$	$8.588^{+0.271+0.141}_{-0.095-0.141}\cdot 10^{-2}$
115	$7.805^{+2.550+0.164}_{-1.608-0.164}\cdot 10^{-2}$	$7.951^{+0.713+0.170}_{-0.424-0.170}\cdot 10^{-2}$	$7.933^{+0.252+0.132}_{-0.096-0.132}\cdot 10^{-2}$
120	$7.202^{+2.401+0.154}_{-1.509-0.154}\cdot 10^{-2}$	$7.349^{+0.668+0.159}_{-0.399-0.159}\cdot 10^{-2}$	$7.331^{+0.231+0.124}_{-0.092-0.124}\cdot 10^{-2}$
125	$6.646^{+2.267+0.143}_{-1.409-0.143}\cdot 10^{-2}$	$6.797^{+0.619+0.148}_{-0.381-0.148}\cdot 10^{-2}$	$6.781^{+0.212+0.116}_{-0.092-0.116}\cdot 10^{-2}$
130	$6.142^{+2.130+0.134}_{-1.323-0.134}\cdot 10^{-2}$	$6.297^{+0.576+0.139}_{-0.369-0.139}\cdot 10^{-2}$	$6.276^{+0.198+0.109}_{-0.086-0.109}\cdot 10^{-2}$
135	$5.676^{+2.008+0.126}_{-1.236-0.126}\cdot 10^{-2}$	$5.824^{+0.549+0.130}_{-0.344-0.130}\cdot 10^{-2}$	$5.811^{+0.185+0.102}_{-0.083-0.102}\cdot 10^{-2}$
140	$5.254^{+1.887+0.118}_{-1.162-0.118}\cdot 10^{-2}$	$5.401^{+0.505+0.122}_{-0.330-0.122}\cdot 10^{-2}$	$5.384^{+0.173+0.095}_{-0.078-0.095}\cdot 10^{-2}$
145	$4.861^{+1.777+0.110}_{-1.087-0.110}\cdot 10^{-2}$	$5.007^{+0.474+0.115}_{-0.314-0.115}\cdot 10^{-2}$	$4.993^{+0.157+0.090}_{-0.076-0.090}\cdot 10^{-2}$
150	$4.501^{+1.680+0.103}_{-1.018-0.103}\cdot 10^{-2}$	$4.642^{+0.447+0.107}_{-0.295-0.107}\cdot 10^{-2}$	$4.630^{+0.151+0.084}_{-0.074-0.084}\cdot 10^{-2}$
155	$4.172^{+1.578+0.097}_{-0.956-0.097}\cdot 10^{-2}$	$4.310^{+0.417+0.101}_{-0.283-0.101}\cdot 10^{-2}$	$4.297^{+0.138+0.079}_{-0.072-0.079}\cdot 10^{-2}$
160	$3.867^{+1.486+0.091}_{-0.894-0.091}\cdot 10^{-2}$	$4.003^{+0.389+0.095}_{-0.270-0.095}\cdot 10^{-2}$	$3.991^{+0.131+0.074}_{-0.070-0.074}\cdot 10^{-2}$
165	$3.586^{+1.399+0.085}_{-0.837-0.085}\cdot 10^{-2}$	$3.717^{+0.366+0.089}_{-0.255-0.089}\cdot 10^{-2}$	$3.706^{+0.121+0.070}_{-0.066-0.070}\cdot 10^{-2}$
170	$3.327^{+1.317+0.080}_{-0.784-0.080}\cdot 10^{-2}$	$3.456^{+0.343+0.084}_{-0.243-0.084}\cdot 10^{-2}$	$3.445^{+0.111+0.066}_{-0.065-0.066}\cdot 10^{-2}$
175	$3.087^{+1.239+0.075}_{-0.735-0.075}\cdot 10^{-2}$	$3.213^{+0.322+0.079}_{-0.230-0.079}\cdot 10^{-2}$	$3.202^{+0.103+0.062}_{-0.062-0.062}\cdot 10^{-2}$
180	$2.867^{+1.169+0.071}_{-0.689-0.071}\cdot 10^{-2}$	$2.989^{+0.301+0.074}_{-0.219-0.074}\cdot 10^{-2}$	$2.980^{+0.097+0.058}_{-0.060-0.058}\cdot 10^{-2}$
185	$2.663^{+1.102+0.067}_{-0.646-0.067}\cdot 10^{-2}$	$2.783^{+0.284+0.070}_{-0.208-0.070}\cdot 10^{-2}$	$2.772^{+0.090+0.055}_{-0.056-0.055}\cdot 10^{-2}$
190	$2.475^{+1.036+0.063}_{-0.606-0.063}\cdot 10^{-2}$	$2.591^{+0.265+0.066}_{-0.198-0.066}\cdot 10^{-2}$	$2.581^{+0.085+0.052}_{-0.054-0.052}\cdot 10^{-2}$
195	$2.301^{+0.976+0.059}_{-0.569-0.059}\cdot 10^{-2}$	$2.413^{+0.249+0.062}_{-0.189-0.062}\cdot 10^{-2}$	$2.403^{+0.078+0.049}_{-0.052-0.049}\cdot 10^{-2}$
200	$2.140^{+0.919+0.056}_{-0.533-0.056}\cdot 10^{-2}$	$2.249^{+0.233+0.058}_{-0.178-0.058}\cdot 10^{-2}$	$2.239^{+0.073+0.046}_{-0.050-0.046}\cdot 10^{-2}$
210	$1.853^{+0.816+0.049}_{-0.470-0.049}\cdot 10^{-2}$	$1.954^{+0.203+0.052}_{-0.161-0.052}\cdot 10^{-2}$	$1.945^{+0.063+0.041}_{-0.046-0.041}\cdot 10^{-2}$
220	$1.607^{+0.724+0.044}_{-0.414-0.044}\cdot 10^{-2}$	$1.700^{+0.181+0.046}_{-0.144-0.046}\cdot 10^{-2}$	$1.692^{+0.055+0.036}_{-0.042-0.036}\cdot 10^{-2}$
230	$1.395^{+0.643+0.039}_{-0.365-0.039}\cdot 10^{-2}$	$1.480^{+0.160+0.041}_{-0.129-0.041}\cdot 10^{-2}$	$1.474^{+0.049+0.032}_{-0.038-0.032}\cdot 10^{-2}$
240	$1.212^{+0.571+0.035}_{-0.322-0.035}\cdot 10^{-2}$	$1.291^{+0.141+0.037}_{-0.116-0.037}\cdot 10^{-2}$	$1.285^{+0.043+0.029}_{-0.035-0.029}\cdot 10^{-2}$
250	$1.054^{+0.508+0.031}_{-0.283-0.031}\cdot 10^{-2}$	$1.127^{+0.125+0.033}_{-0.105-0.033}\cdot 10^{-2}$	$1.122^{+0.037+0.026}_{-0.032-0.026}\cdot 10^{-2}$
260	$9.177^{+4.510+0.276}_{-2.502-0.276}\cdot 10^{-3}$	$9.846^{+1.101+0.293}_{-0.940-0.293}\cdot 10^{-3}$	$9.797^{+0.326+0.232}_{-0.291-0.232}\cdot 10^{-3}$
270	$8.000^{+4.011+0.246}_{-2.213-0.246}\cdot 10^{-3}$	$8.614^{+0.973+0.263}_{-0.848-0.263}\cdot 10^{-3}$	$8.564^{+0.293+0.208}_{-0.264-0.208}\cdot 10^{-3}$
280	$6.977^{+3.568+0.220}_{-1.954-0.220}\cdot 10^{-3}$	$7.536^{+0.862+0.235}_{-0.760-0.235}\cdot 10^{-3}$	$7.497^{+0.257+0.186}_{-0.242-0.186}\cdot 10^{-3}$
290	$6.089^{+3.171+0.197}_{-1.725-0.197}\cdot 10^{-3}$	$6.601^{+0.764+0.211}_{-0.683-0.211}\cdot 10^{-3}$	$6.567^{+0.221+0.167}_{-0.223-0.167}\cdot 10^{-3}$
300	$5.318^{+2.824+0.176}_{-1.524-0.176}\cdot 10^{-3}$	$5.786^{+0.677+0.189}_{-0.614-0.189}\cdot 10^{-3}$	$5.754^{+0.196+0.150}_{-0.200-0.150}\cdot 10^{-3}$

Table B.5: Total VBF cross sections at the Tevatron, $\sqrt{S} = 1.96\,\text{TeV}$ at LO, NLO and NNLO in QCD. Errors shown are respectively scale and PDF uncertainities. Scale uncertainities are evaluated by varying μ_r and μ_f in the interval $\mu_r, \mu_f \in [Q/4, 4Q]$. The NNPDF2.1 [77] PDF set has been used. Numbers are in pb.

m_H [GeV]	σ_{LO}	σ_{NLO}	σ_{NNLO}
90	$1.856^{+0.140+0.013}_{-0.140-0.013}$	$1.797^{+0.062+0.013}_{-0.022-0.013}$	$1.820^{+0.021+0.014}_{-0.029-0.014}$
95	$1.758^{+0.146+0.013}_{-0.138-0.013}$	$1.709^{+0.059+0.013}_{-0.025-0.013}$	$1.728^{+0.024+0.013}_{-0.027-0.013}$
100	$1.667^{+0.146+0.012}_{-0.135-0.012}$	$1.622^{+0.059+0.012}_{-0.024-0.012}$	$1.643^{+0.022+0.012}_{-0.026-0.012}$
105	$1.585^{+0.147+0.011}_{-0.133-0.011}$	$1.544^{+0.054+0.011}_{-0.026-0.011}$	$1.560^{+0.024+0.012}_{-0.021-0.012}$
110	$1.506^{+0.148+0.011}_{-0.130-0.011}$	$1.466^{+0.058+0.011}_{-0.022-0.011}$	$1.483^{+0.026+0.011}_{-0.022-0.011}$
115	$1.431^{+0.148+0.010}_{-0.129-0.010}$	$1.394^{+0.058+0.010}_{-0.018-0.010}$	$1.411^{+0.022+0.011}_{-0.014-0.011}$
120	$1.363^{+0.145+0.010}_{-0.128-0.010}$	$1.330^{+0.054+0.010}_{-0.021-0.010}$	$1.345^{+0.022+0.010}_{-0.016-0.010}$
125	$1.297^{+0.146+0.009}_{-0.125-0.009}$	$1.267^{+0.054+0.009}_{-0.020-0.009}$	$1.285^{+0.020+0.010}_{-0.022-0.010}$
130	$1.236^{+0.145+0.009}_{-0.122-0.009}$	$1.209^{+0.051+0.009}_{-0.021-0.009}$	$1.223^{+0.022+0.009}_{-0.013-0.009}$
135	$1.180^{+0.142+0.008}_{-0.121-0.008}$	$1.153^{+0.052+0.009}_{-0.018-0.009}$	$1.168^{+0.021+0.009}_{-0.018-0.009}$
140	$1.125^{+0.142+0.008}_{-0.118-0.008}$	$1.101^{+0.051+0.008}_{-0.016-0.008}$	$1.116^{+0.021+0.008}_{-0.013-0.008}$
145	$1.074^{+0.139+0.008}_{-0.115-0.008}$	$1.052^{+0.049+0.008}_{-0.017-0.008}$	$1.067^{+0.019+0.008}_{-0.017-0.008}$
150	$1.026^{+0.138+0.007}_{-0.112-0.007}$	$1.006^{+0.049+0.008}_{-0.018-0.008}$	$1.018^{+0.021+0.008}_{-0.011-0.008}$
155	$9.804^{+1.349+0.072}_{-1.090-0.072}\cdot10^{-1}$	$9.622^{+0.458+0.073}_{-0.157-0.073}\cdot10^{-1}$	$9.731^{+0.209+0.074}_{-0.096-0.074}\cdot10^{-1}$
160	$9.371^{+1.335+0.069}_{-1.062-0.069}\cdot10^{-1}$	$9.207^{+0.461+0.070}_{-0.157-0.070}\cdot10^{-1}$	$9.340^{+0.170+0.071}_{-0.116-0.071}\cdot10^{-1}$
165	$8.971^{+1.304+0.066}_{-1.033-0.066}\cdot10^{-1}$	$8.816^{+0.442+0.067}_{-0.147-0.067}\cdot10^{-1}$	$8.937^{+0.158+0.068}_{-0.098-0.068}\cdot10^{-1}$
170	$8.581^{+1.297+0.064}_{-1.005-0.064}\cdot10^{-1}$	$8.442^{+0.425+0.065}_{-0.147-0.065}\cdot10^{-1}$	$8.560^{+0.164+0.066}_{-0.116-0.066}\cdot10^{-1}$
175	$8.211^{+1.247+0.061}_{-0.977-0.061}\cdot10^{-1}$	$8.076^{+0.423+0.062}_{-0.139-0.062}\cdot10^{-1}$	$8.199^{+0.168+0.063}_{-0.075-0.063}\cdot10^{-1}$
180	$7.873^{+1.246+0.059}_{-0.954-0.059}\cdot10^{-1}$	$7.752^{+0.411+0.060}_{-0.136-0.060}\cdot10^{-1}$	$7.855^{+0.162+0.061}_{-0.068-0.061}\cdot10^{-1}$
185	$7.547^{+1.213+0.057}_{-0.939-0.057}\cdot10^{-1}$	$7.431^{+0.405+0.058}_{-0.129-0.058}\cdot10^{-1}$	$7.544^{+0.155+0.059}_{-0.092-0.059}\cdot10^{-1}$
190	$7.235^{+1.190+0.055}_{-0.915-0.055}\cdot10^{-1}$	$7.143^{+0.380+0.056}_{-0.141-0.056}\cdot10^{-1}$	$7.252^{+0.127+0.057}_{-0.098-0.057}\cdot10^{-1}$
195	$6.947^{+1.159+0.053}_{-0.897-0.053}\cdot10^{-1}$	$6.857^{+0.368+0.054}_{-0.142-0.054}\cdot10^{-1}$	$6.955^{+0.137+0.055}_{-0.087-0.055}\cdot10^{-1}$
200	$6.664^{+1.144+0.051}_{-0.861-0.051}\cdot10^{-1}$	$6.573^{+0.377+0.052}_{-0.117-0.052}\cdot10^{-1}$	$6.686^{+0.115+0.053}_{-0.075-0.053}\cdot10^{-1}$
210	$6.139^{+1.092+0.048}_{-0.814-0.048}\cdot10^{-1}$	$6.074^{+0.341+0.049}_{-0.130-0.049}\cdot10^{-1}$	$6.177^{+0.114+0.049}_{-0.067-0.049}\cdot10^{-1}$
220	$5.673^{+1.047+0.045}_{-0.771-0.045}\cdot10^{-1}$	$5.619^{+0.324+0.045}_{-0.129-0.045}\cdot10^{-1}$	$5.709^{+0.117+0.046}_{-0.050-0.046}\cdot10^{-1}$
230	$5.251^{+1.002+0.042}_{-0.742-0.042}\cdot10^{-1}$	$5.205^{+0.315+0.043}_{-0.125-0.043}\cdot10^{-1}$	$5.290^{+0.108+0.043}_{-0.052-0.043}\cdot10^{-1}$
240	$4.853^{+0.960+0.039}_{-0.687-0.039}\cdot10^{-1}$	$4.819^{+0.298+0.040}_{-0.115-0.040}\cdot10^{-1}$	$4.904^{+0.102+0.040}_{-0.040-0.040}\cdot10^{-1}$
250	$4.510^{+0.908+0.037}_{-0.665-0.037}\cdot10^{-1}$	$4.475^{+0.291+0.037}_{-0.105-0.037}\cdot10^{-1}$	$4.555^{+0.096+0.038}_{-0.036-0.038}\cdot10^{-1}$
260	$4.182^{+0.871+0.035}_{-0.624-0.035}\cdot10^{-1}$	$4.158^{+0.266+0.035}_{-0.107-0.035}\cdot10^{-1}$	$4.238^{+0.090+0.036}_{-0.030-0.036}\cdot10^{-1}$
270	$3.888^{+0.833+0.033}_{-0.592-0.033}\cdot10^{-1}$	$3.872^{+0.248+0.033}_{-0.107-0.033}\cdot10^{-1}$	$3.943^{+0.092+0.034}_{-0.026-0.034}\cdot10^{-1}$
280	$3.618^{+0.797+0.031}_{-0.561-0.031}\cdot10^{-1}$	$3.607^{+0.243+0.031}_{-0.101-0.031}\cdot10^{-1}$	$3.675^{+0.083+0.032}_{-0.023-0.032}\cdot10^{-1}$
290	$3.370^{+0.762+0.029}_{-0.533-0.029}\cdot10^{-1}$	$3.364^{+0.228+0.030}_{-0.101-0.030}\cdot10^{-1}$	$3.434^{+0.071+0.030}_{-0.029-0.030}\cdot10^{-1}$
300	$3.143^{+0.726+0.028}_{-0.502-0.028}\cdot10^{-1}$	$3.142^{+0.212+0.028}_{-0.096-0.028}\cdot10^{-1}$	$3.210^{+0.065+0.028}_{-0.027-0.028}\cdot10^{-1}$
320	$2.742^{+0.660+0.025}_{-0.457-0.025}\cdot10^{-1}$	$2.749^{+0.192+0.025}_{-0.095-0.025}\cdot10^{-1}$	$2.807^{+0.061+0.025}_{-0.018-0.025}\cdot10^{-1}$
340	$2.398^{+0.605+0.022}_{-0.407-0.022}\cdot10^{-1}$	$2.413^{+0.171+0.023}_{-0.089-0.023}\cdot10^{-1}$	$2.463^{+0.053+0.023}_{-0.015-0.023}\cdot10^{-1}$
360	$2.108^{+0.549+0.020}_{-0.368-0.020}\cdot10^{-1}$	$2.123^{+0.156+0.020}_{-0.081-0.020}\cdot10^{-1}$	$2.168^{+0.050+0.020}_{-0.014-0.020}\cdot10^{-1}$
380	$1.857^{+0.503+0.018}_{-0.334-0.018}\cdot10^{-1}$	$1.876^{+0.139+0.018}_{-0.076-0.018}\cdot10^{-1}$	$1.917^{+0.043+0.018}_{-0.013-0.018}\cdot10^{-1}$
400	$1.642^{+0.459+0.016}_{-0.303-0.016}\cdot10^{-1}$	$1.661^{+0.127+0.017}_{-0.071-0.017}\cdot10^{-1}$	$1.700^{+0.037+0.017}_{-0.014-0.017}\cdot10^{-1}$
450	$1.218^{+0.365+0.013}_{-0.236-0.013}\cdot10^{-1}$	$1.239^{+0.098+0.013}_{-0.060-0.013}\cdot10^{-1}$	$1.269^{+0.030+0.013}_{-0.012-0.013}\cdot10^{-1}$
500	$9.161^{+2.940+0.103}_{-1.860-0.103}\cdot10^{-2}$	$9.378^{+0.766+0.104}_{-0.498-0.104}\cdot10^{-2}$	$9.615^{+0.225+0.104}_{-0.107-0.104}\cdot10^{-2}$
550	$6.975^{+2.362+0.082}_{-1.472-0.082}\cdot10^{-2}$	$7.173^{+0.614+0.083}_{-0.407-0.083}\cdot10^{-2}$	$7.363^{+0.175+0.083}_{-0.093-0.083}\cdot10^{-2}$
600	$5.361^{+1.915+0.066}_{-1.172-0.066}\cdot10^{-2}$	$5.547^{+0.489+0.067}_{-0.344-0.067}\cdot10^{-2}$	$5.695^{+0.139+0.067}_{-0.080-0.067}\cdot10^{-2}$
650	$4.157^{+1.553+0.054}_{-0.938-0.054}\cdot10^{-2}$	$4.324^{+0.389+0.054}_{-0.289-0.054}\cdot10^{-2}$	$4.441^{+0.111+0.054}_{-0.067-0.054}\cdot10^{-2}$
700	$3.247^{+1.267+0.044}_{-0.757-0.044}\cdot10^{-2}$	$3.396^{+0.314+0.044}_{-0.241-0.044}\cdot10^{-2}$	$3.492^{+0.089+0.044}_{-0.062-0.044}\cdot10^{-2}$
750	$2.553^{+1.038+0.036}_{-0.611-0.036}\cdot10^{-2}$	$2.683^{+0.256+0.036}_{-0.202-0.036}\cdot10^{-2}$	$2.761^{+0.073+0.036}_{-0.053-0.036}\cdot10^{-2}$
800	$2.018^{+0.851+0.029}_{-0.496-0.029}\cdot10^{-2}$	$2.132^{+0.207+0.030}_{-0.169-0.030}\cdot10^{-2}$	$2.197^{+0.057+0.030}_{-0.047-0.030}\cdot10^{-2}$
850	$1.605^{+0.699+0.024}_{-0.404-0.024}\cdot10^{-2}$	$1.703^{+0.170+0.025}_{-0.141-0.025}\cdot10^{-2}$	$1.753^{+0.046+0.024}_{-0.039-0.024}\cdot10^{-2}$
900	$1.281^{+0.577+0.020}_{-0.330-0.020}\cdot10^{-2}$	$1.366^{+0.140+0.020}_{-0.118-0.020}\cdot10^{-2}$	$1.409^{+0.035+0.020}_{-0.035-0.020}\cdot10^{-2}$
950	$1.026^{+0.478+0.016}_{-0.270-0.016}\cdot10^{-2}$	$1.100^{+0.114+0.017}_{-0.100-0.017}\cdot10^{-2}$	$1.134^{+0.031+0.017}_{-0.030-0.017}\cdot10^{-2}$
1000	$8.249^{+3.952+0.136}_{-2.213-0.136}\cdot10^{-3}$	$8.883^{+0.940+0.140}_{-0.836-0.140}\cdot10^{-3}$	$9.174^{+0.245+0.140}_{-0.252-0.140}\cdot10^{-3}$

Table B.6: Total VBF cross sections at the LHC, $\sqrt{S} = 7\,\text{TeV}$ at LO, NLO and NNLO in QCD. Errors shown are respectively scale and PDF uncertainities. Scale uncertainities are evaluated by varying μ_r and μ_f in the interval $\mu_r, \mu_f \in [Q/4, 4Q]$. The ABKM [70] PDF set has been used. Numbers are in pb.

m_H [GeV]	σ_{LO}	σ_{NLO}	σ_{NNLO}
90	$1.870^{+0.135+0.036}_{-0.129-0.036}$	$1.810^{+0.063+0.036}_{-0.019-0.036}$	$1.801^{+0.026+0.036}_{-0.032-0.036}$
95	$1.776^{+0.136+0.035}_{-0.129-0.035}$	$1.723^{+0.055+0.034}_{-0.024-0.034}$	$1.710^{+0.028+0.034}_{-0.026-0.034}$
100	$1.686^{+0.136+0.033}_{-0.128-0.033}$	$1.637^{+0.054+0.033}_{-0.027-0.033}$	$1.627^{+0.023+0.033}_{-0.030-0.033}$
105	$1.603^{+0.137+0.031}_{-0.128-0.031}$	$1.559^{+0.055+0.031}_{-0.025-0.031}$	$1.545^{+0.025+0.031}_{-0.023-0.031}$
110	$1.524^{+0.140+0.030}_{-0.126-0.030}$	$1.484^{+0.055+0.030}_{-0.025-0.030}$	$1.473^{+0.024+0.030}_{-0.026-0.030}$
115	$1.450^{+0.141+0.029}_{-0.123-0.029}$	$1.411^{+0.055+0.029}_{-0.020-0.029}$	$1.401^{+0.023+0.029}_{-0.022-0.029}$
120	$1.380^{+0.139+0.028}_{-0.121-0.028}$	$1.346^{+0.053+0.028}_{-0.021-0.028}$	$1.335^{+0.025+0.027}_{-0.019-0.027}$
125	$1.314^{+0.140+0.026}_{-0.119-0.026}$	$1.284^{+0.051+0.026}_{-0.021-0.026}$	$1.275^{+0.021+0.026}_{-0.023-0.026}$
130	$1.252^{+0.140+0.025}_{-0.116-0.025}$	$1.225^{+0.050+0.025}_{-0.020-0.025}$	$1.216^{+0.019+0.025}_{-0.019-0.025}$
135	$1.195^{+0.136+0.024}_{-0.114-0.024}$	$1.167^{+0.051+0.024}_{-0.018-0.024}$	$1.158^{+0.024+0.024}_{-0.017-0.024}$
140	$1.141^{+0.133+0.023}_{-0.112-0.023}$	$1.114^{+0.051+0.023}_{-0.015-0.023}$	$1.107^{+0.022+0.023}_{-0.015-0.023}$
145	$1.089^{+0.132+0.022}_{-0.109-0.022}$	$1.067^{+0.047+0.022}_{-0.018-0.022}$	$1.060^{+0.019+0.022}_{-0.018-0.022}$
150	$1.041^{+0.131+0.021}_{-0.108-0.021}$	$1.020^{+0.047+0.021}_{-0.017-0.021}$	$1.013^{+0.020+0.021}_{-0.017-0.021}$
155	$9.962^{+1.292+0.205}_{-1.058-0.205}\cdot10^{-1}$	$9.736^{+0.470+0.206}_{-0.128-0.206}\cdot10^{-1}$	$9.670^{+0.205+0.205}_{-0.117-0.205}\cdot10^{-1}$
160	$9.514^{+1.272+0.196}_{-1.008-0.196}\cdot10^{-1}$	$9.336^{+0.454+0.198}_{-0.147-0.198}\cdot10^{-1}$	$9.278^{+0.189+0.197}_{-0.121-0.197}\cdot10^{-1}$
165	$9.108^{+1.254+0.189}_{-0.999-0.189}\cdot10^{-1}$	$8.935^{+0.458+0.190}_{-0.135-0.190}\cdot10^{-1}$	$8.908^{+0.158+0.190}_{-0.143-0.190}\cdot10^{-1}$
170	$8.721^{+1.238+0.181}_{-0.958-0.181}\cdot10^{-1}$	$8.569^{+0.423+0.183}_{-0.144-0.183}\cdot10^{-1}$	$8.520^{+0.161+0.183}_{-0.133-0.183}\cdot10^{-1}$
175	$8.353^{+1.210+0.174}_{-0.955-0.174}\cdot10^{-1}$	$8.216^{+0.412+0.176}_{-0.129-0.176}\cdot10^{-1}$	$8.182^{+0.119+0.176}_{-0.130-0.176}\cdot10^{-1}$
180	$8.011^{+1.186+0.168}_{-0.933-0.168}\cdot10^{-1}$	$7.867^{+0.404+0.169}_{-0.126-0.169}\cdot10^{-1}$	$7.840^{+0.149+0.169}_{-0.121-0.169}\cdot10^{-1}$
185	$7.684^{+1.169+0.162}_{-0.915-0.162}\cdot10^{-1}$	$7.552^{+0.403+0.163}_{-0.123-0.163}\cdot10^{-1}$	$7.521^{+0.145+0.163}_{-0.108-0.163}\cdot10^{-1}$
190	$7.365^{+1.143+0.155}_{-0.882-0.155}\cdot10^{-1}$	$7.250^{+0.394+0.157}_{-0.122-0.157}\cdot10^{-1}$	$7.216^{+0.152+0.157}_{-0.106-0.157}\cdot10^{-1}$
195	$7.068^{+1.120+0.150}_{-0.853-0.150}\cdot10^{-1}$	$6.959^{+0.388+0.151}_{-0.109-0.151}\cdot10^{-1}$	$6.925^{+0.142+0.151}_{-0.088-0.151}\cdot10^{-1}$
200	$6.782^{+1.097+0.144}_{-0.829-0.144}\cdot10^{-1}$	$6.691^{+0.359+0.146}_{-0.116-0.146}\cdot10^{-1}$	$6.659^{+0.135+0.146}_{-0.086-0.146}\cdot10^{-1}$
210	$6.263^{+1.051+0.134}_{-0.802-0.134}\cdot10^{-1}$	$6.188^{+0.342+0.136}_{-0.116-0.136}\cdot10^{-1}$	$6.149^{+0.136+0.135}_{-0.075-0.135}\cdot10^{-1}$
220	$5.790^{+1.006+0.125}_{-0.762-0.125}\cdot10^{-1}$	$5.713^{+0.330+0.126}_{-0.102-0.126}\cdot10^{-1}$	$5.690^{+0.121+0.126}_{-0.068-0.126}\cdot10^{-1}$
230	$5.350^{+0.977+0.116}_{-0.711-0.116}\cdot10^{-1}$	$5.294^{+0.325+0.118}_{-0.104-0.118}\cdot10^{-1}$	$5.278^{+0.115+0.118}_{-0.062-0.118}\cdot10^{-1}$
240	$4.963^{+0.930+0.108}_{-0.683-0.108}\cdot10^{-1}$	$4.920^{+0.291+0.110}_{-0.101-0.110}\cdot10^{-1}$	$4.896^{+0.107+0.110}_{-0.060-0.110}\cdot10^{-1}$
250	$4.604^{+0.892+0.101}_{-0.647-0.101}\cdot10^{-1}$	$4.569^{+0.286+0.103}_{-0.107-0.103}\cdot10^{-1}$	$4.552^{+0.097+0.103}_{-0.054-0.103}\cdot10^{-1}$
260	$4.277^{+0.850+0.094}_{-0.614-0.094}\cdot10^{-1}$	$4.243^{+0.279+0.096}_{-0.098-0.096}\cdot10^{-1}$	$4.235^{+0.095+0.096}_{-0.046-0.096}\cdot10^{-1}$
270	$3.978^{+0.813+0.088}_{-0.588-0.088}\cdot10^{-1}$	$3.954^{+0.253+0.090}_{-0.099-0.090}\cdot10^{-1}$	$3.944^{+0.095+0.090}_{-0.042-0.090}\cdot10^{-1}$
280	$3.704^{+0.778+0.082}_{-0.554-0.082}\cdot10^{-1}$	$3.688^{+0.248+0.084}_{-0.094-0.084}\cdot10^{-1}$	$3.675^{+0.086+0.084}_{-0.035-0.084}\cdot10^{-1}$
290	$3.453^{+0.748+0.077}_{-0.524-0.077}\cdot10^{-1}$	$3.440^{+0.233+0.079}_{-0.094-0.079}\cdot10^{-1}$	$3.432^{+0.081+0.079}_{-0.032-0.079}\cdot10^{-1}$
300	$3.223^{+0.712+0.073}_{-0.500-0.073}\cdot10^{-1}$	$3.213^{+0.217+0.074}_{-0.087-0.074}\cdot10^{-1}$	$3.206^{+0.077+0.074}_{-0.031-0.074}\cdot10^{-1}$
320	$2.815^{+0.649+0.064}_{-0.451-0.064}\cdot10^{-1}$	$2.812^{+0.198+0.066}_{-0.085-0.066}\cdot10^{-1}$	$2.806^{+0.069+0.066}_{-0.023-0.066}\cdot10^{-1}$
340	$2.465^{+0.597+0.057}_{-0.406-0.057}\cdot10^{-1}$	$2.471^{+0.178+0.058}_{-0.082-0.058}\cdot10^{-1}$	$2.470^{+0.058+0.058}_{-0.021-0.058}\cdot10^{-1}$
360	$2.169^{+0.541+0.050}_{-0.369-0.050}\cdot10^{-1}$	$2.177^{+0.161+0.052}_{-0.075-0.052}\cdot10^{-1}$	$2.175^{+0.053+0.052}_{-0.016-0.052}\cdot10^{-1}$
380	$1.912^{+0.498+0.045}_{-0.334-0.045}\cdot10^{-1}$	$1.927^{+0.144+0.046}_{-0.072-0.046}\cdot10^{-1}$	$1.924^{+0.046+0.046}_{-0.013-0.046}\cdot10^{-1}$
400	$1.692^{+0.454+0.040}_{-0.303-0.040}\cdot10^{-1}$	$1.708^{+0.130+0.041}_{-0.067-0.041}\cdot10^{-1}$	$1.706^{+0.042+0.041}_{-0.011-0.041}\cdot10^{-1}$
450	$1.258^{+0.365+0.031}_{-0.238-0.031}\cdot10^{-1}$	$1.277^{+0.102+0.032}_{-0.057-0.032}\cdot10^{-1}$	$1.276^{+0.032+0.032}_{-0.009-0.032}\cdot10^{-1}$
500	$9.482^{+2.937+0.236}_{-1.882-0.236}\cdot10^{-2}$	$9.674^{+0.804+0.246}_{-0.477-0.246}\cdot10^{-2}$	$9.681^{+0.251+0.247}_{-0.093-0.247}\cdot10^{-2}$
550	$7.236^{+2.369+0.185}_{-1.500-0.185}\cdot10^{-2}$	$7.418^{+0.636+0.194}_{-0.402-0.194}\cdot10^{-2}$	$7.423^{+0.196+0.194}_{-0.080-0.194}\cdot10^{-2}$
600	$5.565^{+1.934+0.147}_{-1.196-0.147}\cdot10^{-2}$	$5.741^{+0.506+0.154}_{-0.338-0.154}\cdot10^{-2}$	$5.749^{+0.155+0.154}_{-0.072-0.154}\cdot10^{-2}$
650	$4.319^{+1.577+0.117}_{-0.961-0.117}\cdot10^{-2}$	$4.478^{+0.408+0.123}_{-0.281-0.123}\cdot10^{-2}$	$4.489^{+0.124+0.124}_{-0.063-0.124}\cdot10^{-2}$
700	$3.376^{+1.292+0.095}_{-0.773-0.095}\cdot10^{-2}$	$3.521^{+0.329+0.100}_{-0.237-0.100}\cdot10^{-2}$	$3.530^{+0.101+0.100}_{-0.055-0.100}\cdot10^{-2}$
750	$2.656^{+1.058+0.077}_{-0.628-0.077}\cdot10^{-2}$	$2.784^{+0.268+0.081}_{-0.197-0.081}\cdot10^{-2}$	$2.794^{+0.080+0.082}_{-0.050-0.082}\cdot10^{-2}$
800	$2.101^{+0.872+0.063}_{-0.510-0.063}\cdot10^{-2}$	$2.214^{+0.217+0.067}_{-0.168-0.067}\cdot10^{-2}$	$2.223^{+0.065+0.067}_{-0.043-0.067}\cdot10^{-2}$
850	$1.670^{+0.718+0.052}_{-0.416-0.052}\cdot10^{-2}$	$1.768^{+0.178+0.055}_{-0.140-0.055}\cdot10^{-2}$	$1.778^{+0.051+0.055}_{-0.038-0.055}\cdot10^{-2}$
900	$1.333^{+0.595+0.043}_{-0.340-0.043}\cdot10^{-2}$	$1.417^{+0.147+0.045}_{-0.118-0.045}\cdot10^{-2}$	$1.426^{+0.042+0.046}_{-0.032-0.046}\cdot10^{-2}$
950	$1.068^{+0.492+0.036}_{-0.279-0.036}\cdot10^{-2}$	$1.142^{+0.120+0.038}_{-0.100-0.038}\cdot10^{-2}$	$1.150^{+0.033+0.038}_{-0.029-0.038}\cdot10^{-2}$
1000	$8.582^{+4.071+0.296}_{-2.286-0.296}\cdot10^{-3}$	$9.224^{+0.991+0.317}_{-0.843-0.317}\cdot10^{-3}$	$9.287^{+0.283+0.319}_{-0.237-0.319}\cdot10^{-3}$

Table B.7: Total VBF cross sections at the LHC, $\sqrt{S} = 7\,\text{TeV}$ at LO, NLO and NNLO in QCD. Errors shown are respectively scale and PDF uncertainities. Scale uncertainities are evaluated by varying μ_r and μ_f in the interval $\mu_r, \mu_f \in [Q/4, 4Q]$. The HERAPDF1.5 [73, 74] PDF set has been used. Numbers are in pb.

m_H [GeV]	σ_{LO}	σ_{NLO}	σ_{NNLO}
90	$1.834^{+0.096+0.023}_{-0.111-0.023}$	$1.776^{+0.047+0.023}_{-0.024-0.023}$	$1.772^{+0.021+0.023}_{-0.026-0.023}$
95	$1.739^{+0.102+0.022}_{-0.107-0.022}$	$1.688^{+0.044+0.022}_{-0.024-0.022}$	$1.684^{+0.019+0.023}_{-0.024-0.023}$
100	$1.654^{+0.105+0.022}_{-0.107-0.022}$	$1.605^{+0.044+0.021}_{-0.021-0.021}$	$1.599^{+0.023+0.022}_{-0.017-0.022}$
105	$1.572^{+0.108+0.021}_{-0.107-0.021}$	$1.530^{+0.045+0.021}_{-0.022-0.021}$	$1.526^{+0.019+0.021}_{-0.022-0.021}$
110	$1.498^{+0.107+0.020}_{-0.108-0.020}$	$1.458^{+0.039+0.020}_{-0.023-0.020}$	$1.453^{+0.014+0.021}_{-0.020-0.021}$
115	$1.428^{+0.105+0.019}_{-0.107-0.019}$	$1.390^{+0.043+0.019}_{-0.023-0.019}$	$1.388^{+0.016+0.020}_{-0.022-0.020}$
120	$1.360^{+0.109+0.019}_{-0.103-0.019}$	$1.325^{+0.042+0.018}_{-0.020-0.018}$	$1.321^{+0.018+0.019}_{-0.018-0.019}$
125	$1.298^{+0.109+0.018}_{-0.105-0.018}$	$1.264^{+0.042+0.018}_{-0.020-0.018}$	$1.260^{+0.017+0.019}_{-0.020-0.019}$
130	$1.239^{+0.112+0.017}_{-0.103-0.017}$	$1.207^{+0.041+0.017}_{-0.018-0.017}$	$1.203^{+0.017+0.018}_{-0.017-0.018}$
135	$1.183^{+0.110+0.017}_{-0.101-0.017}$	$1.152^{+0.041+0.016}_{-0.014-0.016}$	$1.149^{+0.016+0.018}_{-0.014-0.018}$
140	$1.130^{+0.110+0.016}_{-0.099-0.016}$	$1.103^{+0.040+0.016}_{-0.016-0.016}$	$1.098^{+0.018+0.017}_{-0.016-0.017}$
145	$1.080^{+0.110+0.016}_{-0.097-0.016}$	$1.053^{+0.040+0.015}_{-0.014-0.015}$	$1.051^{+0.016+0.017}_{-0.013-0.017}$
150	$1.033^{+0.111+0.015}_{-0.095-0.015}$	$1.010^{+0.039+0.015}_{-0.015-0.015}$	$1.006^{+0.015+0.016}_{-0.014-0.016}$
155	$9.894^{+1.090+0.146}_{-0.946-0.146}\cdot10^{-1}$	$9.676^{+0.368+0.144}_{-0.139-0.144}\cdot10^{-1}$	$9.606^{+0.187+0.159}_{-0.096-0.159}\cdot10^{-1}$
160	$9.464^{+1.078+0.141}_{-0.908-0.141}\cdot10^{-1}$	$9.267^{+0.361+0.140}_{-0.139-0.140}\cdot10^{-1}$	$9.231^{+0.158+0.155}_{-0.137-0.155}\cdot10^{-1}$
165	$9.067^{+1.056+0.137}_{-0.884-0.137}\cdot10^{-1}$	$8.880^{+0.353+0.135}_{-0.132-0.135}\cdot10^{-1}$	$8.847^{+0.141+0.151}_{-0.106-0.151}\cdot10^{-1}$
170	$8.692^{+1.045+0.133}_{-0.887-0.133}\cdot10^{-1}$	$8.516^{+0.349+0.131}_{-0.128-0.131}\cdot10^{-1}$	$8.468^{+0.148+0.146}_{-0.090-0.146}\cdot10^{-1}$
175	$8.336^{+1.028+0.129}_{-0.859-0.129}\cdot10^{-1}$	$8.169^{+0.348+0.127}_{-0.108-0.127}\cdot10^{-1}$	$8.135^{+0.124+0.142}_{-0.088-0.142}\cdot10^{-1}$
180	$7.992^{+1.011+0.125}_{-0.836-0.125}\cdot10^{-1}$	$7.846^{+0.335+0.123}_{-0.126-0.123}\cdot10^{-1}$	$7.806^{+0.134+0.139}_{-0.098-0.139}\cdot10^{-1}$
185	$7.677^{+1.003+0.121}_{-0.832-0.121}\cdot10^{-1}$	$7.544^{+0.328+0.120}_{-0.121-0.120}\cdot10^{-1}$	$7.496^{+0.127+0.135}_{-0.085-0.135}\cdot10^{-1}$
190	$7.373^{+0.975+0.118}_{-0.813-0.118}\cdot10^{-1}$	$7.234^{+0.329+0.116}_{-0.101-0.116}\cdot10^{-1}$	$7.201^{+0.118+0.131}_{-0.077-0.131}\cdot10^{-1}$
195	$7.081^{+0.966+0.114}_{-0.796-0.114}\cdot10^{-1}$	$6.963^{+0.303+0.113}_{-0.114-0.113}\cdot10^{-1}$	$6.911^{+0.125+0.127}_{-0.072-0.127}\cdot10^{-1}$
200	$6.804^{+0.944+0.111}_{-0.772-0.111}\cdot10^{-1}$	$6.691^{+0.302+0.109}_{-0.109-0.109}\cdot10^{-1}$	$6.649^{+0.114+0.124}_{-0.078-0.124}\cdot10^{-1}$
210	$6.286^{+0.913+0.104}_{-0.737-0.104}\cdot10^{-1}$	$6.192^{+0.292+0.103}_{-0.099-0.103}\cdot10^{-1}$	$6.139^{+0.115+0.117}_{-0.053-0.117}\cdot10^{-1}$
220	$5.811^{+0.897+0.098}_{-0.697-0.098}\cdot10^{-1}$	$5.740^{+0.271+0.097}_{-0.101-0.097}\cdot10^{-1}$	$5.701^{+0.095+0.112}_{-0.062-0.112}\cdot10^{-1}$
230	$5.389^{+0.856+0.093}_{-0.668-0.093}\cdot10^{-1}$	$5.323^{+0.273+0.092}_{-0.087-0.092}\cdot10^{-1}$	$5.282^{+0.092+0.106}_{-0.046-0.106}\cdot10^{-1}$
240	$5.002^{+0.820+0.088}_{-0.633-0.088}\cdot10^{-1}$	$4.945^{+0.250+0.087}_{-0.089-0.087}\cdot10^{-1}$	$4.909^{+0.092+0.100}_{-0.044-0.100}\cdot10^{-1}$
250	$4.646^{+0.786+0.083}_{-0.604-0.083}\cdot10^{-1}$	$4.595^{+0.246+0.082}_{-0.078-0.082}\cdot10^{-1}$	$4.559^{+0.091+0.095}_{-0.035-0.095}\cdot10^{-1}$
260	$4.323^{+0.760+0.079}_{-0.575-0.079}\cdot10^{-1}$	$4.284^{+0.229+0.078}_{-0.083-0.078}\cdot10^{-1}$	$4.248^{+0.076+0.090}_{-0.041-0.090}\cdot10^{-1}$
270	$4.025^{+0.730+0.075}_{-0.544-0.075}\cdot10^{-1}$	$3.989^{+0.219+0.074}_{-0.074-0.074}\cdot10^{-1}$	$3.958^{+0.080+0.086}_{-0.029-0.086}\cdot10^{-1}$
280	$3.753^{+0.700+0.071}_{-0.521-0.071}\cdot10^{-1}$	$3.727^{+0.205+0.070}_{-0.076-0.070}\cdot10^{-1}$	$3.693^{+0.072+0.081}_{-0.024-0.081}\cdot10^{-1}$
290	$3.504^{+0.669+0.068}_{-0.495-0.068}\cdot10^{-1}$	$3.479^{+0.201+0.067}_{-0.070-0.067}\cdot10^{-1}$	$3.449^{+0.070+0.077}_{-0.025-0.077}\cdot10^{-1}$
300	$3.270^{+0.641+0.064}_{-0.470-0.064}\cdot10^{-1}$	$3.255^{+0.188+0.064}_{-0.075-0.064}\cdot10^{-1}$	$3.229^{+0.061+0.074}_{-0.025-0.074}\cdot10^{-1}$
320	$2.865^{+0.590+0.058}_{-0.431-0.058}\cdot10^{-1}$	$2.855^{+0.170+0.058}_{-0.070-0.058}\cdot10^{-1}$	$2.830^{+0.055+0.067}_{-0.020-0.067}\cdot10^{-1}$
340	$2.517^{+0.538+0.053}_{-0.392-0.053}\cdot10^{-1}$	$2.514^{+0.155+0.053}_{-0.070-0.053}\cdot10^{-1}$	$2.494^{+0.045+0.061}_{-0.021-0.061}\cdot10^{-1}$
360	$2.214^{+0.497+0.048}_{-0.352-0.048}\cdot10^{-1}$	$2.218^{+0.141+0.048}_{-0.066-0.048}\cdot10^{-1}$	$2.196^{+0.044+0.055}_{-0.012-0.055}\cdot10^{-1}$
380	$1.956^{+0.461+0.044}_{-0.320-0.044}\cdot10^{-1}$	$1.966^{+0.127+0.044}_{-0.062-0.044}\cdot10^{-1}$	$1.944^{+0.041+0.050}_{-0.010-0.050}\cdot10^{-1}$
400	$1.733^{+0.420+0.040}_{-0.290-0.040}\cdot10^{-1}$	$1.744^{+0.116+0.040}_{-0.059-0.040}\cdot10^{-1}$	$1.724^{+0.035+0.045}_{-0.008-0.045}\cdot10^{-1}$
450	$1.294^{+0.339+0.032}_{-0.231-0.032}\cdot10^{-1}$	$1.309^{+0.091+0.032}_{-0.050-0.032}\cdot10^{-1}$	$1.293^{+0.027+0.036}_{-0.008-0.036}\cdot10^{-1}$
500	$9.779^{+2.756+0.261}_{-1.831-0.261}\cdot10^{-2}$	$9.944^{+0.724+0.262}_{-0.424-0.262}\cdot10^{-2}$	$9.810^{+0.212+0.290}_{-0.077-0.290}\cdot10^{-2}$
550	$7.478^{+2.242+0.213}_{-1.469-0.213}\cdot10^{-2}$	$7.638^{+0.587+0.215}_{-0.359-0.215}\cdot10^{-2}$	$7.528^{+0.174+0.234}_{-0.071-0.234}\cdot10^{-2}$
600	$5.765^{+1.834+0.175}_{-1.178-0.175}\cdot10^{-2}$	$5.924^{+0.465+0.177}_{-0.304-0.177}\cdot10^{-2}$	$5.829^{+0.130+0.191}_{-0.061-0.191}\cdot10^{-2}$
650	$4.482^{+1.505+0.144}_{-0.950-0.144}\cdot10^{-2}$	$4.632^{+0.373+0.146}_{-0.260-0.146}\cdot10^{-2}$	$4.552^{+0.109+0.156}_{-0.059-0.156}\cdot10^{-2}$
700	$3.510^{+1.233+0.119}_{-0.770-0.119}\cdot10^{-2}$	$3.645^{+0.303+0.122}_{-0.221-0.122}\cdot10^{-2}$	$3.579^{+0.082+0.128}_{-0.051-0.128}\cdot10^{-2}$
750	$2.764^{+1.014+0.099}_{-0.625-0.099}\cdot10^{-2}$	$2.885^{+0.249+0.102}_{-0.184-0.102}\cdot10^{-2}$	$2.827^{+0.066+0.106}_{-0.044-0.106}\cdot10^{-2}$
800	$2.189^{+0.836+0.082}_{-0.509-0.082}\cdot10^{-2}$	$2.297^{+0.202+0.085}_{-0.157-0.085}\cdot10^{-2}$	$2.248^{+0.055+0.088}_{-0.038-0.088}\cdot10^{-2}$
850	$1.742^{+0.691+0.069}_{-0.417-0.069}\cdot10^{-2}$	$1.836^{+0.167+0.071}_{-0.132-0.071}\cdot10^{-2}$	$1.794^{+0.044+0.073}_{-0.032-0.073}\cdot10^{-2}$
900	$1.391^{+0.573+0.058}_{-0.341-0.058}\cdot10^{-2}$	$1.473^{+0.137+0.060}_{-0.112-0.060}\cdot10^{-2}$	$1.438^{+0.036+0.061}_{-0.029-0.061}\cdot10^{-2}$
950	$1.116^{+0.475+0.048}_{-0.281-0.048}\cdot10^{-2}$	$1.187^{+0.112+0.051}_{-0.095-0.051}\cdot10^{-2}$	$1.157^{+0.029+0.051}_{-0.025-0.051}\cdot10^{-2}$
1000	$8.969^{+3.948+0.407}_{-2.294-0.407}\cdot10^{-3}$	$9.598^{+0.924+0.427}_{-0.808-0.427}\cdot10^{-3}$	$9.340^{+0.238+0.426}_{-0.216-0.426}\cdot10^{-3}$

Table B.8: Total VBF cross sections at the LHC, $\sqrt{S} = 7\,\text{TeV}$ at LO, NLO and NNLO in QCD. Errors shown are respectively scale and PDF uncertainities. Scale uncertainities are evaluated by varying μ_r and μ_f in the interval $\mu_r, \mu_f \in [Q/4, 4Q]$. The JR09 [75, 76] PDF set has been used. Numbers are in pb.

m_H [GeV]	σ_{LO}	σ_{NLO}	σ_{NNLO}
90	$1.674^{+0.127+0.021}_{-0.125-0.021}$	$1.782^{+0.059+0.035}_{-0.026-0.035}$	$1.789^{+0.028+0.032}_{-0.033-0.032}$
95	$1.589^{+0.124+0.020}_{-0.123-0.020}$	$1.697^{+0.053+0.034}_{-0.033-0.034}$	$1.697^{+0.027+0.030}_{-0.026-0.030}$
100	$1.510^{+0.129+0.019}_{-0.126-0.019}$	$1.608^{+0.059+0.032}_{-0.029-0.032}$	$1.616^{+0.025+0.029}_{-0.034-0.029}$
105	$1.435^{+0.129+0.018}_{-0.122-0.018}$	$1.531^{+0.059+0.031}_{-0.028-0.031}$	$1.536^{+0.024+0.027}_{-0.033-0.027}$
110	$1.366^{+0.130+0.017}_{-0.120-0.017}$	$1.456^{+0.055+0.029}_{-0.027-0.029}$	$1.460^{+0.025+0.026}_{-0.027-0.026}$
115	$1.300^{+0.131+0.017}_{-0.118-0.017}$	$1.386^{+0.053+0.028}_{-0.022-0.028}$	$1.391^{+0.026+0.025}_{-0.028-0.025}$
120	$1.239^{+0.132+0.016}_{-0.117-0.016}$	$1.320^{+0.055+0.027}_{-0.026-0.027}$	$1.324^{+0.025+0.024}_{-0.023-0.024}$
125	$1.181^{+0.131+0.015}_{-0.116-0.015}$	$1.258^{+0.057+0.026}_{-0.020-0.026}$	$1.264^{+0.023+0.023}_{-0.023-0.023}$
130	$1.127^{+0.130+0.015}_{-0.112-0.015}$	$1.200^{+0.053+0.024}_{-0.020-0.024}$	$1.203^{+0.026+0.022}_{-0.021-0.022}$
135	$1.075^{+0.129+0.014}_{-0.110-0.014}$	$1.144^{+0.053+0.023}_{-0.018-0.023}$	$1.153^{+0.018+0.021}_{-0.023-0.021}$
140	$1.027^{+0.129+0.014}_{-0.107-0.014}$	$1.094^{+0.051+0.022}_{-0.018-0.022}$	$1.099^{+0.024+0.020}_{-0.019-0.020}$
145	$9.818^{+1.264+0.130}_{-1.063-0.130}\cdot10^{-1}$	$1.045^{+0.050+0.022}_{-0.018-0.022}$	$1.050^{+0.021+0.020}_{-0.021-0.020}$
150	$9.383^{+1.246+0.125}_{-1.026-0.125}\cdot10^{-1}$	$9.998^{+0.486+0.207}_{-0.175-0.207}\cdot10^{-1}$	$1.003^{+0.021+0.019}_{-0.016-0.019}$
155	$8.986^{+1.204+0.121}_{-1.026-0.121}\cdot10^{-1}$	$9.570^{+0.463+0.199}_{-0.185-0.199}\cdot10^{-1}$	$9.599^{+0.209+0.180}_{-0.154-0.180}\cdot10^{-1}$
160	$8.599^{+1.224+0.116}_{-0.997-0.116}\cdot10^{-1}$	$9.161^{+0.450+0.191}_{-0.163-0.191}\cdot10^{-1}$	$9.176^{+0.183+0.173}_{-0.133-0.173}\cdot10^{-1}$
165	$8.233^{+1.199+0.112}_{-0.973-0.112}\cdot10^{-1}$	$8.765^{+0.443+0.184}_{-0.143-0.184}\cdot10^{-1}$	$8.809^{+0.184+0.167}_{-0.150-0.167}\cdot10^{-1}$
170	$7.886^{+1.182+0.108}_{-0.955-0.108}\cdot10^{-1}$	$8.394^{+0.439+0.176}_{-0.151-0.176}\cdot10^{-1}$	$8.411^{+0.202+0.160}_{-0.126-0.160}\cdot10^{-1}$
175	$7.558^{+1.156+0.104}_{-0.931-0.104}\cdot10^{-1}$	$8.037^{+0.435+0.169}_{-0.127-0.169}\cdot10^{-1}$	$8.085^{+0.174+0.154}_{-0.129-0.154}\cdot10^{-1}$
180	$7.244^{+1.148+0.100}_{-0.903-0.100}\cdot10^{-1}$	$7.713^{+0.420+0.163}_{-0.131-0.163}\cdot10^{-1}$	$7.732^{+0.187+0.148}_{-0.105-0.148}\cdot10^{-1}$
185	$6.957^{+1.123+0.096}_{-0.887-0.096}\cdot10^{-1}$	$7.398^{+0.411+0.157}_{-0.123-0.157}\cdot10^{-1}$	$7.412^{+0.185+0.142}_{-0.090-0.142}\cdot10^{-1}$
190	$6.667^{+1.106+0.093}_{-0.854-0.093}\cdot10^{-1}$	$7.105^{+0.384+0.151}_{-0.136-0.151}\cdot10^{-1}$	$7.127^{+0.166+0.137}_{-0.102-0.137}\cdot10^{-1}$
195	$6.404^{+1.093+0.090}_{-0.833-0.090}\cdot10^{-1}$	$6.822^{+0.383+0.146}_{-0.135-0.146}\cdot10^{-1}$	$6.856^{+0.146+0.133}_{-0.114-0.133}\cdot10^{-1}$
200	$6.156^{+1.062+0.087}_{-0.817-0.087}\cdot10^{-1}$	$6.543^{+0.385+0.140}_{-0.116-0.140}\cdot10^{-1}$	$6.580^{+0.143+0.128}_{-0.096-0.128}\cdot10^{-1}$
210	$5.683^{+1.029+0.081}_{-0.767-0.081}\cdot10^{-1}$	$6.049^{+0.351+0.131}_{-0.121-0.131}\cdot10^{-1}$	$6.081^{+0.137+0.119}_{-0.090-0.119}\cdot10^{-1}$
220	$5.256^{+0.986+0.075}_{-0.737-0.075}\cdot10^{-1}$	$5.593^{+0.336+0.121}_{-0.113-0.121}\cdot10^{-1}$	$5.623^{+0.126+0.111}_{-0.075-0.111}\cdot10^{-1}$
230	$4.871^{+0.942+0.070}_{-0.695-0.070}\cdot10^{-1}$	$5.184^{+0.322+0.113}_{-0.109-0.113}\cdot10^{-1}$	$5.213^{+0.114+0.104}_{-0.075-0.104}\cdot10^{-1}$
240	$4.523^{+0.905+0.066}_{-0.672-0.066}\cdot10^{-1}$	$4.811^{+0.295+0.106}_{-0.118-0.106}\cdot10^{-1}$	$4.834^{+0.110+0.097}_{-0.064-0.097}\cdot10^{-1}$
250	$4.200^{+0.868+0.062}_{-0.633-0.062}\cdot10^{-1}$	$4.457^{+0.298+0.099}_{-0.101-0.099}\cdot10^{-1}$	$4.488^{+0.107+0.090}_{-0.055-0.090}\cdot10^{-1}$
260	$3.907^{+0.830+0.058}_{-0.601-0.058}\cdot10^{-1}$	$4.147^{+0.272+0.092}_{-0.102-0.092}\cdot10^{-1}$	$4.175^{+0.098+0.085}_{-0.052-0.085}\cdot10^{-1}$
270	$3.638^{+0.796+0.054}_{-0.574-0.054}\cdot10^{-1}$	$3.860^{+0.258+0.086}_{-0.101-0.086}\cdot10^{-1}$	$3.886^{+0.098+0.079}_{-0.044-0.079}\cdot10^{-1}$
280	$3.391^{+0.762+0.051}_{-0.545-0.051}\cdot10^{-1}$	$3.594^{+0.247+0.081}_{-0.098-0.081}\cdot10^{-1}$	$3.623^{+0.090+0.075}_{-0.043-0.075}\cdot10^{-1}$
290	$3.162^{+0.731+0.048}_{-0.516-0.048}\cdot10^{-1}$	$3.360^{+0.226+0.076}_{-0.101-0.076}\cdot10^{-1}$	$3.380^{+0.086+0.070}_{-0.036-0.070}\cdot10^{-1}$
300	$2.956^{+0.698+0.045}_{-0.492-0.045}\cdot10^{-1}$	$3.137^{+0.217+0.071}_{-0.100-0.071}\cdot10^{-1}$	$3.156^{+0.078+0.066}_{-0.031-0.066}\cdot10^{-1}$
320	$2.587^{+0.640+0.040}_{-0.445-0.040}\cdot10^{-1}$	$2.740^{+0.198+0.063}_{-0.088-0.063}\cdot10^{-1}$	$2.762^{+0.073+0.058}_{-0.027-0.058}\cdot10^{-1}$
340	$2.268^{+0.589+0.035}_{-0.399-0.035}\cdot10^{-1}$	$2.405^{+0.180+0.056}_{-0.081-0.056}\cdot10^{-1}$	$2.424^{+0.066+0.052}_{-0.022-0.052}\cdot10^{-1}$
360	$1.998^{+0.538+0.032}_{-0.362-0.032}\cdot10^{-1}$	$2.119^{+0.161+0.049}_{-0.078-0.049}\cdot10^{-1}$	$2.136^{+0.057+0.046}_{-0.018-0.046}\cdot10^{-1}$
380	$1.766^{+0.494+0.028}_{-0.329-0.028}\cdot10^{-1}$	$1.870^{+0.147+0.044}_{-0.074-0.044}\cdot10^{-1}$	$1.886^{+0.052+0.041}_{-0.014-0.041}\cdot10^{-1}$
400	$1.565^{+0.453+0.025}_{-0.299-0.025}\cdot10^{-1}$	$1.657^{+0.131+0.039}_{-0.070-0.039}\cdot10^{-1}$	$1.671^{+0.045+0.037}_{-0.014-0.037}\cdot10^{-1}$
450	$1.169^{+0.367+0.020}_{-0.236-0.020}\cdot10^{-1}$	$1.235^{+0.103+0.030}_{-0.058-0.030}\cdot10^{-1}$	$1.248^{+0.035+0.028}_{-0.013-0.028}\cdot10^{-1}$
500	$8.851^{+2.964+0.152}_{-1.876-0.152}\cdot10^{-2}$	$9.341^{+0.813+0.229}_{-0.485-0.229}\cdot10^{-2}$	$9.440^{+0.265+0.218}_{-0.110-0.218}\cdot10^{-2}$
550	$6.770^{+2.425+0.120}_{-1.495-0.120}\cdot10^{-2}$	$7.143^{+0.645+0.178}_{-0.404-0.178}\cdot10^{-2}$	$7.225^{+0.209+0.170}_{-0.099-0.170}\cdot10^{-2}$
600	$5.233^{+1.974+0.095}_{-1.203-0.095}\cdot10^{-2}$	$5.516^{+0.514+0.139}_{-0.339-0.139}\cdot10^{-2}$	$5.581^{+0.162+0.134}_{-0.086-0.134}\cdot10^{-2}$
650	$4.076^{+1.621+0.076}_{-0.969-0.076}\cdot10^{-2}$	$4.296^{+0.411+0.110}_{-0.286-0.110}\cdot10^{-2}$	$4.345^{+0.131+0.106}_{-0.072-0.106}\cdot10^{-2}$
700	$3.198^{+1.333+0.061}_{-0.785-0.061}\cdot10^{-2}$	$3.368^{+0.330+0.087}_{-0.239-0.087}\cdot10^{-2}$	$3.408^{+0.109+0.085}_{-0.062-0.085}\cdot10^{-2}$
750	$2.526^{+1.096+0.050}_{-0.638-0.050}\cdot10^{-2}$	$2.658^{+0.268+0.070}_{-0.201-0.070}\cdot10^{-2}$	$2.692^{+0.081+0.068}_{-0.055-0.068}\cdot10^{-2}$
800	$2.007^{+0.906+0.041}_{-0.522-0.041}\cdot10^{-2}$	$2.108^{+0.216+0.056}_{-0.168-0.056}\cdot10^{-2}$	$2.136^{+0.068+0.055}_{-0.047-0.055}\cdot10^{-2}$
850	$1.599^{+0.753+0.033}_{-0.426-0.033}\cdot10^{-2}$	$1.680^{+0.179+0.045}_{-0.140-0.045}\cdot10^{-2}$	$1.702^{+0.056+0.045}_{-0.040-0.045}\cdot10^{-2}$
900	$1.281^{+0.625+0.028}_{-0.349-0.028}\cdot10^{-2}$	$1.345^{+0.145+0.037}_{-0.118-0.037}\cdot10^{-2}$	$1.365^{+0.042+0.037}_{-0.036-0.037}\cdot10^{-2}$
950	$1.030^{+0.521+0.023}_{-0.287-0.023}\cdot10^{-2}$	$1.081^{+0.120+0.030}_{-0.100-0.030}\cdot10^{-2}$	$1.096^{+0.035+0.030}_{-0.030-0.030}\cdot10^{-2}$
1000	$8.307^{+4.344+0.189}_{-2.363-0.189}\cdot10^{-3}$	$8.713^{+0.982+0.243}_{-0.834-0.243}\cdot10^{-3}$	$8.838^{+0.291+0.245}_{-0.259-0.245}\cdot10^{-3}$

Table B.9: Total VBF cross sections at the LHC, $\sqrt{S} = 7\,\text{TeV}$ at LO, NLO and NNLO in QCD. Errors shown are respectively scale and PDF uncertainities. Scale uncertainities are evaluated by varying μ_r and μ_f in the interval $\mu_r, \mu_f \in [Q/4, 4Q]$. The MSTW2008 [63] PDF set (68% CL) has been used. Numbers are in pb.

m_H [GeV]	σ_{LO}	σ_{NLO}	σ_{NNLO}
90	$1.818^{+0.112+0.026}_{-0.118-0.026}$	$1.760^{+0.056+0.026}_{-0.029-0.026}$	$1.774^{+0.029+0.023}_{-0.030-0.023}$
95	$1.726^{+0.114+0.025}_{-0.118-0.025}$	$1.672^{+0.055+0.025}_{-0.026-0.025}$	$1.684^{+0.030+0.022}_{-0.031-0.022}$
100	$1.640^{+0.118+0.024}_{-0.119-0.024}$	$1.591^{+0.052+0.024}_{-0.028-0.024}$	$1.603^{+0.028+0.021}_{-0.028-0.021}$
105	$1.560^{+0.118+0.023}_{-0.118-0.023}$	$1.515^{+0.049+0.023}_{-0.029-0.023}$	$1.522^{+0.028+0.020}_{-0.027-0.020}$
110	$1.482^{+0.121+0.022}_{-0.117-0.022}$	$1.441^{+0.051+0.022}_{-0.023-0.022}$	$1.448^{+0.027+0.019}_{-0.023-0.019}$
115	$1.411^{+0.121+0.021}_{-0.116-0.021}$	$1.372^{+0.050+0.021}_{-0.021-0.021}$	$1.378^{+0.029+0.018}_{-0.024-0.018}$
120	$1.344^{+0.126+0.020}_{-0.116-0.020}$	$1.308^{+0.049+0.020}_{-0.022-0.020}$	$1.318^{+0.021+0.017}_{-0.028-0.017}$
125	$1.280^{+0.124+0.020}_{-0.111-0.020}$	$1.246^{+0.051+0.019}_{-0.018-0.019}$	$1.252^{+0.026+0.016}_{-0.019-0.016}$
130	$1.221^{+0.122+0.019}_{-0.111-0.019}$	$1.189^{+0.050+0.019}_{-0.017-0.019}$	$1.195^{+0.027+0.016}_{-0.018-0.016}$
135	$1.165^{+0.123+0.018}_{-0.109-0.018}$	$1.137^{+0.045+0.018}_{-0.019-0.018}$	$1.143^{+0.022+0.015}_{-0.017-0.015}$
140	$1.112^{+0.122+0.017}_{-0.106-0.017}$	$1.087^{+0.045+0.017}_{-0.021-0.017}$	$1.093^{+0.021+0.015}_{-0.020-0.015}$
145	$1.062^{+0.121+0.017}_{-0.103-0.017}$	$1.037^{+0.047+0.017}_{-0.016-0.017}$	$1.043^{+0.021+0.014}_{-0.015-0.014}$
150	$1.015^{+0.120+0.016}_{-0.102-0.016}$	$9.924^{+0.453+0.160}_{-0.176-0.160}\cdot10^{-1}$	$9.990^{+0.199+0.134}_{-0.190-0.134}\cdot10^{-1}$
155	$9.706^{+1.189+0.154}_{-0.999-0.154}\cdot10^{-1}$	$9.492^{+0.449+0.154}_{-0.143-0.154}\cdot10^{-1}$	$9.541^{+0.199+0.129}_{-0.146-0.129}\cdot10^{-1}$
160	$9.283^{+1.160+0.148}_{-0.969-0.148}\cdot10^{-1}$	$9.086^{+0.440+0.148}_{-0.142-0.148}\cdot10^{-1}$	$9.146^{+0.169+0.124}_{-0.139-0.124}\cdot10^{-1}$
165	$8.890^{+1.167+0.143}_{-0.949-0.143}\cdot10^{-1}$	$8.709^{+0.413+0.143}_{-0.140-0.143}\cdot10^{-1}$	$8.761^{+0.183+0.120}_{-0.148-0.120}\cdot10^{-1}$
170	$8.514^{+1.143+0.137}_{-0.937-0.137}\cdot10^{-1}$	$8.341^{+0.416+0.138}_{-0.136-0.138}\cdot10^{-1}$	$8.390^{+0.174+0.115}_{-0.125-0.115}\cdot10^{-1}$
175	$8.159^{+1.123+0.133}_{-0.929-0.133}\cdot10^{-1}$	$8.006^{+0.388+0.133}_{-0.138-0.133}\cdot10^{-1}$	$8.043^{+0.168+0.111}_{-0.124-0.111}\cdot10^{-1}$
180	$7.831^{+1.096+0.128}_{-0.908-0.128}\cdot10^{-1}$	$7.679^{+0.394+0.128}_{-0.138-0.128}\cdot10^{-1}$	$7.707^{+0.181+0.107}_{-0.108-0.107}\cdot10^{-1}$
185	$7.506^{+1.087+0.123}_{-0.879-0.123}\cdot10^{-1}$	$7.377^{+0.376+0.124}_{-0.131-0.124}\cdot10^{-1}$	$7.411^{+0.156+0.103}_{-0.113-0.103}\cdot10^{-1}$
190	$7.204^{+1.064+0.119}_{-0.856-0.119}\cdot10^{-1}$	$7.065^{+0.377+0.120}_{-0.115-0.120}\cdot10^{-1}$	$7.118^{+0.154+0.100}_{-0.127-0.100}\cdot10^{-1}$
195	$6.904^{+1.057+0.115}_{-0.824-0.115}\cdot10^{-1}$	$6.789^{+0.371+0.116}_{-0.109-0.116}\cdot10^{-1}$	$6.827^{+0.153+0.096}_{-0.094-0.096}\cdot10^{-1}$
200	$6.640^{+1.027+0.111}_{-0.820-0.111}\cdot10^{-1}$	$6.526^{+0.344+0.112}_{-0.110-0.112}\cdot10^{-1}$	$6.557^{+0.156+0.093}_{-0.090-0.093}\cdot10^{-1}$
210	$6.128^{+0.990+0.104}_{-0.776-0.104}\cdot10^{-1}$	$6.037^{+0.327+0.104}_{-0.108-0.104}\cdot10^{-1}$	$6.058^{+0.150+0.087}_{-0.086-0.087}\cdot10^{-1}$
220	$5.656^{+0.960+0.097}_{-0.729-0.097}\cdot10^{-1}$	$5.589^{+0.312+0.098}_{-0.103-0.098}\cdot10^{-1}$	$5.612^{+0.122+0.081}_{-0.074-0.081}\cdot10^{-1}$
230	$5.243^{+0.915+0.091}_{-0.703-0.091}\cdot10^{-1}$	$5.180^{+0.297+0.092}_{-0.101-0.092}\cdot10^{-1}$	$5.202^{+0.115+0.076}_{-0.071-0.076}\cdot10^{-1}$
240	$4.856^{+0.884+0.085}_{-0.665-0.085}\cdot10^{-1}$	$4.809^{+0.279+0.086}_{-0.101-0.086}\cdot10^{-1}$	$4.828^{+0.111+0.071}_{-0.072-0.071}\cdot10^{-1}$
250	$4.512^{+0.843+0.080}_{-0.633-0.080}\cdot10^{-1}$	$4.465^{+0.273+0.080}_{-0.092-0.080}\cdot10^{-1}$	$4.487^{+0.104+0.067}_{-0.057-0.067}\cdot10^{-1}$
260	$4.188^{+0.813+0.075}_{-0.598-0.075}\cdot10^{-1}$	$4.154^{+0.254+0.076}_{-0.095-0.076}\cdot10^{-1}$	$4.176^{+0.097+0.063}_{-0.055-0.063}\cdot10^{-1}$
270	$3.898^{+0.777+0.070}_{-0.570-0.070}\cdot10^{-1}$	$3.872^{+0.240+0.071}_{-0.095-0.071}\cdot10^{-1}$	$3.888^{+0.091+0.059}_{-0.054-0.059}\cdot10^{-1}$
280	$3.631^{+0.743+0.066}_{-0.543-0.066}\cdot10^{-1}$	$3.614^{+0.225+0.067}_{-0.097-0.067}\cdot10^{-1}$	$3.627^{+0.084+0.056}_{-0.044-0.056}\cdot10^{-1}$
290	$3.386^{+0.714+0.062}_{-0.514-0.062}\cdot10^{-1}$	$3.371^{+0.216+0.063}_{-0.088-0.063}\cdot10^{-1}$	$3.384^{+0.082+0.053}_{-0.037-0.053}\cdot10^{-1}$
300	$3.158^{+0.688+0.058}_{-0.489-0.058}\cdot10^{-1}$	$3.146^{+0.210+0.059}_{-0.085-0.059}\cdot10^{-1}$	$3.163^{+0.075+0.050}_{-0.033-0.050}\cdot10^{-1}$
320	$2.762^{+0.629+0.052}_{-0.443-0.052}\cdot10^{-1}$	$2.760^{+0.185+0.053}_{-0.084-0.053}\cdot10^{-1}$	$2.770^{+0.069+0.044}_{-0.030-0.044}\cdot10^{-1}$
340	$2.422^{+0.575+0.047}_{-0.399-0.047}\cdot10^{-1}$	$2.423^{+0.171+0.047}_{-0.077-0.047}\cdot10^{-1}$	$2.435^{+0.062+0.040}_{-0.023-0.040}\cdot10^{-1}$
360	$2.130^{+0.528+0.042}_{-0.364-0.042}\cdot10^{-1}$	$2.138^{+0.153+0.043}_{-0.075-0.043}\cdot10^{-1}$	$2.145^{+0.055+0.036}_{-0.017-0.036}\cdot10^{-1}$
380	$1.879^{+0.481+0.037}_{-0.329-0.037}\cdot10^{-1}$	$1.891^{+0.139+0.038}_{-0.070-0.038}\cdot10^{-1}$	$1.897^{+0.050+0.032}_{-0.013-0.032}\cdot10^{-1}$
400	$1.664^{+0.442+0.034}_{-0.299-0.034}\cdot10^{-1}$	$1.677^{+0.126+0.035}_{-0.066-0.035}\cdot10^{-1}$	$1.682^{+0.045+0.029}_{-0.012-0.029}\cdot10^{-1}$
450	$1.239^{+0.355+0.026}_{-0.236-0.026}\cdot10^{-1}$	$1.256^{+0.098+0.027}_{-0.056-0.027}\cdot10^{-1}$	$1.259^{+0.033+0.023}_{-0.010-0.023}\cdot10^{-1}$
500	$9.335^{+2.889+0.205}_{-1.852-0.205}\cdot10^{-2}$	$9.529^{+0.777+0.212}_{-0.469-0.212}\cdot10^{-2}$	$9.547^{+0.264+0.182}_{-0.086-0.182}\cdot10^{-2}$
550	$7.133^{+2.336+0.162}_{-1.490-0.162}\cdot10^{-2}$	$7.313^{+0.616+0.169}_{-0.396-0.169}\cdot10^{-2}$	$7.330^{+0.197+0.146}_{-0.088-0.146}\cdot10^{-2}$
600	$5.495^{+1.908+0.130}_{-1.189-0.130}\cdot10^{-2}$	$5.665^{+0.495+0.135}_{-0.331-0.135}\cdot10^{-2}$	$5.682^{+0.159+0.118}_{-0.081-0.118}\cdot10^{-2}$
650	$4.268^{+1.559+0.105}_{-0.955-0.105}\cdot10^{-2}$	$4.428^{+0.396+0.110}_{-0.277-0.110}\cdot10^{-2}$	$4.434^{+0.125+0.096}_{-0.064-0.096}\cdot10^{-2}$
700	$3.341^{+1.276+0.085}_{-0.772-0.085}\cdot10^{-2}$	$3.483^{+0.322+0.089}_{-0.235-0.089}\cdot10^{-2}$	$3.490^{+0.096+0.079}_{-0.061-0.079}\cdot10^{-2}$
750	$2.631^{+1.051+0.070}_{-0.625-0.070}\cdot10^{-2}$	$2.758^{+0.261+0.073}_{-0.198-0.073}\cdot10^{-2}$	$2.763^{+0.082+0.065}_{-0.055-0.065}\cdot10^{-2}$
800	$2.085^{+0.863+0.057}_{-0.510-0.057}\cdot10^{-2}$	$2.195^{+0.213+0.060}_{-0.167-0.060}\cdot10^{-2}$	$2.200^{+0.063+0.054}_{-0.046-0.054}\cdot10^{-2}$
850	$1.660^{+0.712+0.047}_{-0.418-0.047}\cdot10^{-2}$	$1.755^{+0.176+0.050}_{-0.141-0.050}\cdot10^{-2}$	$1.758^{+0.052+0.045}_{-0.040-0.045}\cdot10^{-2}$
900	$1.325^{+0.590+0.039}_{-0.340-0.039}\cdot10^{-2}$	$1.410^{+0.142+0.042}_{-0.119-0.042}\cdot10^{-2}$	$1.410^{+0.042+0.037}_{-0.034-0.037}\cdot10^{-2}$
950	$1.063^{+0.489+0.033}_{-0.279-0.033}\cdot10^{-2}$	$1.137^{+0.117+0.035}_{-0.101-0.035}\cdot10^{-2}$	$1.138^{+0.034+0.031}_{-0.030-0.031}\cdot10^{-2}$
1000	$8.551^{+4.076+0.272}_{-2.295-0.272}\cdot10^{-3}$	$9.192^{+0.979+0.290}_{-0.850-0.290}\cdot10^{-3}$	$9.197^{+0.281+0.264}_{-0.254-0.264}\cdot10^{-3}$

Table B.10: Total VBF cross sections at the LHC, $\sqrt{S} = 7\,\text{TeV}$ at LO, NLO and NNLO in QCD. Errors shown are respectively scale and PDF uncertainities. Scale uncertainities are evaluated by varying μ_r and μ_f in the interval $\mu_r, \mu_f \in [Q/4, 4Q]$. The NNPDF2.1 [77] PDF set has been used. Numbers are in pb.

m_H [GeV]	σ_{LO}	σ_{NLO}	σ_{NNLO}
90	$6.204^{+0.000+0.050}_{-0.130-0.050}$	$5.927^{+0.127+0.049}_{-0.080-0.049}$	$5.982^{+0.039+0.049}_{-0.112-0.049}$
95	$5.920^{+0.000+0.047}_{-0.078-0.047}$	$5.698^{+0.081+0.047}_{-0.078-0.047}$	$5.724^{+0.063+0.047}_{-0.082-0.047}$
100	$5.694^{+0.000+0.045}_{-0.117-0.045}$	$5.457^{+0.098+0.044}_{-0.089-0.044}$	$5.503^{+0.031+0.044}_{-0.109-0.044}$
105	$5.425^{+0.022+0.042}_{-0.095-0.042}$	$5.220^{+0.093+0.042}_{-0.079-0.042}$	$5.261^{+0.044+0.042}_{-0.084-0.042}$
110	$5.215^{+0.026+0.040}_{-0.124-0.040}$	$5.011^{+0.100+0.040}_{-0.063-0.040}$	$5.020^{+0.076+0.040}_{-0.045-0.040}$
115	$5.003^{+0.020+0.038}_{-0.128-0.038}$	$4.825^{+0.073+0.038}_{-0.079-0.038}$	$4.854^{+0.026+0.038}_{-0.108-0.038}$
120	$4.796^{+0.054+0.036}_{-0.135-0.036}$	$4.639^{+0.093+0.036}_{-0.069-0.036}$	$4.661^{+0.038+0.037}_{-0.074-0.037}$
125	$4.612^{+0.050+0.035}_{-0.154-0.035}$	$4.443^{+0.092+0.035}_{-0.069-0.035}$	$4.485^{+0.031+0.035}_{-0.076-0.035}$
130	$4.430^{+0.077+0.033}_{-0.151-0.033}$	$4.269^{+0.098+0.033}_{-0.083-0.033}$	$4.308^{+0.034+0.033}_{-0.071-0.033}$
135	$4.265^{+0.079+0.032}_{-0.154-0.032}$	$4.110^{+0.086+0.032}_{-0.052-0.032}$	$4.145^{+0.039+0.032}_{-0.062-0.032}$
140	$4.105^{+0.099+0.030}_{-0.165-0.030}$	$3.960^{+0.089+0.030}_{-0.053-0.030}$	$3.983^{+0.045+0.031}_{-0.049-0.031}$
145	$3.948^{+0.109+0.029}_{-0.166-0.029}$	$3.816^{+0.083+0.029}_{-0.052-0.029}$	$3.839^{+0.053+0.029}_{-0.063-0.029}$
150	$3.802^{+0.123+0.028}_{-0.166-0.028}$	$3.674^{+0.092+0.028}_{-0.051-0.028}$	$3.709^{+0.031+0.028}_{-0.068-0.028}$
155	$3.662^{+0.128+0.027}_{-0.179-0.027}$	$3.544^{+0.089+0.027}_{-0.046-0.027}$	$3.571^{+0.044+0.027}_{-0.048-0.027}$
160	$3.527^{+0.140+0.025}_{-0.174-0.025}$	$3.421^{+0.088+0.026}_{-0.046-0.026}$	$3.444^{+0.039+0.026}_{-0.051-0.026}$
165	$3.406^{+0.140+0.024}_{-0.171-0.024}$	$3.299^{+0.084+0.025}_{-0.047-0.025}$	$3.348^{+0.020+0.025}_{-0.069-0.025}$
170	$3.284^{+0.154+0.023}_{-0.172-0.023}$	$3.191^{+0.065+0.024}_{-0.048-0.024}$	$3.211^{+0.033+0.024}_{-0.049-0.024}$
175	$3.173^{+0.150+0.023}_{-0.182-0.023}$	$3.078^{+0.082+0.023}_{-0.046-0.023}$	$3.103^{+0.032+0.023}_{-0.048-0.023}$
180	$3.066^{+0.147+0.022}_{-0.175-0.022}$	$2.972^{+0.084+0.022}_{-0.029-0.022}$	$3.000^{+0.038+0.022}_{-0.043-0.022}$
185	$2.963^{+0.160+0.021}_{-0.176-0.021}$	$2.871^{+0.077+0.021}_{-0.036-0.021}$	$2.905^{+0.027+0.022}_{-0.041-0.022}$
190	$2.868^{+0.163+0.020}_{-0.183-0.020}$	$2.776^{+0.080+0.020}_{-0.040-0.020}$	$2.802^{+0.042+0.021}_{-0.034-0.021}$
195	$2.767^{+0.171+0.020}_{-0.177-0.020}$	$2.686^{+0.082+0.020}_{-0.036-0.020}$	$2.715^{+0.030+0.020}_{-0.037-0.020}$
200	$2.680^{+0.167+0.019}_{-0.175-0.019}$	$2.604^{+0.080+0.019}_{-0.036-0.019}$	$2.626^{+0.032+0.019}_{-0.035-0.019}$
210	$2.510^{+0.175+0.018}_{-0.174-0.018}$	$2.438^{+0.080+0.018}_{-0.035-0.018}$	$2.467^{+0.029+0.018}_{-0.038-0.018}$
220	$2.355^{+0.174+0.016}_{-0.172-0.016}$	$2.290^{+0.074+0.017}_{-0.037-0.017}$	$2.316^{+0.030+0.017}_{-0.029-0.017}$
230	$2.213^{+0.176+0.015}_{-0.170-0.015}$	$2.152^{+0.079+0.016}_{-0.028-0.016}$	$2.180^{+0.037+0.016}_{-0.031-0.016}$
240	$2.081^{+0.178+0.015}_{-0.165-0.015}$	$2.028^{+0.069+0.015}_{-0.031-0.015}$	$2.051^{+0.026+0.015}_{-0.021-0.015}$
250	$1.961^{+0.177+0.014}_{-0.164-0.014}$	$1.909^{+0.069+0.014}_{-0.021-0.014}$	$1.935^{+0.026+0.014}_{-0.026-0.014}$
260	$1.847^{+0.177+0.013}_{-0.158-0.013}$	$1.801^{+0.069+0.013}_{-0.025-0.013}$	$1.826^{+0.027+0.013}_{-0.027-0.013}$
270	$1.742^{+0.176+0.012}_{-0.155-0.012}$	$1.701^{+0.070+0.012}_{-0.023-0.012}$	$1.724^{+0.026+0.013}_{-0.018-0.013}$
280	$1.645^{+0.174+0.012}_{-0.151-0.012}$	$1.611^{+0.063+0.012}_{-0.026-0.012}$	$1.634^{+0.023+0.012}_{-0.025-0.012}$
290	$1.558^{+0.171+0.011}_{-0.147-0.011}$	$1.523^{+0.063+0.011}_{-0.022-0.011}$	$1.543^{+0.024+0.011}_{-0.017-0.011}$
300	$1.473^{+0.170+0.010}_{-0.142-0.010}$	$1.443^{+0.059+0.011}_{-0.019-0.011}$	$1.463^{+0.025+0.011}_{-0.018-0.011}$
320	$1.325^{+0.164+0.009}_{-0.133-0.009}$	$1.298^{+0.060+0.010}_{-0.019-0.010}$	$1.317^{+0.020+0.010}_{-0.015-0.010}$
340	$1.194^{+0.157+0.009}_{-0.127-0.009}$	$1.176^{+0.054+0.009}_{-0.021-0.009}$	$1.191^{+0.019+0.009}_{-0.015-0.009}$
360	$1.080^{+0.151+0.008}_{-0.121-0.008}$	$1.062^{+0.054+0.008}_{-0.021-0.008}$	$1.079^{+0.018+0.008}_{-0.012-0.008}$
380	$9.793^{+1.448+0.072}_{-1.136-0.072}\cdot 10^{-1}$	$9.637^{+0.505+0.073}_{-0.165-0.073}\cdot 10^{-1}$	$9.810^{+0.160+0.075}_{-0.120-0.075}\cdot 10^{-1}$
400	$8.904^{+1.384+0.066}_{-1.063-0.066}\cdot 10^{-1}$	$8.798^{+0.461+0.067}_{-0.158-0.067}\cdot 10^{-1}$	$8.926^{+0.169+0.069}_{-0.083-0.069}\cdot 10^{-1}$
450	$7.100^{+1.229+0.055}_{-0.925-0.055}\cdot 10^{-1}$	$7.032^{+0.384+0.055}_{-0.138-0.055}\cdot 10^{-1}$	$7.146^{+0.132+0.056}_{-0.075-0.056}\cdot 10^{-1}$
500	$5.738^{+1.084+0.046}_{-0.801-0.046}\cdot 10^{-1}$	$5.695^{+0.332+0.046}_{-0.122-0.046}\cdot 10^{-1}$	$5.794^{+0.117+0.047}_{-0.043-0.047}\cdot 10^{-1}$
550	$4.683^{+0.955+0.039}_{-0.687-0.039}\cdot 10^{-1}$	$4.664^{+0.292+0.039}_{-0.112-0.039}\cdot 10^{-1}$	$4.754^{+0.089+0.040}_{-0.036-0.040}\cdot 10^{-1}$
600	$3.860^{+0.842+0.033}_{-0.595-0.033}\cdot 10^{-1}$	$3.863^{+0.243+0.034}_{-0.112-0.034}\cdot 10^{-1}$	$3.934^{+0.083+0.034}_{-0.027-0.034}\cdot 10^{-1}$
650	$3.209^{+0.743+0.029}_{-0.516-0.029}\cdot 10^{-1}$	$3.222^{+0.212+0.029}_{-0.108-0.029}\cdot 10^{-1}$	$3.286^{+0.064+0.029}_{-0.025-0.029}\cdot 10^{-1}$
700	$2.687^{+0.660+0.025}_{-0.449-0.025}\cdot 10^{-1}$	$2.702^{+0.185+0.025}_{-0.090-0.025}\cdot 10^{-1}$	$2.759^{+0.061+0.025}_{-0.014-0.025}\cdot 10^{-1}$
750	$2.265^{+0.583+0.022}_{-0.390-0.022}\cdot 10^{-1}$	$2.285^{+0.164+0.022}_{-0.085-0.022}\cdot 10^{-1}$	$2.335^{+0.053+0.022}_{-0.015-0.022}\cdot 10^{-1}$
800	$1.922^{+0.514+0.019}_{-0.345-0.019}\cdot 10^{-1}$	$1.943^{+0.147+0.019}_{-0.079-0.019}\cdot 10^{-1}$	$1.982^{+0.051+0.019}_{-0.010-0.019}\cdot 10^{-1}$
850	$1.637^{+0.458+0.017}_{-0.301-0.017}\cdot 10^{-1}$	$1.661^{+0.127+0.017}_{-0.070-0.017}\cdot 10^{-1}$	$1.696^{+0.040+0.017}_{-0.010-0.017}\cdot 10^{-1}$
900	$1.402^{+0.407+0.015}_{-0.265-0.015}\cdot 10^{-1}$	$1.424^{+0.114+0.015}_{-0.062-0.015}\cdot 10^{-1}$	$1.460^{+0.032+0.015}_{-0.013-0.015}\cdot 10^{-1}$
950	$1.205^{+0.362+0.013}_{-0.233-0.013}\cdot 10^{-1}$	$1.229^{+0.097+0.013}_{-0.058-0.013}\cdot 10^{-1}$	$1.260^{+0.030+0.013}_{-0.012-0.013}\cdot 10^{-1}$
1000	$1.040^{+0.323+0.012}_{-0.205-0.012}\cdot 10^{-1}$	$1.063^{+0.086+0.012}_{-0.054-0.012}\cdot 10^{-1}$	$1.091^{+0.024+0.012}_{-0.012-0.012}\cdot 10^{-1}$

Table B.11: Total VBF cross sections at the LHC, $\sqrt{S} = 14$TeV at LO, NLO and NNLO in QCD. Errors shown are respectively scale and PDF uncertainities. Scale uncertainities are evaluated by varying μ_r and μ_f in the interval $\mu_r, \mu_f \in [Q/4, 4Q]$. The ABKM [70] PDF set has been used. Numbers are in pb.

m_H [GeV]	σ_{LO}	σ_{NLO}	σ_{NNLO}
90	$6.192^{+0.000+0.104}_{-0.130-0.104}$	$5.955^{+0.137+0.103}_{-0.076-0.103}$	$5.897^{+0.073+0.102}_{-0.103-0.102}$
95	$5.930^{+0.000+0.101}_{-0.097-0.101}$	$5.701^{+0.108+0.099}_{-0.099-0.099}$	$5.665^{+0.054+0.099}_{-0.100-0.099}$
100	$5.687^{+0.000+0.097}_{-0.074-0.097}$	$5.471^{+0.103+0.096}_{-0.093-0.096}$	$5.448^{+0.025+0.096}_{-0.136-0.096}$
105	$5.438^{+0.013+0.093}_{-0.074-0.093}$	$5.237^{+0.104+0.092}_{-0.059-0.092}$	$5.196^{+0.055+0.092}_{-0.088-0.092}$
110	$5.225^{+0.012+0.090}_{-0.106-0.090}$	$5.026^{+0.072+0.089}_{-0.060-0.089}$	$4.988^{+0.060+0.089}_{-0.081-0.089}$
115	$5.011^{+0.029+0.087}_{-0.096-0.087}$	$4.820^{+0.097+0.086}_{-0.053-0.086}$	$4.786^{+0.039+0.086}_{-0.091-0.086}$
120	$4.816^{+0.031+0.084}_{-0.104-0.084}$	$4.643^{+0.079+0.083}_{-0.074-0.083}$	$4.602^{+0.052+0.083}_{-0.073-0.083}$
125	$4.631^{+0.033+0.081}_{-0.124-0.081}$	$4.450^{+0.095+0.080}_{-0.047-0.080}$	$4.427^{+0.045+0.080}_{-0.077-0.080}$
130	$4.452^{+0.065+0.079}_{-0.133-0.079}$	$4.292^{+0.086+0.078}_{-0.067-0.078}$	$4.264^{+0.037+0.077}_{-0.080-0.077}$
135	$4.283^{+0.078+0.076}_{-0.137-0.076}$	$4.135^{+0.089+0.075}_{-0.056-0.075}$	$4.099^{+0.044+0.075}_{-0.066-0.075}$
140	$4.122^{+0.083+0.073}_{-0.142-0.073}$	$3.980^{+0.088+0.073}_{-0.049-0.073}$	$3.954^{+0.026+0.072}_{-0.077-0.072}$
145	$3.973^{+0.097+0.071}_{-0.148-0.071}$	$3.838^{+0.067+0.070}_{-0.047-0.070}$	$3.823^{+0.020+0.070}_{-0.080-0.070}$
150	$3.830^{+0.099+0.069}_{-0.146-0.069}$	$3.704^{+0.073+0.068}_{-0.050-0.068}$	$3.670^{+0.031+0.068}_{-0.065-0.068}$
155	$3.687^{+0.104+0.067}_{-0.152-0.067}$	$3.565^{+0.071+0.066}_{-0.046-0.066}$	$3.540^{+0.033+0.066}_{-0.067-0.066}$
160	$3.548^{+0.145+0.064}_{-0.149-0.064}$	$3.444^{+0.084+0.064}_{-0.053-0.064}$	$3.413^{+0.033+0.064}_{-0.056-0.064}$
165	$3.432^{+0.123+0.063}_{-0.156-0.063}$	$3.333^{+0.064+0.062}_{-0.057-0.062}$	$3.288^{+0.043+0.062}_{-0.051-0.062}$
170	$3.315^{+0.128+0.061}_{-0.163-0.061}$	$3.205^{+0.078+0.060}_{-0.046-0.060}$	$3.181^{+0.037+0.060}_{-0.050-0.060}$
175	$3.201^{+0.135+0.059}_{-0.158-0.059}$	$3.098^{+0.079+0.058}_{-0.041-0.058}$	$3.079^{+0.040+0.058}_{-0.057-0.058}$
180	$3.090^{+0.139+0.057}_{-0.163-0.057}$	$2.994^{+0.076+0.057}_{-0.047-0.057}$	$2.971^{+0.035+0.056}_{-0.045-0.056}$
185	$2.982^{+0.150+0.055}_{-0.159-0.055}$	$2.899^{+0.073+0.055}_{-0.043-0.055}$	$2.875^{+0.028+0.055}_{-0.049-0.055}$
190	$2.887^{+0.152+0.054}_{-0.160-0.054}$	$2.799^{+0.076+0.053}_{-0.040-0.053}$	$2.786^{+0.023+0.053}_{-0.047-0.053}$
195	$2.792^{+0.149+0.052}_{-0.162-0.052}$	$2.707^{+0.077+0.052}_{-0.036-0.052}$	$2.692^{+0.032+0.052}_{-0.046-0.052}$
200	$2.701^{+0.157+0.051}_{-0.161-0.051}$	$2.623^{+0.070+0.050}_{-0.035-0.050}$	$2.608^{+0.026+0.050}_{-0.039-0.050}$
210	$2.531^{+0.165+0.048}_{-0.160-0.048}$	$2.458^{+0.071+0.047}_{-0.032-0.047}$	$2.449^{+0.026+0.048}_{-0.031-0.048}$
220	$2.376^{+0.161+0.045}_{-0.162-0.045}$	$2.313^{+0.071+0.045}_{-0.031-0.045}$	$2.294^{+0.035+0.045}_{-0.042-0.045}$
230	$2.229^{+0.172+0.043}_{-0.154-0.043}$	$2.175^{+0.065+0.043}_{-0.030-0.043}$	$2.161^{+0.029+0.042}_{-0.036-0.042}$
240	$2.099^{+0.171+0.040}_{-0.150-0.040}$	$2.048^{+0.065+0.040}_{-0.031-0.040}$	$2.034^{+0.029+0.040}_{-0.030-0.040}$
250	$1.984^{+0.161+0.038}_{-0.156-0.038}$	$1.929^{+0.067+0.038}_{-0.028-0.038}$	$1.919^{+0.026+0.038}_{-0.024-0.038}$
260	$1.869^{+0.167+0.036}_{-0.152-0.036}$	$1.821^{+0.066+0.036}_{-0.024-0.036}$	$1.811^{+0.026+0.036}_{-0.032-0.036}$
270	$1.764^{+0.166+0.034}_{-0.149-0.034}$	$1.721^{+0.064+0.035}_{-0.022-0.035}$	$1.710^{+0.026+0.034}_{-0.024-0.034}$
280	$1.667^{+0.165+0.033}_{-0.142-0.033}$	$1.629^{+0.060+0.033}_{-0.023-0.033}$	$1.618^{+0.025+0.033}_{-0.022-0.033}$
290	$1.577^{+0.165+0.031}_{-0.139-0.031}$	$1.541^{+0.059+0.031}_{-0.023-0.031}$	$1.533^{+0.025+0.031}_{-0.022-0.031}$
300	$1.493^{+0.162+0.030}_{-0.137-0.030}$	$1.460^{+0.062+0.030}_{-0.020-0.030}$	$1.454^{+0.022+0.030}_{-0.021-0.030}$
320	$1.344^{+0.155+0.027}_{-0.129-0.027}$	$1.315^{+0.058+0.027}_{-0.019-0.027}$	$1.308^{+0.024+0.027}_{-0.015-0.027}$
340	$1.213^{+0.150+0.025}_{-0.123-0.025}$	$1.191^{+0.052+0.025}_{-0.021-0.025}$	$1.183^{+0.023+0.025}_{-0.016-0.025}$
360	$1.097^{+0.144+0.022}_{-0.116-0.022}$	$1.077^{+0.051+0.023}_{-0.016-0.023}$	$1.073^{+0.018+0.023}_{-0.014-0.023}$
380	$9.950^{+1.400+0.205}_{-1.082-0.205}\cdot10^{-1}$	$9.791^{+0.483+0.207}_{-0.149-0.207}\cdot10^{-1}$	$9.741^{+0.203+0.206}_{-0.108-0.206}\cdot10^{-1}$
400	$9.073^{+1.319+0.188}_{-1.043-0.188}\cdot10^{-1}$	$8.928^{+0.448+0.190}_{-0.143-0.190}\cdot10^{-1}$	$8.891^{+0.168+0.190}_{-0.103-0.190}\cdot10^{-1}$
450	$7.245^{+1.181+0.153}_{-0.896-0.153}\cdot10^{-1}$	$7.145^{+0.402+0.155}_{-0.108-0.155}\cdot10^{-1}$	$7.123^{+0.150+0.155}_{-0.081-0.155}\cdot10^{-1}$
500	$5.859^{+1.053+0.126}_{-0.782-0.126}\cdot10^{-1}$	$5.800^{+0.338+0.128}_{-0.113-0.128}\cdot10^{-1}$	$5.787^{+0.120+0.128}_{-0.061-0.128}\cdot10^{-1}$
550	$4.800^{+0.919+0.105}_{-0.681-0.105}\cdot10^{-1}$	$4.764^{+0.289+0.107}_{-0.106-0.107}\cdot10^{-1}$	$4.749^{+0.098+0.107}_{-0.052-0.107}\cdot10^{-1}$
600	$3.954^{+0.823+0.088}_{-0.584-0.088}\cdot10^{-1}$	$3.940^{+0.254+0.090}_{-0.098-0.090}\cdot10^{-1}$	$3.931^{+0.091+0.090}_{-0.039-0.090}\cdot10^{-1}$
650	$3.299^{+0.726+0.074}_{-0.518-0.074}\cdot10^{-1}$	$3.290^{+0.221+0.076}_{-0.091-0.076}\cdot10^{-1}$	$3.287^{+0.072+0.076}_{-0.030-0.076}\cdot10^{-1}$
700	$2.764^{+0.647+0.063}_{-0.449-0.063}\cdot10^{-1}$	$2.775^{+0.184+0.065}_{-0.091-0.065}\cdot10^{-1}$	$2.765^{+0.061+0.065}_{-0.023-0.065}\cdot10^{-1}$
750	$2.332^{+0.574+0.054}_{-0.392-0.054}\cdot10^{-1}$	$2.344^{+0.166+0.055}_{-0.080-0.055}\cdot10^{-1}$	$2.340^{+0.057+0.055}_{-0.014-0.055}\cdot10^{-1}$
800	$1.981^{+0.509+0.046}_{-0.346-0.046}\cdot10^{-1}$	$1.995^{+0.147+0.048}_{-0.072-0.048}\cdot10^{-1}$	$1.995^{+0.045+0.048}_{-0.015-0.048}\cdot10^{-1}$
850	$1.689^{+0.456+0.040}_{-0.302-0.040}\cdot10^{-1}$	$1.709^{+0.129+0.041}_{-0.069-0.041}\cdot10^{-1}$	$1.707^{+0.040+0.041}_{-0.010-0.041}\cdot10^{-1}$
900	$1.447^{+0.405+0.035}_{-0.267-0.035}\cdot10^{-1}$	$1.468^{+0.114+0.036}_{-0.061-0.036}\cdot10^{-1}$	$1.467^{+0.036+0.036}_{-0.010-0.036}\cdot10^{-1}$
950	$1.246^{+0.363+0.030}_{-0.236-0.030}\cdot10^{-1}$	$1.269^{+0.098+0.032}_{-0.058-0.032}\cdot10^{-1}$	$1.267^{+0.032+0.032}_{-0.010-0.032}\cdot10^{-1}$
1000	$1.078^{+0.322+0.027}_{-0.211-0.027}\cdot10^{-1}$	$1.099^{+0.088+0.028}_{-0.054-0.028}\cdot10^{-1}$	$1.096^{+0.029+0.028}_{-0.008-0.028}\cdot10^{-1}$

Table B.12: Total VBF cross sections at the LHC, $\sqrt{S} = 14\,\text{TeV}$ at LO, NLO and NNLO in QCD. Errors shown are respectively scale and PDF uncertainities. Scale uncertainities are evaluated by varying μ_r and μ_f in the interval $\mu_r, \mu_f \in [Q/4, 4Q]$. The HERAPDF1.5 [73, 74] PDF set has been used. Numbers are in pb.

m_H [GeV]	σ_{LO}	σ_{NLO}	σ_{NNLO}
90	$5.930^{+0.018+0.065}_{-0.184-0.065}$	$5.691^{+0.122+0.065}_{-0.071-0.065}$	$5.724^{+0.048+0.060}_{-0.098-0.060}$
95	$5.689^{+0.021+0.063}_{-0.178-0.063}$	$5.401^{+0.181+0.062}_{-0.058-0.062}$	$5.473^{+0.056+0.057}_{-0.098-0.057}$
100	$5.452^{+0.002+0.060}_{-0.146-0.060}$	$5.236^{+0.111+0.060}_{-0.072-0.060}$	$5.250^{+0.041+0.055}_{-0.095-0.055}$
105	$5.227^{+0.000+0.058}_{-0.109-0.058}$	$5.018^{+0.109+0.057}_{-0.057-0.057}$	$5.029^{+0.062+0.053}_{-0.067-0.053}$
110	$5.025^{+0.000+0.056}_{-0.080-0.056}$	$4.828^{+0.085+0.055}_{-0.060-0.055}$	$4.852^{+0.041+0.051}_{-0.078-0.051}$
115	$4.824^{+0.000+0.054}_{-0.064-0.054}$	$4.642^{+0.092+0.053}_{-0.056-0.053}$	$4.656^{+0.046+0.049}_{-0.066-0.049}$
120	$4.636^{+0.004+0.052}_{-0.072-0.052}$	$4.461^{+0.084+0.051}_{-0.050-0.051}$	$4.473^{+0.047+0.047}_{-0.070-0.047}$
125	$4.464^{+0.004+0.050}_{-0.087-0.050}$	$4.293^{+0.077+0.049}_{-0.047-0.049}$	$4.305^{+0.035+0.046}_{-0.068-0.046}$
130	$4.293^{+0.017+0.048}_{-0.084-0.048}$	$4.136^{+0.068+0.048}_{-0.051-0.048}$	$4.152^{+0.026+0.044}_{-0.072-0.044}$
135	$4.132^{+0.021+0.047}_{-0.089-0.047}$	$3.986^{+0.081+0.046}_{-0.046-0.046}$	$3.996^{+0.040+0.043}_{-0.054-0.043}$
140	$3.985^{+0.028+0.045}_{-0.100-0.045}$	$3.840^{+0.074+0.045}_{-0.041-0.045}$	$3.850^{+0.038+0.042}_{-0.050-0.042}$
145	$3.838^{+0.034+0.044}_{-0.102-0.044}$	$3.707^{+0.063+0.043}_{-0.049-0.043}$	$3.706^{+0.033+0.040}_{-0.052-0.040}$
150	$3.703^{+0.037+0.042}_{-0.111-0.042}$	$3.562^{+0.079+0.042}_{-0.037-0.042}$	$3.578^{+0.033+0.039}_{-0.049-0.039}$
155	$3.568^{+0.058+0.041}_{-0.112-0.041}$	$3.450^{+0.063+0.041}_{-0.061-0.041}$	$3.452^{+0.032+0.038}_{-0.050-0.038}$
160	$3.445^{+0.065+0.040}_{-0.114-0.040}$	$3.331^{+0.071+0.040}_{-0.034-0.040}$	$3.332^{+0.028+0.037}_{-0.046-0.037}$
165	$3.332^{+0.066+0.039}_{-0.124-0.039}$	$3.216^{+0.073+0.038}_{-0.051-0.038}$	$3.222^{+0.028+0.037}_{-0.049-0.037}$
170	$3.216^{+0.077+0.038}_{-0.121-0.038}$	$3.112^{+0.070+0.037}_{-0.045-0.037}$	$3.114^{+0.025+0.036}_{-0.049-0.036}$
175	$3.111^{+0.070+0.037}_{-0.132-0.037}$	$3.005^{+0.069+0.036}_{-0.031-0.036}$	$3.010^{+0.027+0.035}_{-0.041-0.035}$
180	$3.004^{+0.090+0.036}_{-0.122-0.036}$	$2.912^{+0.063+0.035}_{-0.039-0.035}$	$2.907^{+0.041+0.034}_{-0.037-0.034}$
185	$2.905^{+0.100+0.035}_{-0.123-0.035}$	$2.813^{+0.056+0.034}_{-0.034-0.034}$	$2.815^{+0.024+0.033}_{-0.037-0.033}$
190	$2.813^{+0.101+0.034}_{-0.127-0.034}$	$2.724^{+0.069+0.033}_{-0.034-0.033}$	$2.723^{+0.027+0.033}_{-0.037-0.033}$
195	$2.719^{+0.109+0.033}_{-0.123-0.033}$	$2.638^{+0.066+0.032}_{-0.035-0.032}$	$2.637^{+0.027+0.032}_{-0.032-0.032}$
200	$2.633^{+0.113+0.032}_{-0.128-0.032}$	$2.555^{+0.065+0.032}_{-0.031-0.032}$	$2.557^{+0.038+0.031}_{-0.037-0.031}$
210	$2.473^{+0.119+0.030}_{-0.130-0.030}$	$2.407^{+0.057+0.030}_{-0.035-0.030}$	$2.401^{+0.025+0.030}_{-0.039-0.030}$
220	$2.327^{+0.119+0.029}_{-0.135-0.029}$	$2.257^{+0.065+0.029}_{-0.029-0.029}$	$2.258^{+0.023+0.029}_{-0.028-0.029}$
230	$2.188^{+0.124+0.028}_{-0.128-0.028}$	$2.126^{+0.062+0.027}_{-0.021-0.027}$	$2.129^{+0.019+0.028}_{-0.035-0.028}$
240	$2.063^{+0.121+0.026}_{-0.133-0.026}$	$2.005^{+0.055+0.026}_{-0.025-0.026}$	$2.002^{+0.026+0.027}_{-0.025-0.027}$
250	$1.946^{+0.129+0.025}_{-0.133-0.025}$	$1.895^{+0.055+0.025}_{-0.026-0.025}$	$1.890^{+0.020+0.026}_{-0.022-0.026}$
260	$1.840^{+0.128+0.024}_{-0.129-0.024}$	$1.790^{+0.053+0.024}_{-0.022-0.024}$	$1.788^{+0.018+0.025}_{-0.022-0.025}$
270	$1.739^{+0.129+0.023}_{-0.128-0.023}$	$1.697^{+0.048+0.023}_{-0.026-0.023}$	$1.692^{+0.018+0.024}_{-0.022-0.024}$
280	$1.645^{+0.131+0.022}_{-0.123-0.022}$	$1.603^{+0.051+0.022}_{-0.021-0.022}$	$1.600^{+0.021+0.023}_{-0.019-0.023}$
290	$1.558^{+0.131+0.021}_{-0.122-0.021}$	$1.520^{+0.050+0.021}_{-0.017-0.021}$	$1.518^{+0.018+0.022}_{-0.019-0.022}$
300	$1.478^{+0.130+0.020}_{-0.119-0.020}$	$1.442^{+0.048+0.020}_{-0.018-0.020}$	$1.439^{+0.019+0.022}_{-0.017-0.022}$
320	$1.331^{+0.130+0.019}_{-0.114-0.019}$	$1.297^{+0.052+0.018}_{-0.013-0.018}$	$1.299^{+0.017+0.020}_{-0.016-0.020}$
340	$1.204^{+0.124+0.017}_{-0.110-0.017}$	$1.180^{+0.042+0.017}_{-0.017-0.017}$	$1.174^{+0.018+0.019}_{-0.013-0.019}$
360	$1.092^{+0.122+0.016}_{-0.103-0.016}$	$1.071^{+0.041+0.016}_{-0.015-0.016}$	$1.067^{+0.017+0.018}_{-0.012-0.018}$
380	$9.938^{+1.175+0.150}_{-0.990-0.150}\cdot10^{-1}$	$9.766^{+0.391+0.148}_{-0.159-0.148}\cdot10^{-1}$	$9.713^{+0.139+0.166}_{-0.102-0.166}\cdot10^{-1}$
400	$9.057^{+1.142+0.140}_{-0.938-0.140}\cdot10^{-1}$	$8.907^{+0.377+0.138}_{-0.128-0.138}\cdot10^{-1}$	$8.861^{+0.137+0.156}_{-0.089-0.156}\cdot10^{-1}$
450	$7.266^{+1.039+0.118}_{-0.826-0.118}\cdot10^{-1}$	$7.165^{+0.326+0.117}_{-0.104-0.117}\cdot10^{-1}$	$7.126^{+0.109+0.134}_{-0.072-0.134}\cdot10^{-1}$
500	$5.901^{+0.934+0.101}_{-0.722-0.101}\cdot10^{-1}$	$5.831^{+0.288+0.100}_{-0.091-0.100}\cdot10^{-1}$	$5.797^{+0.095+0.116}_{-0.049-0.116}\cdot10^{-1}$
550	$4.847^{+0.828+0.088}_{-0.637-0.088}\cdot10^{-1}$	$4.804^{+0.244+0.086}_{-0.088-0.086}\cdot10^{-1}$	$4.765^{+0.087+0.100}_{-0.040-0.100}\cdot10^{-1}$
600	$4.011^{+0.745+0.076}_{-0.549-0.076}\cdot10^{-1}$	$3.989^{+0.227+0.075}_{-0.082-0.075}\cdot10^{-1}$	$3.958^{+0.069+0.088}_{-0.033-0.088}\cdot10^{-1}$
650	$3.351^{+0.661+0.066}_{-0.483-0.066}\cdot10^{-1}$	$3.343^{+0.190+0.066}_{-0.076-0.066}\cdot10^{-1}$	$3.313^{+0.057+0.076}_{-0.024-0.076}\cdot10^{-1}$
700	$2.816^{+0.593+0.058}_{-0.426-0.058}\cdot10^{-1}$	$2.818^{+0.168+0.058}_{-0.071-0.058}\cdot10^{-1}$	$2.788^{+0.055+0.067}_{-0.014-0.067}\cdot10^{-1}$
750	$2.382^{+0.531+0.051}_{-0.374-0.051}\cdot10^{-1}$	$2.393^{+0.145+0.051}_{-0.074-0.051}\cdot10^{-1}$	$2.363^{+0.048+0.059}_{-0.011-0.059}\cdot10^{-1}$
800	$2.027^{+0.471+0.046}_{-0.328-0.046}\cdot10^{-1}$	$2.038^{+0.132+0.045}_{-0.061-0.045}\cdot10^{-1}$	$2.014^{+0.041+0.052}_{-0.008-0.052}\cdot10^{-1}$
850	$1.733^{+0.424+0.041}_{-0.292-0.041}\cdot10^{-1}$	$1.746^{+0.116+0.040}_{-0.058-0.040}\cdot10^{-1}$	$1.727^{+0.036+0.046}_{-0.008-0.046}\cdot10^{-1}$
900	$1.488^{+0.380+0.036}_{-0.259-0.036}\cdot10^{-1}$	$1.507^{+0.099+0.036}_{-0.058-0.036}\cdot10^{-1}$	$1.486^{+0.030+0.041}_{-0.008-0.041}\cdot10^{-1}$
950	$1.283^{+0.338+0.032}_{-0.229-0.032}\cdot10^{-1}$	$1.300^{+0.090+0.032}_{-0.050-0.032}\cdot10^{-1}$	$1.284^{+0.025+0.036}_{-0.008-0.036}\cdot10^{-1}$
1000	$1.110^{+0.304+0.029}_{-0.204-0.029}\cdot10^{-1}$	$1.128^{+0.081+0.029}_{-0.046-0.029}\cdot10^{-1}$	$1.112^{+0.023+0.032}_{-0.007-0.032}\cdot10^{-1}$

Table B.13: Total VBF cross sections at the LHC, $\sqrt{S} = 14\,\text{TeV}$ at LO, NLO and NNLO in QCD. Errors shown are respectively scale and PDF uncertainities. Scale uncertainities are evaluated by varying μ_r and μ_f in the interval $\mu_r, \mu_f \in [Q/4, 4Q]$. The JR09 [75, 76] PDF set has been used. Numbers are in pb.

m_H [GeV]	σ_{LO}	σ_{NLO}	σ_{NNLO}
90	$5.508^{+0.000+0.059}_{-0.151-0.059}$	$5.809^{+0.147+0.105}_{-0.072-0.105}$	$5.857^{+0.076+0.094}_{-0.098-0.094}$
95	$5.266^{+0.000+0.057}_{-0.094-0.057}$	$5.583^{+0.124+0.101}_{-0.068-0.101}$	$5.644^{+0.045+0.091}_{-0.146-0.091}$
100	$5.040^{+0.000+0.055}_{-0.079-0.055}$	$5.352^{+0.110+0.097}_{-0.069-0.097}$	$5.382^{+0.052+0.086}_{-0.104-0.086}$
105	$4.837^{+0.000+0.053}_{-0.070-0.053}$	$5.141^{+0.101+0.093}_{-0.066-0.093}$	$5.147^{+0.073+0.083}_{-0.075-0.083}$
110	$4.645^{+0.001+0.051}_{-0.092-0.051}$	$4.939^{+0.081+0.090}_{-0.061-0.090}$	$4.961^{+0.027+0.080}_{-0.119-0.080}$
115	$4.456^{+0.007+0.049}_{-0.145-0.049}$	$4.748^{+0.068+0.086}_{-0.072-0.086}$	$4.752^{+0.054+0.077}_{-0.089-0.077}$
120	$4.285^{+0.019+0.048}_{-0.113-0.048}$	$4.548^{+0.095+0.083}_{-0.062-0.083}$	$4.562^{+0.082+0.074}_{-0.044-0.074}$
125	$4.115^{+0.021+0.046}_{-0.119-0.046}$	$4.375^{+0.077+0.080}_{-0.052-0.080}$	$4.391^{+0.040+0.072}_{-0.087-0.072}$
130	$3.961^{+0.040+0.044}_{-0.131-0.044}$	$4.219^{+0.071+0.077}_{-0.062-0.077}$	$4.224^{+0.091+0.069}_{-0.075-0.069}$
135	$3.802^{+0.058+0.043}_{-0.128-0.043}$	$4.064^{+0.073+0.075}_{-0.076-0.075}$	$4.076^{+0.030+0.067}_{-0.081-0.067}$
140	$3.670^{+0.061+0.042}_{-0.137-0.042}$	$3.906^{+0.087+0.072}_{-0.043-0.072}$	$3.926^{+0.030+0.064}_{-0.084-0.064}$
145	$3.531^{+0.075+0.040}_{-0.142-0.040}$	$3.764^{+0.080+0.070}_{-0.044-0.070}$	$3.781^{+0.039+0.062}_{-0.071-0.062}$
150	$3.405^{+0.085+0.039}_{-0.145-0.039}$	$3.630^{+0.084+0.067}_{-0.063-0.067}$	$3.642^{+0.042+0.060}_{-0.077-0.060}$
155	$3.283^{+0.100+0.038}_{-0.149-0.038}$	$3.498^{+0.081+0.065}_{-0.044-0.065}$	$3.514^{+0.042+0.058}_{-0.068-0.058}$
160	$3.165^{+0.107+0.037}_{-0.156-0.037}$	$3.377^{+0.087+0.063}_{-0.050-0.063}$	$3.385^{+0.039+0.056}_{-0.068-0.056}$
165	$3.053^{+0.104+0.035}_{-0.149-0.035}$	$3.258^{+0.079+0.061}_{-0.044-0.061}$	$3.275^{+0.037+0.055}_{-0.067-0.055}$
170	$2.947^{+0.123+0.034}_{-0.149-0.034}$	$3.150^{+0.079+0.059}_{-0.046-0.059}$	$3.160^{+0.042+0.053}_{-0.060-0.053}$
175	$2.851^{+0.115+0.033}_{-0.159-0.033}$	$3.046^{+0.076+0.057}_{-0.047-0.057}$	$3.075^{+0.016+0.052}_{-0.081-0.052}$
180	$2.756^{+0.124+0.032}_{-0.160-0.032}$	$2.938^{+0.079+0.055}_{-0.040-0.055}$	$2.950^{+0.040+0.050}_{-0.062-0.050}$
185	$2.663^{+0.129+0.031}_{-0.158-0.031}$	$2.842^{+0.076+0.054}_{-0.040-0.054}$	$2.853^{+0.049+0.048}_{-0.054-0.048}$
190	$2.571^{+0.136+0.031}_{-0.152-0.031}$	$2.749^{+0.070+0.052}_{-0.035-0.052}$	$2.760^{+0.041+0.047}_{-0.048-0.047}$
195	$2.491^{+0.139+0.030}_{-0.154-0.030}$	$2.650^{+0.088+0.050}_{-0.030-0.050}$	$2.668^{+0.041+0.045}_{-0.045-0.045}$
200	$2.412^{+0.144+0.029}_{-0.158-0.029}$	$2.574^{+0.077+0.049}_{-0.036-0.049}$	$2.581^{+0.040+0.044}_{-0.047-0.044}$
210	$2.262^{+0.148+0.027}_{-0.156-0.027}$	$2.416^{+0.074+0.046}_{-0.035-0.046}$	$2.423^{+0.040+0.041}_{-0.045-0.041}$
220	$2.120^{+0.156+0.026}_{-0.150-0.026}$	$2.267^{+0.075+0.044}_{-0.029-0.044}$	$2.276^{+0.037+0.039}_{-0.039-0.039}$
230	$1.998^{+0.154+0.025}_{-0.152-0.025}$	$2.132^{+0.074+0.041}_{-0.027-0.041}$	$2.142^{+0.033+0.037}_{-0.033-0.037}$
240	$1.880^{+0.156+0.023}_{-0.149-0.023}$	$2.010^{+0.072+0.039}_{-0.031-0.039}$	$2.018^{+0.033+0.035}_{-0.032-0.035}$
250	$1.773^{+0.155+0.022}_{-0.147-0.022}$	$1.894^{+0.074+0.037}_{-0.028-0.037}$	$1.903^{+0.028+0.033}_{-0.037-0.033}$
260	$1.673^{+0.156+0.021}_{-0.143-0.021}$	$1.785^{+0.068+0.035}_{-0.025-0.035}$	$1.796^{+0.032+0.032}_{-0.031-0.032}$
270	$1.580^{+0.156+0.020}_{-0.141-0.020}$	$1.691^{+0.061+0.033}_{-0.030-0.033}$	$1.695^{+0.032+0.030}_{-0.028-0.030}$
280	$1.496^{+0.153+0.019}_{-0.139-0.019}$	$1.598^{+0.064+0.032}_{-0.025-0.032}$	$1.604^{+0.028+0.029}_{-0.028-0.029}$
290	$1.416^{+0.155+0.018}_{-0.135-0.018}$	$1.512^{+0.062+0.030}_{-0.020-0.030}$	$1.519^{+0.027+0.027}_{-0.023-0.027}$
300	$1.342^{+0.150+0.017}_{-0.132-0.017}$	$1.430^{+0.067+0.029}_{-0.020-0.029}$	$1.442^{+0.024+0.026}_{-0.025-0.026}$
320	$1.208^{+0.149+0.016}_{-0.124-0.016}$	$1.288^{+0.063+0.026}_{-0.018-0.026}$	$1.298^{+0.024+0.024}_{-0.021-0.024}$
340	$1.093^{+0.143+0.014}_{-0.121-0.014}$	$1.165^{+0.054+0.024}_{-0.016-0.024}$	$1.172^{+0.023+0.022}_{-0.019-0.022}$
360	$9.925^{+1.344+0.133}_{-1.156-0.133}\cdot10^{-1}$	$1.055^{+0.054+0.022}_{-0.015-0.022}$	$1.061^{+0.021+0.020}_{-0.015-0.020}$
380	$8.999^{+1.354+0.122}_{-1.073-0.122}\cdot10^{-1}$	$9.599^{+0.490+0.199}_{-0.142-0.199}\cdot10^{-1}$	$9.656^{+0.190+0.181}_{-0.141-0.181}\cdot10^{-1}$
400	$8.192^{+1.294+0.112}_{-0.997-0.112}\cdot10^{-1}$	$8.746^{+0.478+0.183}_{-0.157-0.183}\cdot10^{-1}$	$8.780^{+0.205+0.166}_{-0.110-0.166}\cdot10^{-1}$
450	$6.573^{+1.137+0.092}_{-0.878-0.092}\cdot10^{-1}$	$7.008^{+0.394+0.149}_{-0.129-0.149}\cdot10^{-1}$	$7.045^{+0.156+0.136}_{-0.101-0.136}\cdot10^{-1}$
500	$5.330^{+1.018+0.077}_{-0.761-0.077}\cdot10^{-1}$	$5.677^{+0.342+0.123}_{-0.117-0.123}\cdot10^{-1}$	$5.714^{+0.127+0.113}_{-0.067-0.113}\cdot10^{-1}$
550	$4.372^{+0.908+0.064}_{-0.663-0.064}\cdot10^{-1}$	$4.654^{+0.302+0.102}_{-0.115-0.102}\cdot10^{-1}$	$4.678^{+0.118+0.094}_{-0.046-0.094}\cdot10^{-1}$
600	$3.621^{+0.809+0.054}_{-0.580-0.054}\cdot10^{-1}$	$3.852^{+0.253+0.086}_{-0.106-0.086}\cdot10^{-1}$	$3.877^{+0.091+0.079}_{-0.042-0.079}\cdot10^{-1}$
650	$3.024^{+0.713+0.046}_{-0.504-0.046}\cdot10^{-1}$	$3.211^{+0.220+0.073}_{-0.100-0.073}\cdot10^{-1}$	$3.232^{+0.079+0.067}_{-0.028-0.067}\cdot10^{-1}$
700	$2.539^{+0.640+0.039}_{-0.442-0.039}\cdot10^{-1}$	$2.694^{+0.201+0.062}_{-0.089-0.062}\cdot10^{-1}$	$2.716^{+0.070+0.057}_{-0.022-0.057}\cdot10^{-1}$
750	$2.148^{+0.569+0.034}_{-0.388-0.034}\cdot10^{-1}$	$2.283^{+0.166+0.053}_{-0.087-0.053}\cdot10^{-1}$	$2.297^{+0.063+0.049}_{-0.017-0.049}\cdot10^{-1}$
800	$1.827^{+0.511+0.029}_{-0.340-0.029}\cdot10^{-1}$	$1.937^{+0.150+0.045}_{-0.075-0.045}\cdot10^{-1}$	$1.955^{+0.054+0.042}_{-0.013-0.042}\cdot10^{-1}$
850	$1.563^{+0.456+0.025}_{-0.300-0.025}\cdot10^{-1}$	$1.656^{+0.130+0.039}_{-0.068-0.039}\cdot10^{-1}$	$1.673^{+0.041+0.037}_{-0.015-0.037}\cdot10^{-1}$
900	$1.342^{+0.408+0.022}_{-0.265-0.022}\cdot10^{-1}$	$1.421^{+0.116+0.034}_{-0.063-0.034}\cdot10^{-1}$	$1.436^{+0.037+0.032}_{-0.014-0.032}\cdot10^{-1}$
950	$1.158^{+0.363+0.019}_{-0.234-0.019}\cdot10^{-1}$	$1.226^{+0.101+0.030}_{-0.057-0.030}\cdot10^{-1}$	$1.237^{+0.035+0.028}_{-0.012-0.028}\cdot10^{-1}$
1000	$1.002^{+0.326+0.017}_{-0.208-0.017}\cdot10^{-1}$	$1.062^{+0.090+0.026}_{-0.053-0.026}\cdot10^{-1}$	$1.070^{+0.030+0.024}_{-0.011-0.024}\cdot10^{-1}$

Table B.14: Total VBF cross sections at the LHC, $\sqrt{S} = 14\,\text{TeV}$ at LO, NLO and NNLO in QCD. Errors shown are respectively scale and PDF uncertainities. Scale uncertainities are evaluated by varying μ_r and μ_f in the interval $\mu_r, \mu_f \in [Q/4, 4Q]$. The MSTW2008 [63] PDF set (68% CL) has been used. Numbers are in pb.

m_H [GeV]	σ_{LO}	σ_{NLO}	σ_{NNLO}
90	$5.980^{+0.022+0.080}_{-0.186-0.080}$	$5.712^{+0.163+0.078}_{-0.068-0.078}$	$5.810^{+0.056+0.072}_{-0.132-0.072}$
95	$5.733^{+0.011+0.076}_{-0.182-0.076}$	$5.498^{+0.128+0.075}_{-0.069-0.075}$	$5.565^{+0.062+0.069}_{-0.111-0.069}$
100	$5.497^{+0.015+0.073}_{-0.147-0.073}$	$5.265^{+0.122+0.072}_{-0.088-0.072}$	$5.344^{+0.049+0.066}_{-0.115-0.066}$
105	$5.262^{+0.000+0.070}_{-0.101-0.070}$	$5.065^{+0.105+0.069}_{-0.071-0.069}$	$5.106^{+0.072+0.063}_{-0.085-0.063}$
110	$5.055^{+0.000+0.067}_{-0.080-0.067}$	$4.862^{+0.100+0.066}_{-0.077-0.066}$	$4.913^{+0.045+0.060}_{-0.108-0.060}$
115	$4.848^{+0.012+0.065}_{-0.114-0.065}$	$4.668^{+0.090+0.064}_{-0.067-0.064}$	$4.716^{+0.061+0.058}_{-0.085-0.058}$
120	$4.684^{+0.000+0.062}_{-0.107-0.062}$	$4.490^{+0.090+0.061}_{-0.069-0.061}$	$4.542^{+0.040+0.055}_{-0.093-0.055}$
125	$4.479^{+0.017+0.060}_{-0.089-0.060}$	$4.317^{+0.083+0.059}_{-0.061-0.059}$	$4.363^{+0.047+0.053}_{-0.081-0.053}$
130	$4.307^{+0.024+0.058}_{-0.100-0.058}$	$4.148^{+0.078+0.057}_{-0.055-0.057}$	$4.218^{+0.019+0.051}_{-0.104-0.051}$
135	$4.148^{+0.026+0.056}_{-0.110-0.056}$	$4.002^{+0.071+0.055}_{-0.057-0.055}$	$4.035^{+0.045+0.049}_{-0.071-0.049}$
140	$3.996^{+0.029+0.054}_{-0.122-0.054}$	$3.854^{+0.068+0.053}_{-0.050-0.053}$	$3.890^{+0.031+0.047}_{-0.081-0.047}$
145	$3.846^{+0.044+0.052}_{-0.116-0.052}$	$3.714^{+0.070+0.051}_{-0.052-0.051}$	$3.747^{+0.039+0.046}_{-0.067-0.046}$
150	$3.725^{+0.042+0.051}_{-0.138-0.051}$	$3.561^{+0.093+0.049}_{-0.038-0.049}$	$3.616^{+0.035+0.044}_{-0.075-0.044}$
155	$3.575^{+0.068+0.049}_{-0.113-0.049}$	$3.449^{+0.081+0.048}_{-0.051-0.048}$	$3.487^{+0.032+0.042}_{-0.082-0.042}$
160	$3.449^{+0.067+0.047}_{-0.134-0.047}$	$3.325^{+0.086+0.046}_{-0.035-0.046}$	$3.362^{+0.039+0.041}_{-0.068-0.041}$
165	$3.333^{+0.081+0.046}_{-0.142-0.046}$	$3.212^{+0.084+0.045}_{-0.037-0.045}$	$3.257^{+0.026+0.040}_{-0.070-0.040}$
170	$3.213^{+0.088+0.044}_{-0.138-0.044}$	$3.109^{+0.076+0.044}_{-0.044-0.044}$	$3.135^{+0.034+0.038}_{-0.061-0.038}$
175	$3.105^{+0.095+0.043}_{-0.142-0.043}$	$3.001^{+0.082+0.042}_{-0.042-0.042}$	$3.033^{+0.034+0.037}_{-0.060-0.037}$
180	$2.993^{+0.113+0.041}_{-0.137-0.041}$	$2.900^{+0.071+0.041}_{-0.036-0.041}$	$2.932^{+0.029+0.036}_{-0.058-0.036}$
185	$2.902^{+0.107+0.040}_{-0.150-0.040}$	$2.810^{+0.074+0.040}_{-0.041-0.040}$	$2.830^{+0.033+0.035}_{-0.048-0.035}$
190	$2.804^{+0.120+0.039}_{-0.143-0.039}$	$2.714^{+0.076+0.039}_{-0.039-0.039}$	$2.742^{+0.033+0.034}_{-0.049-0.034}$
195	$2.707^{+0.126+0.038}_{-0.142-0.038}$	$2.625^{+0.071+0.037}_{-0.034-0.037}$	$2.651^{+0.034+0.033}_{-0.051-0.033}$
200	$2.628^{+0.117+0.037}_{-0.149-0.037}$	$2.542^{+0.076+0.036}_{-0.033-0.036}$	$2.565^{+0.037+0.032}_{-0.046-0.032}$
210	$2.461^{+0.131+0.035}_{-0.147-0.035}$	$2.387^{+0.069+0.034}_{-0.031-0.034}$	$2.406^{+0.036+0.030}_{-0.042-0.030}$
220	$2.311^{+0.141+0.033}_{-0.152-0.033}$	$2.244^{+0.071+0.033}_{-0.034-0.033}$	$2.263^{+0.032+0.028}_{-0.037-0.028}$
230	$2.174^{+0.141+0.031}_{-0.151-0.031}$	$2.112^{+0.064+0.031}_{-0.031-0.031}$	$2.128^{+0.031+0.026}_{-0.038-0.026}$
240	$2.045^{+0.143+0.029}_{-0.144-0.029}$	$1.989^{+0.066+0.029}_{-0.030-0.029}$	$2.000^{+0.032+0.025}_{-0.033-0.025}$
250	$1.927^{+0.148+0.028}_{-0.141-0.028}$	$1.874^{+0.065+0.028}_{-0.024-0.028}$	$1.890^{+0.028+0.024}_{-0.032-0.024}$
260	$1.821^{+0.142+0.027}_{-0.143-0.027}$	$1.772^{+0.061+0.027}_{-0.027-0.027}$	$1.784^{+0.028+0.022}_{-0.028-0.022}$
270	$1.718^{+0.146+0.025}_{-0.138-0.025}$	$1.673^{+0.059+0.025}_{-0.025-0.025}$	$1.685^{+0.027+0.021}_{-0.027-0.021}$
280	$1.624^{+0.147+0.024}_{-0.135-0.024}$	$1.585^{+0.056+0.024}_{-0.022-0.024}$	$1.595^{+0.029+0.020}_{-0.026-0.020}$
290	$1.538^{+0.145+0.023}_{-0.132-0.023}$	$1.501^{+0.060+0.023}_{-0.023-0.023}$	$1.511^{+0.029+0.019}_{-0.024-0.019}$
300	$1.457^{+0.144+0.022}_{-0.129-0.022}$	$1.424^{+0.053+0.022}_{-0.022-0.022}$	$1.436^{+0.021+0.018}_{-0.027-0.018}$
320	$1.310^{+0.142+0.020}_{-0.123-0.020}$	$1.278^{+0.055+0.020}_{-0.018-0.020}$	$1.291^{+0.023+0.017}_{-0.022-0.017}$
340	$1.186^{+0.135+0.018}_{-0.121-0.018}$	$1.158^{+0.053+0.018}_{-0.016-0.018}$	$1.167^{+0.021+0.015}_{-0.018-0.015}$
360	$1.073^{+0.132+0.017}_{-0.113-0.017}$	$1.051^{+0.047+0.017}_{-0.014-0.017}$	$1.056^{+0.022+0.014}_{-0.015-0.014}$
380	$9.737^{+1.290+0.155}_{-1.059-0.155}\cdot10^{-1}$	$9.551^{+0.467+0.155}_{-0.151-0.155}\cdot10^{-1}$	$9.612^{+0.184+0.129}_{-0.153-0.129}\cdot10^{-1}$
400	$8.859^{+1.226+0.143}_{-1.002-0.143}\cdot10^{-1}$	$8.711^{+0.421+0.144}_{-0.141-0.144}\cdot10^{-1}$	$8.764^{+0.169+0.119}_{-0.125-0.119}\cdot10^{-1}$
450	$7.079^{+1.118+0.118}_{-0.868-0.118}\cdot10^{-1}$	$6.985^{+0.368+0.119}_{-0.115-0.119}\cdot10^{-1}$	$7.024^{+0.152+0.098}_{-0.102-0.098}\cdot10^{-1}$
500	$5.733^{+1.011+0.098}_{-0.750-0.098}\cdot10^{-1}$	$5.675^{+0.321+0.099}_{-0.106-0.099}\cdot10^{-1}$	$5.704^{+0.114+0.082}_{-0.077-0.082}\cdot10^{-1}$
550	$4.696^{+0.899+0.083}_{-0.664-0.083}\cdot10^{-1}$	$4.660^{+0.277+0.084}_{-0.100-0.084}\cdot10^{-1}$	$4.679^{+0.108+0.069}_{-0.050-0.069}\cdot10^{-1}$
600	$3.877^{+0.794+0.070}_{-0.573-0.070}\cdot10^{-1}$	$3.860^{+0.246+0.071}_{-0.097-0.071}\cdot10^{-1}$	$3.881^{+0.087+0.059}_{-0.042-0.059}\cdot10^{-1}$
650	$3.236^{+0.699+0.060}_{-0.506-0.060}\cdot10^{-1}$	$3.228^{+0.210+0.061}_{-0.086-0.061}\cdot10^{-1}$	$3.241^{+0.077+0.051}_{-0.031-0.051}\cdot10^{-1}$
700	$2.711^{+0.626+0.051}_{-0.440-0.051}\cdot10^{-1}$	$2.717^{+0.184+0.052}_{-0.084-0.052}\cdot10^{-1}$	$2.724^{+0.070+0.044}_{-0.021-0.044}\cdot10^{-1}$
750	$2.289^{+0.564+0.044}_{-0.385-0.044}\cdot10^{-1}$	$2.305^{+0.156+0.046}_{-0.081-0.046}\cdot10^{-1}$	$2.310^{+0.057+0.038}_{-0.021-0.038}\cdot10^{-1}$
800	$1.945^{+0.497+0.039}_{-0.340-0.039}\cdot10^{-1}$	$1.959^{+0.141+0.040}_{-0.071-0.040}\cdot10^{-1}$	$1.967^{+0.048+0.033}_{-0.014-0.033}\cdot10^{-1}$
850	$1.662^{+0.442+0.034}_{-0.300-0.034}\cdot10^{-1}$	$1.681^{+0.120+0.035}_{-0.067-0.035}\cdot10^{-1}$	$1.684^{+0.043+0.029}_{-0.012-0.029}\cdot10^{-1}$
900	$1.425^{+0.396+0.029}_{-0.265-0.029}\cdot10^{-1}$	$1.442^{+0.111+0.030}_{-0.058-0.030}\cdot10^{-1}$	$1.446^{+0.038+0.026}_{-0.010-0.026}\cdot10^{-1}$
950	$1.227^{+0.354+0.026}_{-0.234-0.026}\cdot10^{-1}$	$1.246^{+0.096+0.027}_{-0.056-0.027}\cdot10^{-1}$	$1.250^{+0.032+0.023}_{-0.010-0.023}\cdot10^{-1}$
1000	$1.060^{+0.317+0.023}_{-0.207-0.023}\cdot10^{-1}$	$1.080^{+0.086+0.024}_{-0.049-0.024}\cdot10^{-1}$	$1.083^{+0.030+0.020}_{-0.010-0.020}\cdot10^{-1}$

Table B.15: Total VBF cross sections at the LHC, $\sqrt{S} = 14\,\text{TeV}$ at LO, NLO and NNLO in QCD. Errors shown are respectively scale and PDF uncertainities. Scale uncertainities are evaluated by varying μ_r and μ_f in the interval $\mu_r, \mu_f \in [Q/4, 4Q]$. The NNPDF2.1 [77] PDF set has been used. Numbers are in pb.

References

[1] A. Djouadi, Phys.Rept. **457**, 1 (2008), arXiv:hep-ph/0503172.

[2] R. Harlander, J. Phys. **G35**, 033001 (2008).

[3] G. Giudice, C. Grojean, A. Pomarol, and R. Rattazzi, JHEP **0706**, 045 (2007), arXiv:hep-ph/0703164.

[4] R. Harlander and W. B. Kilgore, Phys.Rev.Lett. **88**, 201801 (2002), arXiv:hep-ph/0201206.

[5] C. Anastasiou and K. Melnikov, Nucl.Phys. **B646**, 220 (2002), arXiv:hep-ph/0207004.

[6] V. Ravindran, J. Smith, and W. L. van Neerven, Nucl.Phys. **B665**, 325 (2003), arXiv:hep-ph/0302135.

[7] O. Brein, A. Djouadi, and R. Harlander, Phys.Lett. **B579**, 149 (2004), arXiv:hep-ph/0307206.

[8] LHC Higgs Cross Section Working Group, S. Dittmaier *et al.*, (2011), arXiv:1101.0593.

[9] R. N. Cahn and S. Dawson, Phys. Lett. **B136**, 196 (1984).

[10] G. L. Kane, W. W. Repko, and W. B. Rolnick, Phys. Lett. **B148**, 367 (1984).

[11] R. Kleiss and W. Stirling, Phys.Lett. **B182**, 75 (1986).

[12] D. L. Rainwater and D. Zeppenfeld, JHEP **9712**, 005 (1997), arXiv:hep-ph/9712271.

[13] D. L. Rainwater, D. Zeppenfeld, and K. Hagiwara, Phys. Rev. **D59**, 014037 (1998), arXiv:hep-ph/9808468.

[14] N. Kauer, T. Plehn, D. L. Rainwater, and D. Zeppenfeld, Phys.Lett. **B503**, 113 (2001), arXiv:hep-ph/0012351.

[15] M. L. Mangano *et al.*, Phys. Lett. **B556**, 50 (2003), arXiv:hep-ph/0210261.

[16] T. Han, G. Valencia, and S. Willenbrock, Phys.Rev.Lett. **69**, 3274 (1992), arXiv:hep-ph/9206246.

[17] T. Figy, C. Oleari, and D. Zeppenfeld, Phys. Rev. **D68**, 073005 (2003), arXiv:hep-ph/0306109.

[18] M. Ciccolini, A. Denner, and S. Dittmaier, Phys.Rev.Lett. **99**, 161803 (2007), arXiv:0707.0381.

[19] M. Ciccolini, A. Denner, and S. Dittmaier, Phys.Rev. **D77**, 013002 (2008), arXiv:0710.4749.

[20] P. Bolzoni, F. Maltoni, S. Moch, and M. Zaro, Phys.Rev.Lett. **105**, 011801 (2010), arXiv:1003.4451.

[21] P. Bolzoni, M. Zaro, F. Maltoni, and S. Moch, Nucl.Phys.Proc.Suppl. **205-206**, 314 (2010), arXiv:1006.2323.

[22] C. Csaki *et al.*, Phys.Rev. **D69**, 055006 (2004), arXiv:hep-ph/0305237.

[23] C. Csaki, C. Grojean, L. Pilo, and J. Terning, Phys.Rev.Lett. **92**, 101802 (2004), arXiv:hep-ph/0308038.

[24] M. Zaro, P. Bolzoni, F. Maltoni, and S.-O. Moch, PoS **CHARGED2010**, 028 (2010), arXiv:1012.1806.

[25] E. N. Argyres *et al.*, Phys. Lett. **B358**, 339 (1995), arXiv:hep-ph/9507216.

[26] R. Harlander, J. Vollinga, and M. M. Weber, Phys.Rev. **D77**, 053010 (2008), arXiv:0801.3355.

[27] J. R. Andersen and J. M. Smillie, Phys. Rev. **D75**, 037301 (2007), arXiv:hep-ph/0611281.

[28] J. R. Andersen, T. Binoth, G. Heinrich, and J. M. Smillie, JHEP **02**, 057 (2008), arXiv:0709.3513.

[29] A. Ballestrero *et al.*, Comput.Phys.Commun. **180**, 401 (2009), arXiv:0801.3359.

[30] A. Ballestrero, G. Bevilacqua, D. B. Franzosi, and E. Maina, JHEP **0911**, 126 (2009), arXiv:0909.3838.

[31] B. Jäger, C. Oleari, and D. Zeppenfeld, Phys. Rev. **D73**, 113006 (2006), arXiv:hep-ph/0604200.

[32] B. Jäger, C. Oleari, and D. Zeppenfeld, JHEP **07**, 015 (2006), arXiv:hep-ph/0603177.

[33] G. Bozzi, B. Jäger, C. Oleari, and D. Zeppenfeld, Phys. Rev. **D75**, 073004 (2007), arXiv:hep-ph/0701105.

[34] K. Arnold *et al.*, (2011), arXiv:1107.4038.

[35] Particle Data Group, K. Nakamura *et al.*, J.Phys.G **G37**, 075021 (2010).

[36] D. A. Dicus and S. S. D. Willenbrock, Phys. Rev. **D32**, 1642 (1985).

[37] W. A. Bardeen, A. J. Buras, D. W. Duke, and T. Muta, Phys. Rev. **D18**, 3998 (1978).

[38] S. Moch, J. Vermaseren, and A. Vogt, Nucl.Phys. **B688**, 101 (2004), arXiv:hep-ph/0403192.

[39] A. Vogt, Comput.Phys.Commun. **170**, 65 (2005), arXiv:hep-ph/0408244.

[40] W. L. van Neerven and A. Vogt, Nucl. Phys. **B588**, 345 (2000), arXiv:hep-ph/0006154.

[41] W. van Neerven and E. Zijlstra, Phys.Lett. **B272**, 127 (1991).

[42] E. B. Zijlstra and W. L. van Neerven, Nucl. Phys. **B383**, 525 (1992).

[43] E. B. Zijlstra and W. L. van Neerven, Phys. Lett. **B297**, 377 (1992).

[44] S. Moch and J. Vermaseren, Nucl.Phys. **B573**, 853 (2000), arXiv:hep-ph/9912355.

[45] A. Vogt, S. Moch, and J. Vermaseren, Nucl.Phys. **B691**, 129 (2004), arXiv:hep-ph/0404111.

[46] J. Vermaseren, A. Vogt, and S. Moch, Nucl.Phys. **B724**, 3 (2005), arXiv:hep-ph/0504242.

[47] S. Moch, J. A. M. Vermaseren, and A. Vogt, Nucl. Phys. **B813**, 220 (2009), arXiv:0812.4168.

[48] E. Remiddi and J. Vermaseren, Int.J.Mod.Phys. **A15**, 725 (2000), arXiv:hep-ph/9905237.

[49] T. Gehrmann and E. Remiddi, Comput.Phys.Commun. **141**, 296 (2001), arXiv:hep-ph/0107173.

[50] T. Figy, V. Hankele, and D. Zeppenfeld, JHEP **02**, 076 (2008), arXiv:0710.5621.

[51] W. L. van Neerven and J. A. M. Vermaseren, Phys. Lett. **B137**, 241 (1984).

[52] A. Denner and S. Dittmaier, Nucl. Phys. **B658**, 175 (2003), arXiv:hep-ph/0212259.

[53] J. Fleischer and T. Riemann, Phys. Rev. **D83**, 073004 (2011), arXiv:1009.4436.

[54] R. K. Ellis and G. Zanderighi, JHEP **02**, 002 (2008), arXiv:0712.1851.

[55] V. Hirschi *et al.*, JHEP **05**, 044 (2011), arXiv:1103.0621.

[56] R. Frederix, S. Frixione, F. Maltoni, and T. Stelzer, JHEP **10**, 003 (2009), arXiv:0908.4272.

[57] A. Martin, R. Roberts, W. Stirling, and R. Thorne, Eur. Phys. J. **C28**, 455 (2003), arXiv:hep-ph/0211080.

[58] A. Bredenstein, A. Denner, S. Dittmaier, and M. Weber, Phys.Rev. **D74**, 013004 (2006), arXiv:hep-ph/0604011.

[59] A. Bredenstein, A. Denner, S. Dittmaier, and M. M. Weber, JHEP **02**, 080 (2007), arXiv:hep-ph/0611234.

[60] M. Zaro, P. Bolzoni, F. Maltoni, and S. Moch, PoS **DIS2010**, 211 (2010).

[61] B. A. Kniehl, Phys. Rev. **D42**, 3100 (1990).

[62] B. A. Kniehl, Phys. Rev. **D42**, 2253 (1990).

[63] A. Martin, W. Stirling, R. Thorne, and G. Watt, Eur.Phys.J. **C63**, 189 (2009), arXiv:0901.0002.

[64] B. A. Kniehl and J. H. Kühn, Nucl.Phys. **B329**, 547 (1990).

[65] R. J. Gonsalves, C.-M. Hung, and J. Pawlowski, Phys.Rev. **D46**, 4930 (1992).

[66] R. Mertig, M. Bohm, and A. Denner, Comput.Phys.Commun. **64**, 345 (1991).

[67] F. Maltoni and T. Stelzer, JHEP **0302**, 027 (2003), arXiv:hep-ph/0208156.

[68] J. Alwall *et al.*, JHEP **09**, 028 (2007), arXiv:0706.2334.

[69] W. Bernreuther *et al.*, Nucl.Phys. **B723**, 91 (2005), arXiv:hep-ph/0504190.

[70] S. Alekhin, J. Blümlein, S. Klein, and S. Moch, Phys.Rev. **D81**, 014032 (2010), arXiv:0908.2766.

[71] HAWK, A. Denner, S. Dittmaier, and A. Mück, `http://omnibus.uni-freiburg.de/~sd565/programs/hawk/hawk.html`.

[72] S. Alekhin, J. Blümlein, and S. Moch, PoS **DIS2010**, 021 (2010), arXiv:1007.3657.

[73] H1 and ZEUS Collaboration, F. Aaron *et al.*, JHEP **1001**, 109 (2010), arXiv:0911.0884.

[74] HERAPDF, `https://www.desy.de/h1zeus/combined_results/proton_structure/Fits/HERAPDF1.0_NNLO_1145.LHgrid.gz`.

[75] P. Jimenez-Delgado and E. Reya, Phys.Rev. **D79**, 074023 (2009), arXiv:0810.4274.

[76] P. Jimenez-Delgado and E. Reya, Phys.Rev. **D80**, 114011 (2009), arXiv:0909.1711.

[77] The NNPDF Collaboration, R. D. Ball *et al.*, Nucl.Phys. **B855**, 153 (2012), arXiv:1107.2652.

[78] VBF@NNLO, P. Bolzoni, F. Maltoni, S. Moch, and M. Zaro, `http://vbf-nnlo.phys.ucl.ac.be/vbf.html` .

[79] T. Plehn, D. L. Rainwater, and D. Zeppenfeld, Phys.Rev.Lett. **88**, 051801 (2002), arXiv:hep-ph/0105325.

[80] Y. Takubo *et al.*, (2010), arXiv:1006.3427.

[81] V. Hankele, G. Klamke, D. Zeppenfeld, and T. Figy, Phys.Rev. **D74**, 095001 (2006), arXiv:hep-ph/0609075.

[82] K. Arnold *et al.*, Comput.Phys.Commun. **180**, 1661 (2009), arXiv:0811.4559.

[83] W. Hollik, T. Plehn, M. Rauch, and H. Rzehak, Phys.Rev.Lett. **102**, 091802 (2009), arXiv:arXiv:0804.2676.

[84] S. Heinemeyer, W. Hollik, and G. Weiglein, Eur.Phys.J. **C9**, 343 (1999), arXiv:hep-ph/9812472.

[85] G. Degrassi *et al.*, Eur.Phys.J. **C28**, 133 (2003), arXiv:hep-ph/0212020.

[86] M. Frank *et al.*, JHEP **0702**, 047 (2007), arXiv:hep-ph/0611326.

[87] S. Kanemura, Phys.Rev. **D61**, 095001 (2000), arXiv:hep-ph/9710237.

[88] E. Asakawa, S. Kanemura, and J. Kanzaki, Phys.Rev. **D75**, 075022 (2007), arXiv:hep-ph/0612271.

[89] E. L. Berger, T. Han, J. Jiang, and T. Plehn, Phys.Rev. **D71**, 115012 (2005), arXiv:hep-ph/0312286.

[90] C. Weydert *et al.*, Eur.Phys.J. **C67**, 617 (2010), arXiv:0912.3430.

[91] H. Georgi and M. Machacek, Nucl.Phys. **B262**, 463 (1985).

[92] J. Gunion, R. Vega, and J. Wudka, Phys.Rev. **D42**, 1673 (1990).

[93] R. Vega and D. A. Dicus, Nucl.Phys. **B329**, 533 (1990).

[94] S. Godfrey and K. Moats, Phys.Rev. **D81**, 075026 (2010), arXiv:1003.3033.

[95] R. Chivukula *et al.*, Phys.Rev. **D74**, 075011 (2006), arXiv:hep-ph/0607124.

[96] H.-J. He *et al.*, Phys.Rev. **D78**, 031701 (2008), arXiv:0708.2588.

[97] K. Agashe *et al.*, Phys.Rev. **D76**, 115015 (2007), arXiv:0709.0007.

[98] K. Agashe *et al.*, Phys.Rev. **D80**, 075007 (2009), arXiv:0810.1497.

[99] L. Da Rold and A. Pomarol, Nucl. Phys. **B721**, 79 (2005), arXiv:hep-ph/0501218.

[100] A. Falkowski *et al.*, JHEP **1111**, 028 (2011), arXiv:1108.1183.

[101] A. Daleo, A. Gehrmann-De Ridder, T. Gehrmann, and G. Luisoni, JHEP **1001**, 118 (2010), arXiv:0912.0374.

[102] G. Ferrera, M. Grazzini, and F. Tramontano, Phys.Rev.Lett. **107**, 152003 (2011), arXiv:1107.1164.

[103] N. D. Christensen and C. Duhr, Comput.Phys.Commun. **180**, 1614 (2009), arXiv:0806.4194.

[104] J. Alwall *et al.*, JHEP **06**, 128 (2011), arXiv:1106.0522.

[105] G. Ossola, C. G. Papadopoulos, and R. Pittau, JHEP **03**, 042 (2008), arXiv:0711.3596.

[106] D. Binosi and L. Theussl, Comput.Phys.Commun. **161**, 76 (2004), arXiv:hep-ph/0309015.

[107] J. Vermaseren, Comput.Phys.Commun. **83**, 45 (1994).

[108] G. Lepage, J.Comput.Phys. **27**, 192 (1978).